Università degli Studi di Cagliari
PhD program in Life, Environmental and Drug Sciences
Curriculum Drug Sciences
XXXIV° Cycle

Strategies to promote the delivery of anti-inflammatory agents through different nanotechnological approaches

SSD: CHIM/09

PhD candidate: Luca Casula

Supervisor: Prof. Anna Maria Fadda

Final exam. Academic Year 2020–2021
Thesis defence: April 2022 Session

Index of contents

Abstract

Non-steroidal anti-inflammatory drugs (NSAIDs) and glucocorticoids are some of the most widely prescribed drugs in the world and are commonly used to treat inflammatory disorders and the related effects (e.g. fever and pain), but also inflammation in chronic diseases such as rheumatoid arthritis and osteoarthritis. These molecules inhibit the formation of chemical mediators, responsible for the propagation of the inflammation cascade, through different mechanisms.

However, some of these active ingredients are characterized by poor aqueous solubility, low bioavailability and poor stability. In order to overcome these limits, various strategies have been studied over the years such as the use of nanotechnology to produce drug delivery systems.

In this thesis, different technological approaches have been developed to enhance delivery of poorly soluble drugs with anti-inflammatory activity, i.e., production of nanosuspensions (Part 1), liposomes and polymeric nanofibers (Part 2).

Part 1 of this thesis investigates the potential of nanocrystals suspension for inhalation drug delivery for the treatment of pulmonary inflammatory conditions, such as chronic obstructive pulmonary disease (COPD) and chronic asthma.

More in detail, Chapter 1 focuses on the ability of electronic nicotine delivery systems (ENDS) to deliver drug nanocrystals through the produced aerosol. A nanocrystal nanosuspension of beclomethasone dipropionate, a synthetic chlorinated corticosteroid diester commonly used by inhalation in the treatment of asthma and chronic obstructive pulmonary disease, was prepared with a wet media milling technique using Poloxamer 188 as stabilizer. The obtained nanosuspension was thoroughly characterized by different techniques: transmission electron microscopy, photon correlation spectroscopy, X-ray powder diffractometry and Fourier transform infrared spectroscopy. The nanosuspension was then loaded in the cartomizer of the electronic cigarette and the produced aerosol was collected and analysed, confirming the presence of drug nanocrystals. The results of this study suggested the possible alternative use of ENDS as medical device for the delivery of poorly soluble drugs.

In Chapter 2, the combination of a conventional glucocorticoid drug and a natural active compound was studied. Curcumin has shown a potential extraordinary activity as an add-on ingredient in asthma treatment, due to its immunomodulatory and anti-inflammatory mechanism of action. However, its low water solubility and bioavailability lead to a poor therapeutic effect, which can be overcome by its formulation as nanocrystals. The aim of this study was to prepare a multicomponent formulation for the delivery of curcumin (CUR) and beclomethasone dipropionate (BDP) into the lungs as water-based nanosuspensions (NS). Single component formulations (CUR-NS, BDP-NS) and a multi-component formulation (CUR+BDP-NS) were prepared through a wet ball media milling technique, using P188 as a non-toxic stabilizer. Characterization was carried out in terms of size, size distribution, zeta potential, nanocrystals morphology and solid-state properties. Moreover, the inhalation delivery efficiency was studied with Next Generation Impactor (NGI, Apparatus E Ph. Eu). CUR-NS was optimized and showed a long-term stability and improved nanocrystals apparent solubility. The three formulations exhibited a nanocrystal mean diameter in the range 200-240 nm and a homogenous particle size distribution. Aggregation or sedimentation phenomena were not observed in the multicomponent formulation on 90 days storage at room temperature. Finally, the nebulization tests of the three samples showed optimal aerodynamic parameters and MMAD < 5 μm.

In Part 2 of the thesis, a combination of two different technological approaches, namely liposomes and nanofibers, was used to improve the delivery of the poorly soluble drug simvastatin. Simvastatin, as part of the statins group, is mostly used for its lipid lowering effect. However, recent studies have highlighted the anti-inflammatory and immunomodulatory activity of the drug both *in vitro* and in vivo. At first, simvastatin was encapsulated in liposomes through the direct sonication methods. In order to avoid degradation phenomena, increasing amounts of antioxidant were used for the preparation of the samples. The different formulations were characterized in terms of size, size distribution, zeta potential, drug content and encapsulation efficiency. Once the liposomal formulations had been optimized, three formulations were chosen for the preparation of the polymeric solutions. Nanofibers were prepared through a green electrospinning technique and their morphology was investigated using scanning and transmission electron microscopy. The three different liposomes-composite nanofibrous systems were

characterized for drug content and entrapment efficiency, drug release (both in sink and non-sink conditions), protection of the active compound by the antioxidant. Moreover, the innovative Multi-Angle Dynamic Light Scattering Technology (MADLS) was used to investigate the release of liposomes from the nanofibrous mats. Finally, in vitro tests were carried out to study the cytotoxicity of the different formulations on human keratinocytes their ability to inhibit lymphocytes proliferation.

List of abbreviations

AA	arachidonic acid
ATR-FTIR	attenuated total reflectance-fourier transform infrared
BCS	biopharmaceutics classification system
BDP	beclomethasone dipropionate
BDP-NS	beclomethasone dipropionate nanosuspension
BHA	butylated hydroxyanisole
CAMs	cell adhesion molecules
COPD	chronic obstructive pulmonary disease
COX	cyclooxygenase
CS	corticosteroids
CUR	curcumin
CUR+BDP-NS	curcumin/beclomethasone dipropionate multicomponent nanosuspension
CUR-NS	curcumin nanosuspension
DAMPs	danger-associated molecular patterns
DEE	drug entrapment efficiency
DL	drug loading
DLS	dynamic light scattering
DMEM	Dulbecco's modified eagle medium
DMSO	dimethyl sulfoxide

DSC	differential scanning calorimetry
EA	edge activator
ED	emitted dose
EE	encapsulation efficiency
ENDS	electronic nicotine delivery systems
EPAG	european pharmaceutical aerosol group
ESEM	environmental scanning electron microscope
FBS	fetal bovine serum
FPD	fine particle dose
FPF	fine particle fraction
FTIR	fourier transform infrared
GSD	geometric standard deviation
HMG-CoA	3-hydroxy-3-methyl-gutaryl coenzyme a
hs-CRP	high-sensivity C-reactive proteins
IFN	interferon
IL	interleukin
LABA	long-acting beta2-agonist
LIPO	liposomes
LOX	lipoxygenase
LOX	lipoxygenase

LT	leukotrien
LTRA	leukotriene receptor antagonist
LUVs	large unilamellar vesicles
LX	lipoxin
MADLS	multi-angle dynamic light scattering
MHC II	major histocompatibility class ii
MLVs	multilamellar vesicles
MMAD	mass median aerodynamic diameter
MMPs	matrix metalloproteinases
NF	nanofibers
Nf-κB	nuclear factor κb
NGI	next generation impactor
NS	nanosuspension(s)
NSAIDs	non-steroidal anti-inflammatory drugs
OCS	oral corticosteroids
OTC	over-the-counter
P188	poloxamer 188
P90G	phospolipon 90g
PAF	platelet-activating factor
PAI-1	plasminogen activator inhibitor-1

PAMPs	pathogen-associated molecular patterns
PDI	polydispersity index
PEO	poly(ethylene) oxide
PG	prostaglandin
PGHS	prostaglandin H synthase
PHA	phytohemagglutinin
PLA2	phospholipase A2
PMN	polymorphonuclear cells
PRRs	pattern-recognition receptors
RH	relative humidity
SABA	short-acting beta2-agonist
SDS	sodium dodecyl sulphate
SEM	scanning electron microscope
SIM	simvastatin
SUVs	small unilamellar vesicles
TEM	transmission electron microscopy
TF	tissue factor
TNF	tumor necrosis factor
TPD	tobacco products directive
TX	thromboxane

WBM	wet ball media milling
XRPD	x-ray powder diffractometry
ZP	zeta potential

General introduction

1 The Inflammatory process

Inflammation is a physiological process activated as a response against infectious agents or injurious insults. The early phase involves the so-called *acute* inflammation, whose final point is usually a positive resolution. Nevertheless, it might become prolonged or *chronic* and thus, promote or aggravate existing disease conditions, such as asthma, atherosclerosis and cancer [1]. The typical signals of tissue inflammation were already documented by Celsus in the 1st century AD as *rubor* (redness), *tumor* (swelling), *calor* (heat) and *dolor* (pain) [2]. This complex mechanism involves activation of immune cells and release of chemical mediators, aimed at removing the trigger insult, isolating the affected area and commencing the restoration and healing of the tissue integrity and functionality [1], [3].

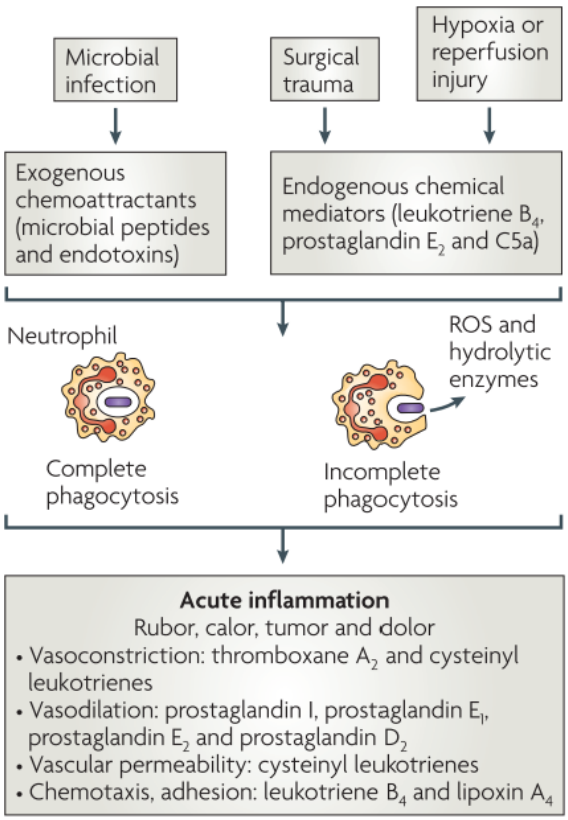

Figure 1. Schematic representation of the acute inflammation process [4].

The first steps are carried out by the cells of the innate and adaptive immune systems, which recognize through the pattern-recognition receptors (PRRs) the pathogen-associated molecular patterns (PAMPs) of infecting microorganisms or the danger-associated molecular patterns (DAMPs) deriving from any cellular damage [5]. Their stimulation leads to activation of transmitting signals to the nucleus with a consequential initiation of transcriptional mechanisms and production of proinflammatory cytokines and chemokines [6], [7]. A large amount of transcriptions factors play a key-role in the induction of inflammatory genes. Among the others, Nf-κB is one of the most studied and is also believed to have a relevant importance in the progression of chronic inflammatory diseases, such as bronchial asthma [5], [8].

Once the trigger stimulus has been sensed and the chemotactic molecules have been released, time-dependent progression of phagocytic cells infiltration to the tissue proceeds via diapedesis, primarily with neutrophils and secondly with monocytes. These polymorphonuclear (PMN) cells are attracted from postcapillary venules to the site of inflammation by the presence not only of the endogenous chemokines and cytokines, but also of the exogenous chemoattractants released by the invading microorganisms [4]. The chemotactic stimuli bring about an upregulation of the cell surface receptors and the activation of a group of cell surface molecules. Simultaneously, the expression of selectin molecules on the surface of endothelial cells (L-, P-, and E-selectins) and integrin molecules on the neutrophils are upregulated, aiding the immobilization of the PMN and the attachment to the surface of the vascular endothelium. The interactions of the integrins with the cell adhesion molecules (CAMs) lead to the extravasation of neutrophils and monocytes in the injured tissue area. Once the monocytes infiltrate in the tissue, they differentiate into macrophages and dendritic cells, which act together with neutrophils as the major protagonists in propagating the inflammatory response [1], [9]. Nonetheless, many others cell types are implicated in the execution of the process, such as mast cells and lymphocytes, which release several chemokines responsible of enhancing the vascular endothelial permeability and the recruitment of other inflammatory cells [2], [5], [10].

1.1 Chemical mediators of Inflammation

During the complex and interconnected mechanisms of inflammation, a large amount of chemical substances is involved in the control of the whole process, to prevent further damage and promote healing and restoration of the tissue. These chemical messengers might include exogenous substances (such as bacterial products and toxins), and endogenous substances, which are released in the human body [11]. The latter can be identified as *inflammatory mediators:* molecules that induce vasodilation, enhance blood flow and vessel permeability, and promote emigration of inflammatory cells from the vessels. Whilst some mediators are preformed and gathered in granules (histamine, serotonin), some others are produced ex novo by the cells. In particular, peptide (kinins) and lipid mediators (eicosanoids) are obtained through multi-step enzymatic reactions when these cells are activated [11], [12].

Among the various chemicals, some are identified as vasoactive mediators, such as histamine, serotonin, and bradykinin [13]. Histamine (β-Imidazolylethylamine), a vasoactive amine produced by mast cells and basophil leukocytes, determines an increase in vascular permeability, chemokinesis, mucus production and smooth muscle contraction and plays a relevant role in allergic inflammatory reactions. Serotonin (5-Hydroxytryptamine), another amine with vascular effects, is produced through tryptophan metabolism by mast cells and platelets and is mostly known for its role as neurotransmitter. Bradykinin is a nonapeptide hormone created from plasma Kinin–Kallikrein system, showing not only vascular effects, but also stimulation of pain receptors and swelling [14]–[16].

Particular importance is given to the role played by cytokines. Cytokines are small proteins released from the focus of inflammation with some peculiar actions on the modulation of the process and the communication between inflammatory cells. They are often produced through a self-perpetuating mechanism, with one cytokine stimulating the target cells to produce more cytokines. These molecules can have an effect on the same cells that secrete them (autocrine action), on nearby cells (paracrine action), and rarely on distant cells (endocrine action). Furthermore, they can act synergistically or antagonistically with other cytokines or other classes of mediators. Cytokines classification can be made according to their cells-producer: lymphokine (produced by lymphocytes), monokine (from monocytes)

and interleukin (made by leukocytes and acting on other leukocytes) [17], [18]. Eighteen cytokines are part of the interleukin (IL) subgroup, whereas some others have maintained their biological activity-name, such as tumor necrosis factor (TNF). Furthermore, their role on the inflammation leads to categorization on proinflammatory cytokines, which promote inflammation, and anti-inflammatory cytokines, which suppress the activity of the proinflammatory ones. Among the first group, IL-1, TNF- α, and IFN- γ are potent activators of the process, whereas IL-4, IL-6, IL-10, IL-11, and IL-13 are part of the second group [19], [20].

Chemokines, one particular subgroup of low molecular weight cytokines, are known to induce chemotaxis. They show a predominant chemoattractant function, activating the migration of leukocytes and their production is commonly accomplished by monocytes, macrophages or epithelial, endothelial, and fibroblastic cells after their stimulation by proinflammatory cytokines or bacterial lipopolysaccharides (LPS) [21], [22].

Additionally, lipid compounds represent another interesting class of mediators. Among them, the platelet-activating factor (PAF) is an ether-linked phospholipid produced by basophils, neutrophils monocytes and macrophages, responsible of platelet and neutrophils activation, increase of vascular permeability and smooth muscle contraction [11], [12]. As a matter of fact, the major lipid mediators playing a major role in regulating the inflammatory cascade are the metabolites of the arachidonic acid (AA), also known as eicosanoids (Figure 2). Cellular levels of AA are usually regulated by a multitude of enzymes, that keep it esterified unless some stimulation induces the mobilization by phospholipase A2 (PLA2). According to the stimulus and the type of cell involved, different pathways might be induced. In particular, the cyclooxygenase (COX) and the lipoxygenase (LOX) pathways are the most important in the inflammatory process [13], [23].

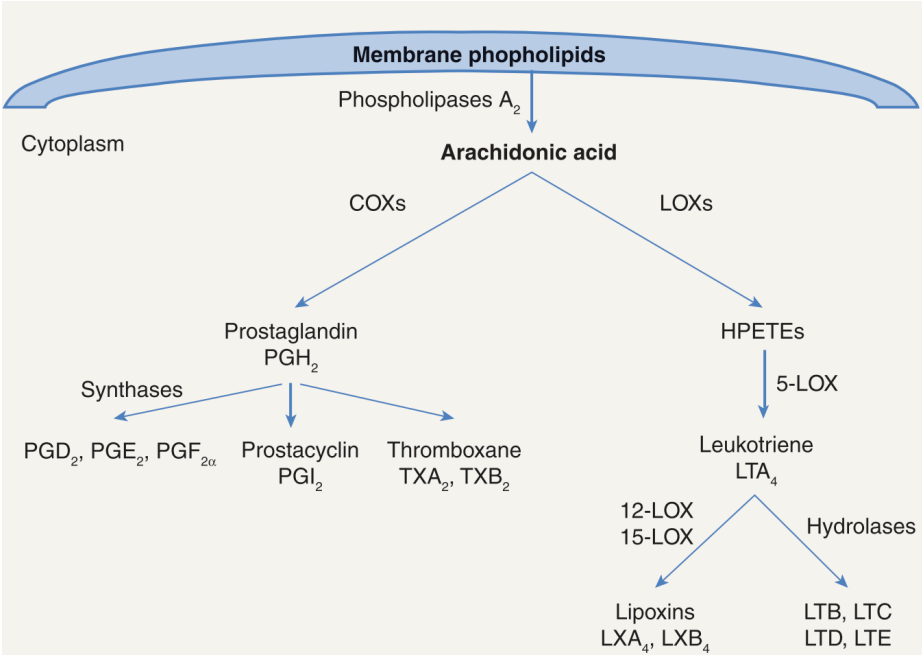

Figure 2. Schematic representation of the arachidonic acid metabolic pathway [24]. COX= cyclooxygenase, LOX= lipoxygenase, HPETE= hydroperoxyeicosatetraenoic acid.

Following the prostaglandin pathway, AA is metabolized by most cells in our body to an intermediate prostaglandin PGH2, by prostaglandin H synthase (PGHS; also known as COX). There are at least two isoforms of COX: basal and constitutive prostaglandin synthesis might be attributed to COX-1, whereas COX-2 is induced in inflammatory conditions [25]. Moreover, COX-3 is a splice variant of COX-1 that has been identified with a higher expression in microvessels of the brain and heart [26], [27]. PGH2 is then converted into several active molecules by enzymatically-catalysed reactions. Particularly, prostaglandin synthase leads to the production of PGD2, PGE2, PGA2 and PGF2α, whereas prostacyclin synthase generates PGI2, and thromboxane synthase of TXA2 and TXB2. These mediators act producing sensations of pruritus and pain, fever, increased vascular permeability, modulation of platelet aggregation and degranulation and smooth muscle contraction [12], [16], [28].

As concerns the lipoxygenase pathway, leukotrienes are produced preponderantly in inflammatory cells like polymorphonuclear leukocytes, macrophages, and mast cells. AA is transformed by 5-lipoxygenase (5-LOX) to the epoxide LTA4 in a multi-step reaction. LTA4 transformation can then undergo through different mechanisms (hydrolysis, conjugation with glutathione, or transcellular metabolism) to generate active eicosanoids (LTB4, LTC4,

LTD4 and LTE4) or lipoxins (LXA4, LXB4). These molecules have a wide spectrum of biological effects: from pro-inflammatory activity of the leukotrienes, to the anti-inflammatory action of the lipoxins [25], [29], [30].

2 Anti-inflammatory drugs

The use of extracts of salicylate-containing plants, for the treatment of fever, pain and inflammatory conditions, represents the origin of anti-inflammatory analgesic drugs. In the early 19th century, the active salicylate components were isolated and in the mid-late 19th century, salicylic and acetylsalicylic acids were synthesized for the first time in Europe. The latter has then been commercialised by Bayer AG as Aspirin™ over 100 years ago [31]. Soon after, other drugs having similar actions to aspirin were discovered.

2.1 Non-steroidal anti-inflammatory drugs (NSAIDs)

Aspirin can be recognised as the progenitor of what are known as the non-steroidal anti-inflammatory drugs (NSAIDs), followed by phenylbutazone in 1946 (by JR Geigy, Basel, Switzerland) and indomethacin in the 1960's (by Merck & Co, Rahway, NJ, USA). In the 1960's, Ibuprofen was the second NSAID approved as over-the-counter or OTC NSAID (other than aspirin). After its discovery and commercialisation, several pharmaceutical companies implemented the development of NSAIDs with a variety of chemical and biological properties [32]. Nowadays, diclofenac and ibuprofen are the most widely used NSAIDs, with ibuprofen-based NSAIDs representing the most typical OTC NSAID used on an as-needed basis [33].

NSAIDs act via inhibition of prostanoid biosynthesis, through their activity on the COX enzymes: COX-1 and COX-2. As already mentioned, the two isoforms undertake different functions and evidence suggests that the therapeutic effects of NSAIDs largely result from COX-2 inhibition at inflammation sites, whereas side effects - particularly gastrointestinal side effects - are mostly due to the inhibition of COX-1 [34].

Different criteria can be used to classify NSAIDs, such as chemical classes, pharmacological properties, and COX selectivity. As concerns their structure, they are generally chemically similar and behave as moderately lipid-soluble weak acids. Selectivity of the NSAIDs is determined by their affinity as inhibitor of COX-1 and COX-2, ranging from (i) weak inhibitors of COX-1 and COX-2, (ii) poorly selective full inhibitors of both isoforms, (iii) preferential selectivity towards COX-2, and (iv) exceptional selectivity towards COX-2 [35].

The latter, also called COXIBs, provide the same pharmacological effects and reduced or absent gastrointestinal toxicity due to diminished or none inhibition of COX-1. Nevertheless, evidence suggests a significantly increased risk of cardiovascular side effects most probably due to the inhibition of COX-2 dependent PGI2 [36].

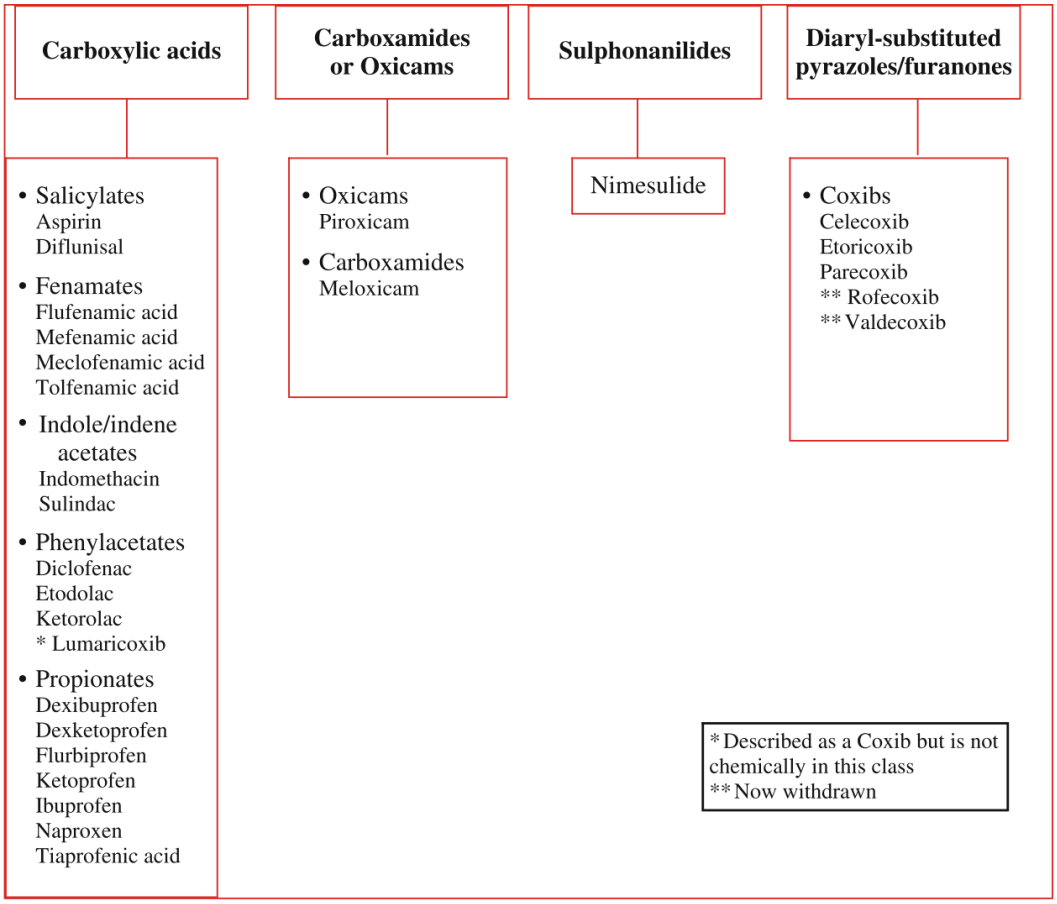

Figure 3. Chemical Classification of the NSAIDs [32].

2.2 Corticosteroids

Another important drug class at the forefront for its anti-inflammatory and immunomodulatory activity is represented by corticosteroids. First discovered in 1940s, this class include a wide variety of compounds whose effects can generally be divided into two major categories: glucocorticoids, which play their effect on metabolism and inflammation, and mineralocorticoids, known as sodium and water levels regulators. Both activities might be provided by the same compound, and therefore glucocorticoids are carefully chosen for the intended treatment [37].

The anti-inflammatory properties of steroids have been attributed to three independent mechanisms: the induction of lipocortin-I, the induction of MAPK phosphatase 1, and the repression of transcription factors. Lipocortin-I interacts with and inhibits PLA2, preventing the release of AA and the production of eicosanoids. As concerns the glucocorticoid-induced MAPK phosphatase 1, it dephosphorylates and inactivates several kinases and enzymes involved in the diffusion of the signalling cascade. Moreover, these molecules act by blocking several transcription factors (AP-1 and NF-κB) that control the production of inflammatory mediators (IL-1, TNF-α, IL-2, IL-5, IFN-γ, I-CAM, V-CAM, E-selectin), and, most importantly, COX-2 synthesis [38].

Corticosteroids are ideal anti-inflammatory drugs, mostly used in case of sepsis or persistent inflammation conditions due to allergies, asthma or autoimmune diseases [39], [40]. However, their wide range spectrum activity might lead to plural side effects when used as chronic therapy in high doses: abnormalities of fat distribution, loss of muscle mass, osteoporosis, skin changes, cardiovascular complications, immunodeficiency, electrolyte imbalance, stimulation of appetite and consequent obesity [41].

2.3 New therapeutic approaches

In the last decades, new revolutionary drugs have emerged for the treatment of complex inflammatory status, such as autoimmune diseases. As mentioned above, a sophisticated and interconnected system of chemical mediators are involved in the recruitment and activation of inflammatory and immune cells.

Among the others, cytokines have been studied as therapeutic targets to control and ameliorate the progress of sever diseases (rheumatoid arthritis, psoriasis, osteoarthritis, inflammatory bowel disease, etc.). Most of the developed and already licensed drugs involve the cytokines TNFa, IL-6, and IL-1 [42]. Nevertheless, new approaches concerning different mechanisms and mediators are under study, such as the NF-κB, P38 and STAT1 pathways [43]–[45].

3 Methods to improve the delivery of poorly aqueous soluble drugs

NSAIDs and corticosteroids are the first line therapy for the management and treatment of inflammation and to get relief from pain. Although, a large part of these drugs is poorly-water soluble, leading to reduced bioavailability and thus compromised therapeutic activity. The poor solubility is also a rate-limiting step in the absorption of locally administered drugs, bringing about a significant impediment in the rapid onset of action [46]. The different procedures to improve the aqueous solubility of anti-inflammatory compounds and to obtain desired therapeutic efficacy can exploit both chemical and physical modifications. The most used and known methods include prodrug design, pH modifications, formation of salts, micronization, use of surfactants and co-solvents, modification of the solid state, etc. [47], [48].

Furthermore, in the last decades there has been an ever-growing attention in new technological approaches to overcome these limits [49]. In the first place, reduction of the size and production of nanocrystals suspension represent one of the simplest but more successful techniques [50], [51]. In the second place, lipid-based systems such as liposomes, solid lipid nanoparticles, nanoemulsions and self-emulsifying systems are often used as drug delivery systems [52]–[55]. Lastly, use of polymers might lead to the production of not only drug delivery systems such as polymeric nanoparticles and microneedle arrays, but also more complex structures like polymeric nanofibers, which might act as drug nanocarriers and tissue scaffolds [56]–[58].

3.1 Nanosuspensions

Micronization has been widely applied for many years as a conventional method to formulate poorly soluble drugs. Through the jet milling or the colloid milling process, coarse drug powders are micronized to ultrafine powders, with an average drug crystal diameter of 2-5 µm. The resulting increased surface area enhances the dissolution velocity, as described by the Noyes–Whitney equation [59], [60]. Nonetheless, compound characterised by a very poor saturation solubility, e.g. below the mg/mL level, micronization is not a satisfactory technique to obtain a high bioavailability. Thus, the subsequent phase is the nanosizing

approach and in the 1990s, the production of nanocrystals became a new drug production technology. Nanocrystals are carrier-free nanoparticles of pure drug with a minimum of stabilizer (surfactants or polymers), characterized by an average diameter of 200-500 nm. They can be formulated as colloidal nanosuspension in water or non-water media, and the presence of the stabilizer is desired to avoid the particles to agglomerate and to ensure a stable system [50], [61].

According to the Prandtl equation, the nanosizing process increases the dissolution velocity not only through the increased particle surface area, but also by the reduction of the diffusion layer thickness [62]. Moreover, nanocrystals might achieve higher bioavailability owing to the increased saturation solubility, not observed for the microparticles [63]. Nanocrystals might further be formulated as tablets, pellets, capsules, or be injected parenterally, due to the adequate small diameter and safe composition.

Nanosizing methods can be divided into the bottom-up, in which the nanocrystals can be formed from the molecules, and the top-down methods, where the coarse powder is disintegrated to form the nanocrystals [59]. Additionally, a combination of the two techniques might be used.

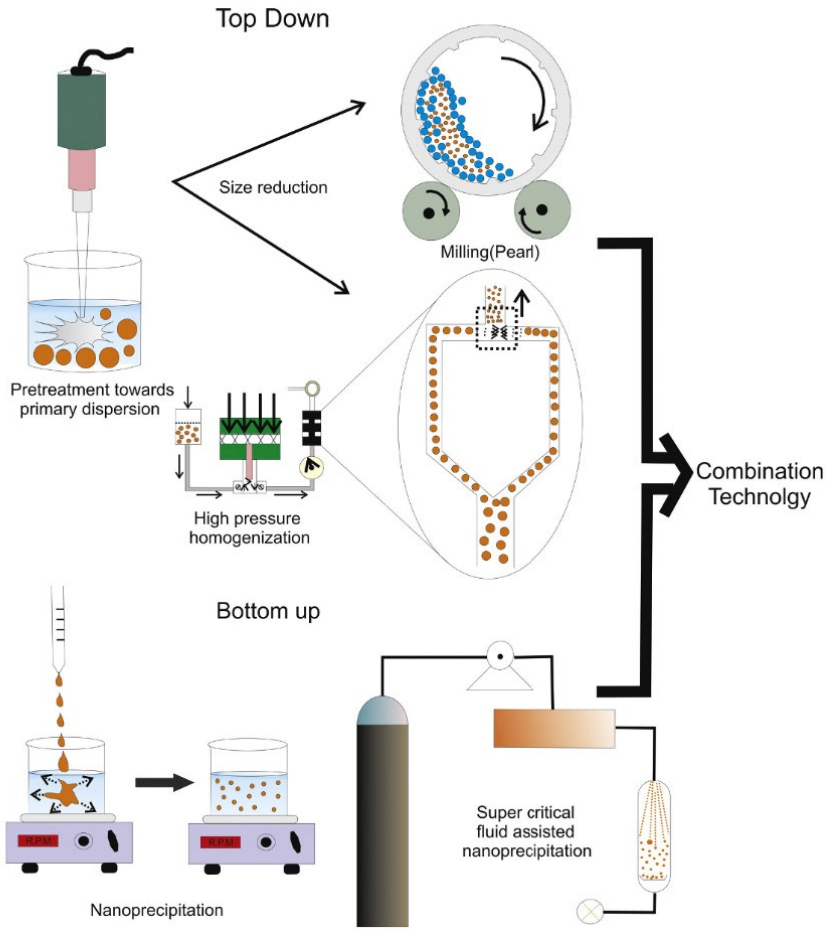

Figure 4. Nanocrystals production methods [64]

In the bottom-up methods, also called nanoprecipitation, the low water-soluble drugs are molecularly dissolved in a solvent (usually organic solvent) to form a supersaturated solution. The variation in the solubility of the drug, induced by reduction of temperature, evaporation of the solvent or by mixing it with an antisolvent (usually water), results in nucleation and precipitation in the form of nanocrystals. In the antisolvent technique, the antisolvent is usually an aqueous solution with a stabilizer, to avoid aggregation phenomena and microparticle formation [65].

The top-down process is based on particle size reduction from micro-range to nanometer-range through different wet milling techniques, such as ball media milling, microfluidization and high-pressure homogenization. In the early 1990s, the first wet media-based milling to obtain nanoparticles was certified with the trade name NanoCrystal® by the company Elan Pharma lnternational Ltd. Since then, the wet ball media milling (WBM) has been applied as reference technique in the production of pharmaceutical nanosuspensions [50]. The media milling beads are mixed in a becker or a roller plate or a mixer with a coarse aqueous suspension of the drug containing the stabilizer (polymer or surfactant). A combination of cleavage, abrasion and fractures, due to continuous powerful collisions between the beads and the drug particles, result in the reduction of the drug crystals size in the nanometer range [66]. This approach does not make use of aggressive solvents and is considered as the most versatile top-down process, appropriate for all poor soluble drugs and drugs insoluble in any solvent ("brick dust drugs") [50], [67].

3.2 Liposomes

Since the 1960s, several colloidal systems have been investigated for drug delivery and biomedical applications, such as vesicles, microemulsions, and lipid nanoparticles. Among them, liposomes are spherical vesicles of phospholipid bilayers with an interior aqueous core. First prepared by A.D. Bangham in the early 1960s, they can encapsulate molecules with different physicochemical properties. In particular, hydrophilic ingredients can be dissolved in the aqueous core, while lipophilic ingredients can incorporated into the lipid bilayers [48], [68]. They can be classified into several types according to their size and number of lamellae: large unilamellar vesicles (LUVs) with a size > 100 nm, small unilamellar vesicles (SUVs) with a size ranging from 20 nm to 100 nm, and multilamellar vesicles (MLVs) with a size > 0.5 µm [69], [70].

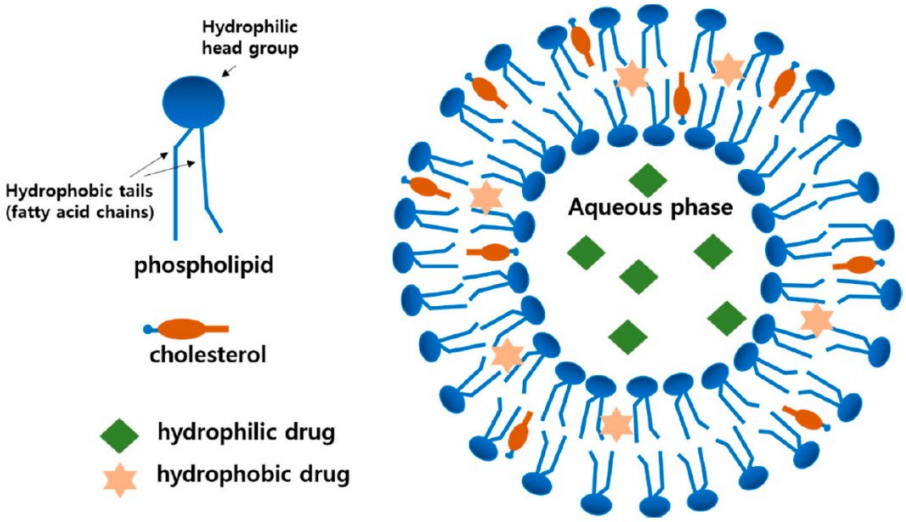

Figure 5. Structure of a conventional liposome [71].

Liposomes have been recognized as new drug delivery systems suitable for transporting drug molecules with several advantages. In fact, they provide active ingredient protection, modified pharmacokinetic and distribution, superior drug transport to target sites, and prolonged or controlled drug release. Moreover, due to their composition, they exhibit high biocompatibility, low toxicity and biodegradability [72].

Even though they can be prepared using different methods, the most used one is film hydration that was developed in 1965. This procedure is usually followed by sonication or extrusion, in order to reduce particle size and to obtain SUVs. Other techniques include reversed phase evaporation, solvent injection, dual asymmetric centrifugation, supercritical fluid [49], [73]. Most recently, direct sonication and microfluidic have gained a growing attention due to their production efficiency [74], [75].

Since their initial discovery, study and exploration in the field of vesicular carriers have considerably expanded. The classic composition of liposomes has evolved with the introduction of new additives. In 1992, highly deformable and elastic liposomes were for the first time created by Cevc and Blume (Transfersomes®). They can be classified as phospholipid-based vesicles with an additional component, usually a single-chain surfactant, named “edge activator” (EA). The EA – sodium cholate, sodium deoxycholate, or one of the Tween/Span series – makes the system more elastic and deformable with his large radius

chain curvature. Transfersomes are mostly studied for transdermal drug delivery, and the lipid film hydration method is usually the most used technique [52], [76].

In 2000, the introduction of high concentrations of ethanol (20-50%) into the phospholipid vesicle led to the formation of ethosomes. In contrast with the common thought that high amounts of alcohol might destroy the membrane structure, the integrity of the vesicles, their high stability up to one year of storage and the high encapsulation efficiency of actives with different physicochemical properties were demonstrated [72], [77].

As far as the vesicles stability is concerned, proliposomes have been investigated as an efficient alternative for drug delivery. In fact, the storage of aqueous liposomal dispersions might reveal product instability, which can be overcome by the transformation of the formulation into a dry product. Proliposomes can be described as dry powders able to form MLVs after hydration with water. Different techniques can be used to produce them: lipid film deposition method, lipid-drug matrix method, supercritical anti-solvent method, spray-drying and lyophilization. Hydration with water immediately before use, or in vivo contact with physiological fluids, leads to the formation of liposomes with similar characteristics and uniform vesicle size than the conventional liposomes [78], [79].

3.3 Nanofibers

Nanofibers are polymeric nanostructured delivery systems, with several extraordinary properties. They consist of solid fibers with nanoscale diameter, high surface-to-volume ratio, porous structure, theoretically unlimited length and enhanced mechanical properties [80]. The increasing interest in pharmaceuticals and biomedicine is due to the possibility of combining the drug delivery activity with the ability to mimic biological microenvironments, support damaged tissues and stimulate tissue regeneration [81], [82]. As far as the structure is concerned, nanofibers can be classified as monolithic, core-shell and hollow fibers. The active ingredients can be incorporated into nanofibers in amorphous or crystalline form, or attached to its surface [83].

Nanofibers can be obtained using different methods such as melt blowing, phase separation, self-assembly, template melt extrusion, template synthesis, drawing, electrospinning, interfacial polymerization, and force-spinning [83], [84]. Electrospinning is the most

frequently used technique due to its versatility and simplicity [85]. Among its advantages, the possibility to control the morphology and load different therapeutics agents (e.g. drugs, proteins, DNA, growth factors) are the most remarkable [86]–[89].

The electrospinning technique leads to the production of nanofibers through the use of a high voltage. Few essential elements are needed: a syringe fitted with a metal nozzle, a high voltage supply and a collector. The syringe is filled with the polymer solution and mounted on a pump, which provides a constant flow rate. A high voltage is applied at the tip of the capillary of the nozzle, resulting in an electric field which determines the formation of a conical shape, known as Taylor cone, from the pendant hemispherical polymer drop. When the electrical field reaches a critical value, at which the repulsive electrostatic force overcomes the surface tension of the liquid, a jet is ejected from the cone tip. The jet is exposed to bending instabilities and continuously lengthened and stretched towards the collector. Simultaneously, the solvent evaporates resulting in solid nanofibers deposited on the collector [90], [91].

Even though electrospinning seems to be very simple in terms of equipment and gives the impression of an easily controlled procedure, it is an extremely complex technique due to the different physics governing the process. The different parameters affecting the final outcome can be classified into three main categories: solution, ambient, and process parameters. The morphology of the obtained nanofibers is not only influenced by each parameter, but also by the interconnectivity among them [83], [92].

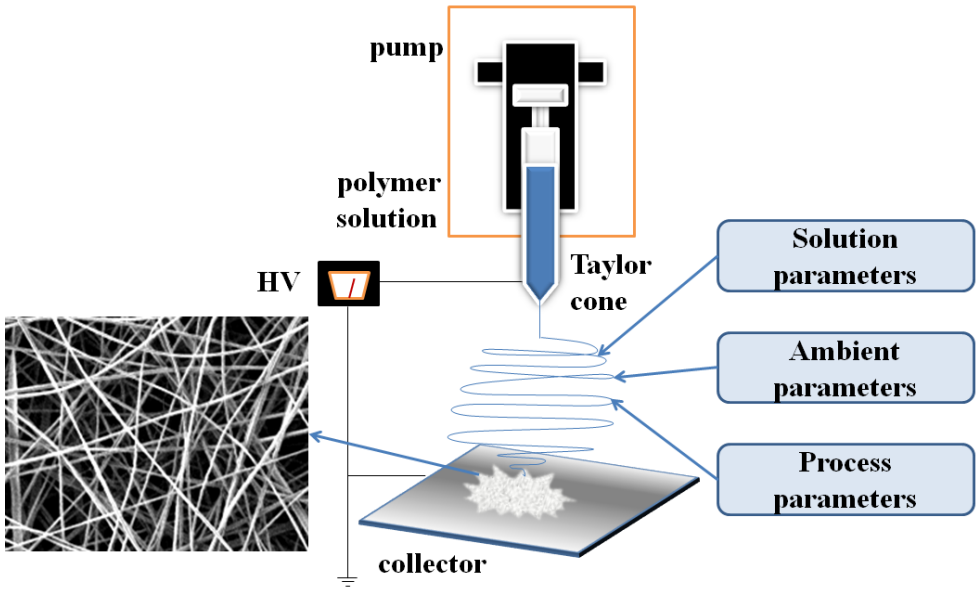

Figure 6. Schematic representation of the electrospinning setup and the parameters affecting the process.

The solution parameters are determined by the choice of the solvent and the polymer characteristics and concentration, and affect some physics properties such as surface tension, viscosity and conductivity [83], [93]. Process parameters, such as flow rate and applied voltage, are often interconnected with the polymer solution properties. Higher voltage is required when the solution has a low conductivity, high surface tension and/or high viscosity. Moreover, flow rate and applied voltage should accurately be monitored in relation with the volatility of the solvent [94]–[96]. Temperature and relative humidity (RH) represent two important ambient parameters affecting the morphology of the final product, whose effects depend also on the properties of the polymer used. Hydrophobic polymers dissolved in organic solvents determine the formation of porous nanofibers in case of high values of RH. With aqueous polymer solutions, nanofibers morphology and properties are determined by proper values of RH. Low RH values result in rapid solvent evaporation, resulting in thicker nanofibers. With high RH values, the velocity of the evaporation is decreased, resulting in thinner nanofibers and gradually, in the formation of bead-on-a-string morphology and a deposition of a wet polymer film [92].

Aim

Nanotechnology is a growing science undergoing outstanding development in various areas of medicine. In the pharmaceutical field, it is widely used to overcome drug delivery and bioavailability issues and to improve efficacy, safety and patient compliance. The choice and composition of nano-based drug delivery systems is critical to guarantee high therapeutic performances. Applications of nanotechnology are widespread in the diagnosis and treatment of inflammatory diseases.

Therefore, the aim of this thesis was to use nanotechnology to achieve:

i. improved delivery of poorly water-soluble drugs,
ii. co-delivery of more drugs for combination therapy,
iii. local delivery of drugs in a cell- or tissue-specific manner through the combination of different nanotechnological approaches.

To reach this purpose, different strategies were exploited. In Part 1, the production of nanocrystal suspensions through a wet ball media milling technique was used to improve the poor water solubility of anti-inflammatory drugs. In Chapter 1, the ability of an electronic cigarette to deliver the obtained nanosuspension and its possible application as an alternative inhalation medical device were then investigated. Whereas in Chapter 2, a multicomponent formulation with a corticosteroid and a natural adjuvant compound was developed, and studied for inhalation therapy. In Part 2 of the thesis, liposomes production through direct sonication method and polymeric nanofibers through a green electrospinning approach were investigated. A combination of the two nanotechnology techniques was used to produce a liposomes-nanofibrous composite scaffold for wound healing.

Part 1: Nanosuspension formulation for inhalation drug delivery

Chapter 1: Electronic cigarette as an alternative delivery system of a beclomethasone dipropionate nanosuspension

The majority of this chapter has been directly copied or modified from *International Journal of Pharmaceutics* ***2021****, 596; https://doi.org/10.1016/j.ijpharm.2021.120293* "Delivery of beclomethasone dipropionate nanosuspensions with an electronic cigarette" by **Casula, L.**, Sinico, C., Valenti, D., Pini, E., Pireddu, R., Schlich, M., Lai, F., Fadda, A.M.

1 Introduction

Electronic nicotine delivery systems (ENDS) – commonly called electronic cigarettes, or E-cigarettes – are marketed as aerosol producing devices for the delivery of tobacco-free nicotine, usually in propylene glycol or glycerine solutions. The main components are an aerosol generator with a heating element ('atomiser'), a liquid storage area ('cartridge'), a flow sensor (in some devices), and a re-chargeable battery. Atomizer and cartridge are often combined together to form a 'cartomizer'[97]. Since e-cigarettes were developed with the aim of mimicking the action of smoking, their design and the vapour production remind of traditional cigarettes. In order to activate the heating element, the button placed on the surface of the atomiser has to be pressed. The aerosol is then produced from the liquid in the cartridge (e-liquid) and delivered upon inhalation. The E-liquid can be easily refilled after consumption, and its composition can slightly differ on the propylene glycol-glycerine ratio. [98].

Since tobacco smoke or combustion are not involved, e-cigarettes appear to be safer than conventional cigarettes. However, various toxic and carcinogenic substances have been found in ENDS vapours and components [99]. In particular, metal and silicate particles – including nanoparticles – have been found in cartomizer fluid and aerosol produced by some e-cigarettes made of low-quality materials. Diameter of these nanoparticles was in the range of 10-1000 nm, showing the ability of the e-cigarette aerosol to deliver nanosized material [100]. Nevertheless, the level of carcinogen biomarkers and toxicants has been proven to be lower when switching from conventional cigarette to e-cigarette [101]–[103].

The Tobacco Products Directive 2014/40/EU (TPD) introduced new rules for nicotine-containing electronic cigarettes and became applicable in EU countries in May 2016. However, the TDP does not apply to those e-cigarettes and refill liquids that are authorised as medicines, including nicotine-free vaping devices [104]. In fact, there has been an increasing interest in the scientific community in the alternative applications of ENDS to deliver different substances. At first, illegal drug vaping has been widely reported [105], [106]. Afterwards, various studies focused on cannabis delivery – cannavaping – have been carried out [107]–[110]. These studies highlighted the versatility of this device and its possible use for therapeutic purposes. Purchez et al. studied the ability of a high-power ENDS to deliver bronchodilators for pulmonary disease treatment. Their results showed the capacity of the device to generate submicron carrier-droplets containing drug molecules dissolved in the e-liquid [111]. In all these studies, the delivered drugs are soluble in the e-liquid. However, most of the newly developed drugs are poorly hydrosoluble and their bioavailability is limited by their slow dissolution rate. Therefore, their formulation is still challenging, and research has been testing several new approaches and alternative administration routes. Drug nanonization or the use of nanocarriers have already shown their potential in improving bioavailability of drugs classified in class II and class IV of the Biopharmaceutics Classification System (BCS), whose principles can partly be transposed on pulmonary-delivered drugs, taking into consideration the effect of the complex physiology of the respiratory system [112], [113]. Therefore, it is worthy of investigation the capability of ENDS to deliver nanoparticles, i.e., both drug nanocrystals and drug loaded nanocarriers. Nanocrystals are nanoparticles of pure drug without any matrix material with an average diameter below 1 µm (typically in the range of 200-500 nm). The drug nanocrystals can be suspended in an outer liquid phase, usually composed of water and/or water-miscible solvents and stabilized using an ionic or non-ionic surfactant or polymers, to obtain a nanosuspension. The reduction of the drug crystal mean diameter below 1 µm dramatically increases the particle surface area and decreases the diffusion layer thickness if compared to coarse and micronized drug, as described by the Prandtl equation, thus, speeding up the dissolution rate [62]. In addition, nanocrystals are characterized by an enhanced saturation solubility, according to the Freundlich– Ostwald equation [63]. Moreover, nanosuspensions have shown to be suitable to formulate poorly soluble drugs for lung delivery and to have

superior pharmacokinetics properties when compared to solutions or coarse suspensions of the same drug [114]–[119].

Since the presence of metal and silicate (nano)particles in the aerosol produced by e-cigarettes has been demonstrated, the aim of the present work was to investigate the ability of the ENDS-aerosol to deliver nanocrystals of poorly water-soluble drugs. Beclomethasone dipropionate (BDP) was chosen as a model drug for its well-known effect on the treatment of asthma and chronic obstructive pulmonary disease (COPD) [120]–[122].

BDP nanosuspensions were prepared by a top down - media milling method. Characterization of the nanosuspensions was carried out via different techniques: Dynamic Light Scattering (DLS), transmission electron microscopy (TEM), differential scanning calorimetry (DSC), X-ray powder diffractometry (XRPD) and Fourier transform infrared (FTIR) spectroscopy. In addition, solubility studies and vaping tests were performed.

2 Materials and Methods

2.1 Materials

Beclomethasone dipropionate and Kolliphor P188 (Poloxamer 188, P188) were obtained from Sigma Aldrich (Italy). Vegetable glycerol and propylene glycol were purchased from Galeno srl (Italy). All the other products were of analytical grade.

2.2 Preparation of BDP nanosuspension

The nanosuspensions were prepared using a wet ball media milling technique. BDP was dispersed in a Poloxamer 188 (P188) water solution using an Ultra Turrax T25 basic for 6 min at 8000 rpm. Nanosuspensions were prepared using a 2:1 (w/w) BDP:P188 ratio. This coarse suspension was divided in 1.5 ml conical microtubes containing about 0.4 g of 0.1-0.2 mm yttrium-stabilized zirconia-silica beads (Silibeads® Typ ZY Sigmund Lindner, Germany). The microtubes were oscillated at 3000 rpm for 150 minutes using a beads-milling cell disruptor equipment (Disruptor Genie®, Scientific Industries, USA). The obtained nanosuspensions of each microtubes were gathered and then separated from the milling beads by sieving. In the preliminary studies, the nanosuspensions were prepared directly in the conical microtubes, without any preliminary homogenisation with the Ultra Turrax, in order to evaluate the optimum milling time. The formulation had a final concentration of 1% BDP and 0.5% P188.

2.3 Particle size analysis

Average diameter and polydispersity index (PDI, as a measure of the size distribution width) of the samples were determined by Dynamic Light Scattering (DLS) using a Zetasizer nano (Malvern Instrument, Worcestershire, United Kingdom). Samples were backscattered by a helium–neon laser (633 nm) at an angle of 173° and a constant temperature of 25°C. Zeta potential was estimated using the Zetasizer nano by means of the M3-PALS (Phase Analysis Light Scattering) technique. Just before the analysis, nanosuspensions were diluted with distilled water. Furthermore, a medium-term stability study of the BDP nanosuspension stored at room temperature was performed by monitoring average size, polydispersity index, and zeta potential for 30 days. The nanosuspensions were visually inspected before

every DLS measurement to check the absence of large precipitated aggregates or phase separation. All the measurements were made in triplicate.

2.4 Lyophilization of BDP nanosuspension

BDP nanosuspensions (1 mL samples) were frozen at -80 °C and then freeze dried for 24 h at -86 °C and 0 mmTorr, using an FDU-8606 Freeze Dryer (Operon Co, Korea).

2.5 Preparation of Poloxamer 188/BDP physical mixture

Drug physical mixtures were prepared by blending Poloxamer 188/BDP in an agata mortar until a homogeneous mixture was obtained. The same ratio of drug/surfactant (2:1, w/w) of the nanosuspension was used.

2.6 Solubility studies

BDP solubility in a home-made e-cigarette liquid (water:vegetable glycerol:propylene glycol=20:40:40 w/w) was measured for the BDP bulk, freeze dried BDP nanocrystals and the Poloxamer 188/BDP physical mixture. The formulations (n = 3) were kept under constant stirring for 48 h at room temperature. Samples were withdrawn and centrifuged at 12,000 rpm for 60 min; the supernatant was centrifuged again at 12,000 rpm for 60 min. Then, 0.2 ml of the clear supernatant were diluted with methanol and analysed by HPLC for BDP content.

2.7 HPLC analysis

Quantitative determination of BDP was performed by HPLC using a liquid chromatograph Alliance 2690 (Waters Corp, Milford, MA) equipped with a photodiode array detector and a computer integrating apparatus (Empower 3). Analyses were performed at 240 nm with a X-Select C18 column (3.5 µm, 4.6 mm × 100 mm, Waters). The mobile phase was a mixture of acetonitrile, water and acetic acid (68.45:31.5:0.05, v/v), delivered at a flow rate of 1 mL/min. Samples (10µL) were injected using an auto sampler. The stock standard solution of BDP was prepared by dissolving the drug in methanol and stored at 4 °C. A standard calibration curve (peak area of BDP vs. known drug concentration) was built up by using standard solutions prepared by dilution of the stock standard solution with the mobile

phase. Calibration graphs were plotted according to the linear regression analysis, which gave a correlation coefficient value (R2) of 0.999. The BDP retention time was 4.15 min. The limit of detection was 0.5 ng while the limit of quantification was 2 ng. Sample preparation and analyses were performed at room temperature.

2.8 Preparation of the e-vaping liquid.

Freeze-dried BDP nanocrystals were dispersed in 200 µL of water, vortexed and made up to 1 mL with a previously prepared solution of vegetable glycerol:propylene glycol (50:50 (w/w)). The final composition of the obtained e-liquid was water:vegetable glycerol:propylene glycol=20:40:40 (w/w). The same procedure was used in case of the vaping tests performed with BDP coarse powder, instead of freeze-dried BDP nanocrystals.

2.9 E-cigarette vaping test

The e-vaping liquid was loaded in the SMOK® QBOX (SmokTech, China) e-cigarette, equipped with a V8-Baby M2 0.25 Ω Dual Coil. The device was fully charged before every vaping test, and the battery level was never lower than 50% during the experiments. A syringe was connected to the atomizer through a plastic tube. The simultaneous activation of the e-cigarette and the retraction of the plunger led to the production of aerosol, which was gradually expelled in a vial immersed in an ice bath for the condensation of the aerosol. The aerosol production was carried out according to the following parameters: 60 mL syringe, 4.0 ± 0.3 seconds-puff, interpuff pause of 30 seconds. The obtained samples were analysed by TEM, DLS and HPLC.

2.10 Transmission electron microscopy

BDP coarse powder, freshly prepared nanosuspensions and condensed aerosol were analysed through transmission electron microscopy (TEM) in order to investigate the presence of crystals and their morphology. After depositing on carbon-coated copper grids (200 mesh), drug crystals were viewed using a JEOL JEM 1400 Plus (CeSAR, Centro Servizi d'Ateneo per la Ricerca, University of Cagliari), with an accelerating voltage of 120 kV in Bright-field mode.

2.11 X-ray powder diffractometry

BDP raw powder, P188 raw powder, physical mixture of P188 and BDP and freeze-dried BDP nanocrystals were investigated by X-ray Powder Diffraction (XRPD). The XRPD patterns were collected with a Rigaku MiniFlex diffractometer, operating at 30 kV and at 15 mA, using, the Cu Kα line at 1.54056 Å as radiation source. Each sample was analysed from 3 to 60 2θ, in steps of 0.02, using a scan step time of 2.00 seconds. The results were then obtained as peak height (intensity) versus 2θ.

2.12 Fourier transform infrared spectroscopy (FTIR)

FT-IR spectra of BDP raw powder, P188 raw powder, physical mixture of P188 and BDP and freeze-dried BDP nanocrystals were collected using the Spectrum One Perkin Elmer (MA, USA) FT-IR Spectrometer in the spectral region between 4000 and 600 cm-1, and analyzed by transmittance technique with 32 scans and 4 cm-1 resolution. Samples were mixed in a mortar with KBr (1:100) and pressed by a hydraulic press (10 tons) into small tablets.

3 Results and discussion

3.1 Preparation and characterization of BDP nanosuspension

BDP nanosuspension were successfully prepared through a wet media milling technique. P188 - chosen as stabilizer - is a non-ionic linear low toxic copolymer, which is used in many commercially available products [123]. The average diameter and PDI modifications as a function of milling time were preliminarily studied (Figure 1).

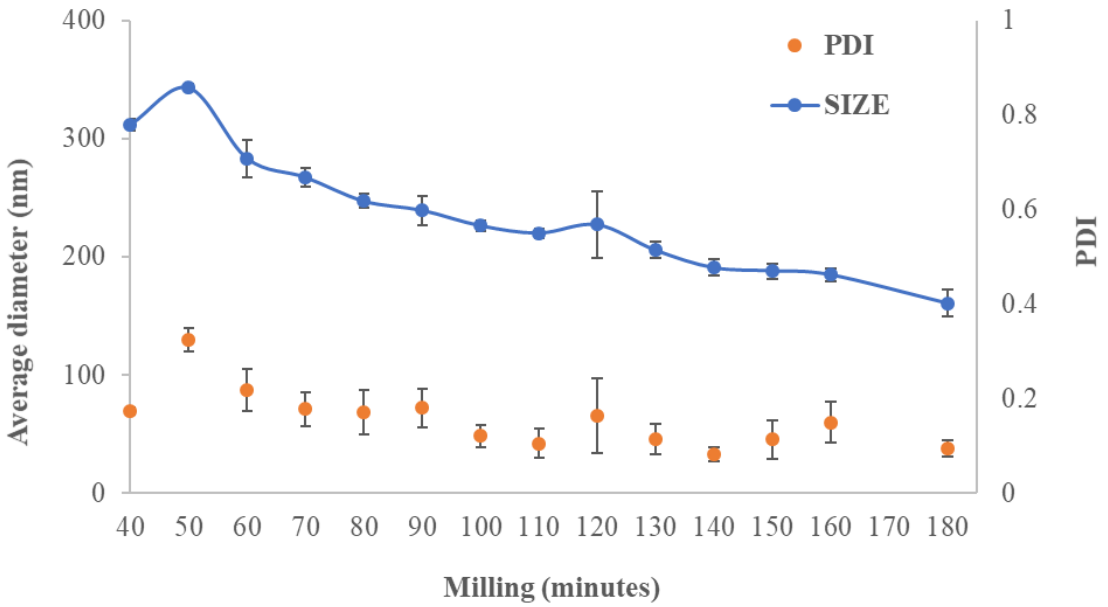

Figure 1. Milling process optimization of BDP nanosuspension as a function of minutes of milling, measured using DLS (average diameter and PDI, mean ± SD; n=3).

In the first 10 cycles (corresponding to 100 minutes of milling), a significant decrease of the mean particle size and PDI was observed. The particle sized reduction slowed down during the last cycles, leading to a final average diameter of approximately 161 nm and a PDI of 0.09 at 180 minutes of milling. In light of these results, we decided to prepare nanosuspensions using a preliminary homogenization with the Ultra Turrax, followed by 150 minutes of milling corresponding to 15 cycles. The composition and physico-chemical data relative to the lead formulation are presented in Table 1. The chosen protocol led to an average diameter of approximately 168 and a PDI of 0.09.

Table 1. Average diameter, polydispersity index (PDI) and Zeta potential of freshly prepared BDP nanosuspension.

Active ingredient	Stabilizer	Properties		
		Average diameter (nm)	PDI	Zeta potential (mV)
BDP 1% (w/w)	P188 0.5% (w/w)	168 ± 5	0.090 ±0.048	-25.65 ± 2.33

Average size, PDI and Zeta-potential were evaluated over a period of 30 days, for a medium-term stability study (Figure 2). As it can be seen in the graphs, an increase in size of ~30% was observed during the 30 days of storage. However, a low mean diameter (229 nm) and low PDI (0.261) were maintained, indicating a fairly narrow size distribution [124]. The zeta potential value was highly negative at the end of the stability test (-27.4 mV).

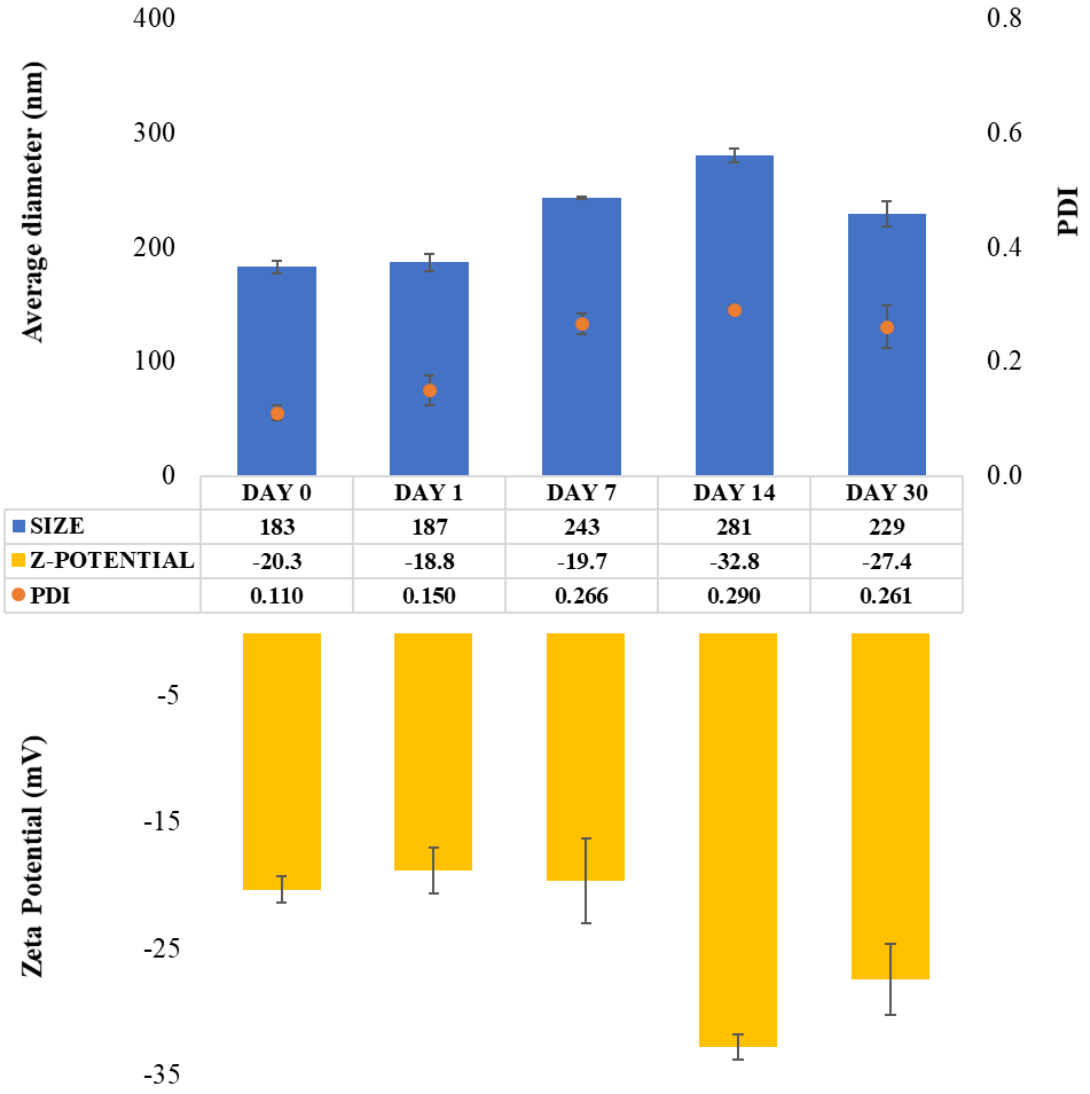

	DAY 0	DAY 1	DAY 7	DAY 14	DAY 30
SIZE	183	187	243	281	229
Z-POTENTIAL	-20.3	-18.8	-19.7	-32.8	-27.4
PDI	0.110	0.150	0.266	0.290	0.261

Figure 2. Average diameter (nm), Zeta Potential (mV) and polydispersity index (PDI) of BDP nanosuspension over 30 days of storage at room temperature. Values are presented as mean values ± standard deviation (n = 3).

The morphological changes of BDP crystals after the milling process were evaluated by TEM imaging (Figure 3).

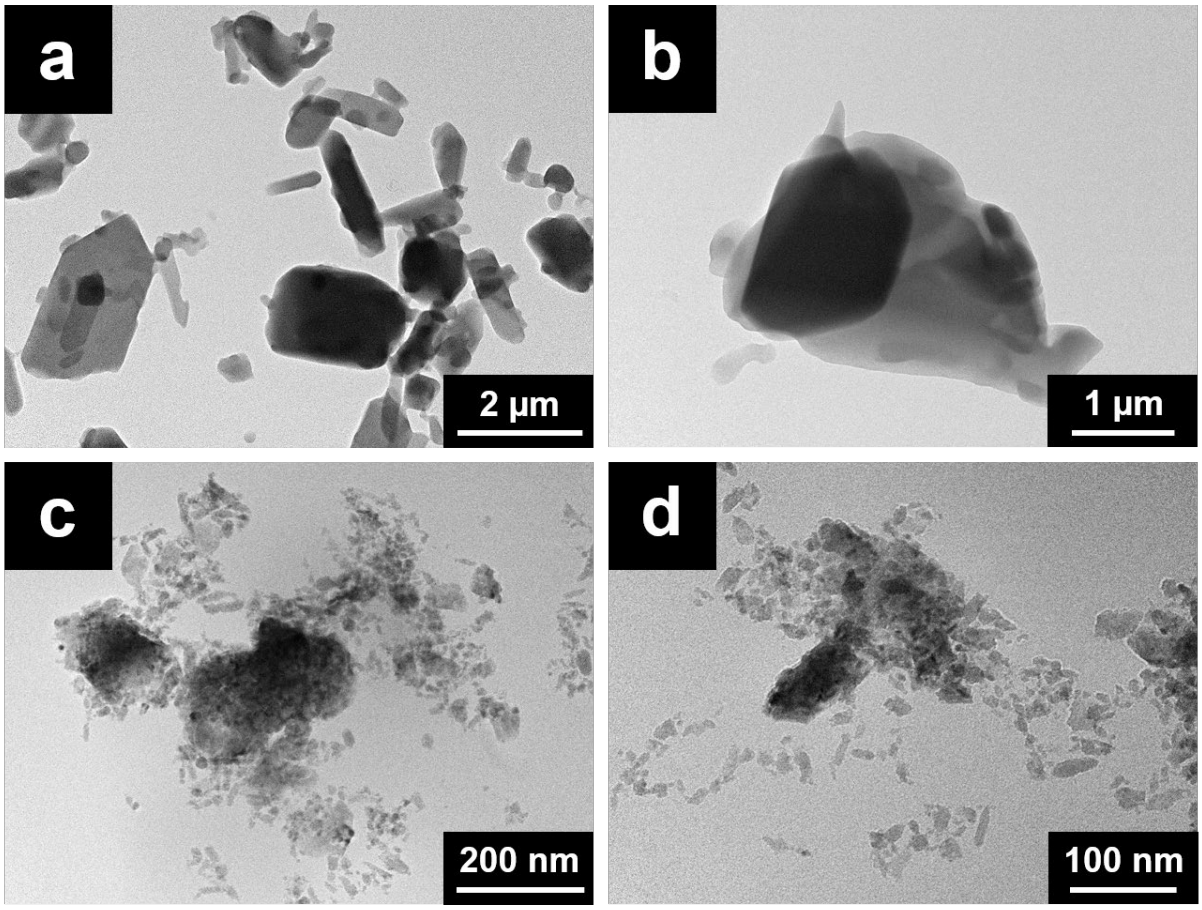

Figure 3. TEM micrographs of BDP raw powder (a-b) and BDP aqueous nanosuspension (c-d).

As can be seen in the TEM micrographs, the milling process modified both the shape and size of BDP crystals. In fact, the high shear forces generated during the process by the collision of the drug crystals and the milling beads – and of the drug crystals themselves – provide the appropriate energy to reduce their size below one micron. BDP nanocrystals (Figure 3c-d) presented a regular and elongated shape, with a homogenous particle size distribution, in accordance with DLS analysis.

As can be seen by the scale bar of the nanosuspension micrographs (Figure 3c-d), the nanocrystals diameter is lower than the value obtained by DLS analysis. This result is in accordance with the literature data [125]–[128], and can be explained by the ability of DLS to measure the hydrodynamic diameter of hydrated particles which is also influenced by all substances adsorbed on the surface of the nanocrystals (hydration layer, polymer shell or surfactants). Thus, it always results larger than the dry particle diameter obtained with TEM or SEM, that measure the geometrical size [129], [130].

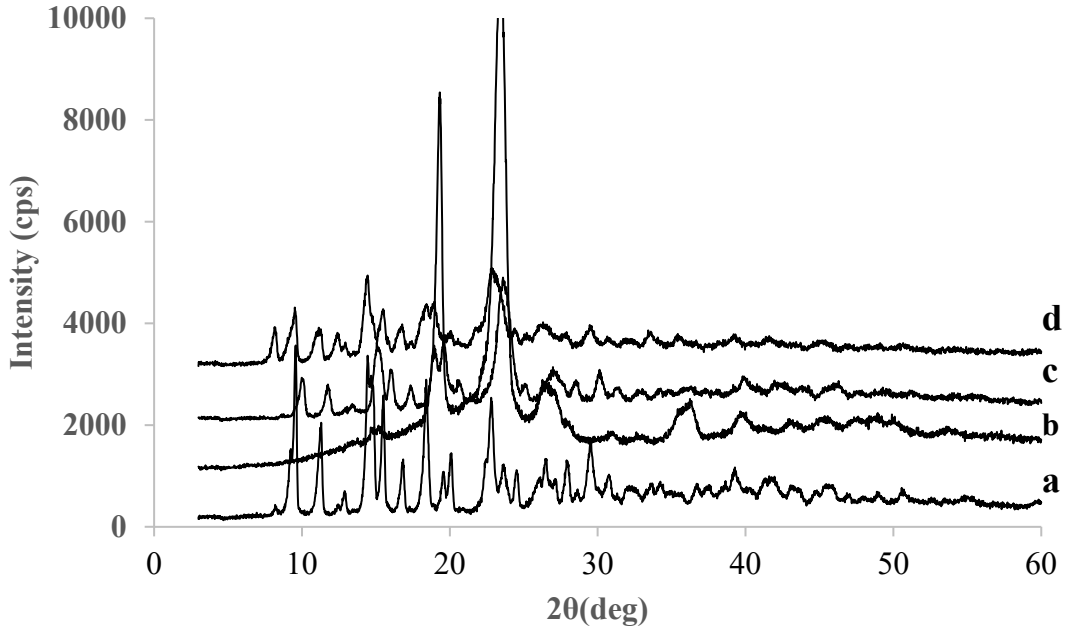

Figure 4 . XRPD analysis of BDP raw powder (a), P188 raw powder (b), physical mixture of P188 and BDP (c) and freeze-dried BDP nanocrystals (d).

XRPD analysis was used to assess the crystallinity of the samples. Commercial BDP showed a crystalline profile with a low intensity signal at 8.5 2ϑ (deg), absent in the physical mixture, which increased in the NS diffractogram confirming the BDP hydration. However, NS analysis evidenced the presence of the signal at 18.4 2θ (Figure 4d), characteristic of the anhydrous BDP [131], suggesting the presence of anhydrous and hydrated BDP in the formulation. Physical mixture and NS still maintained the crystalline profile.

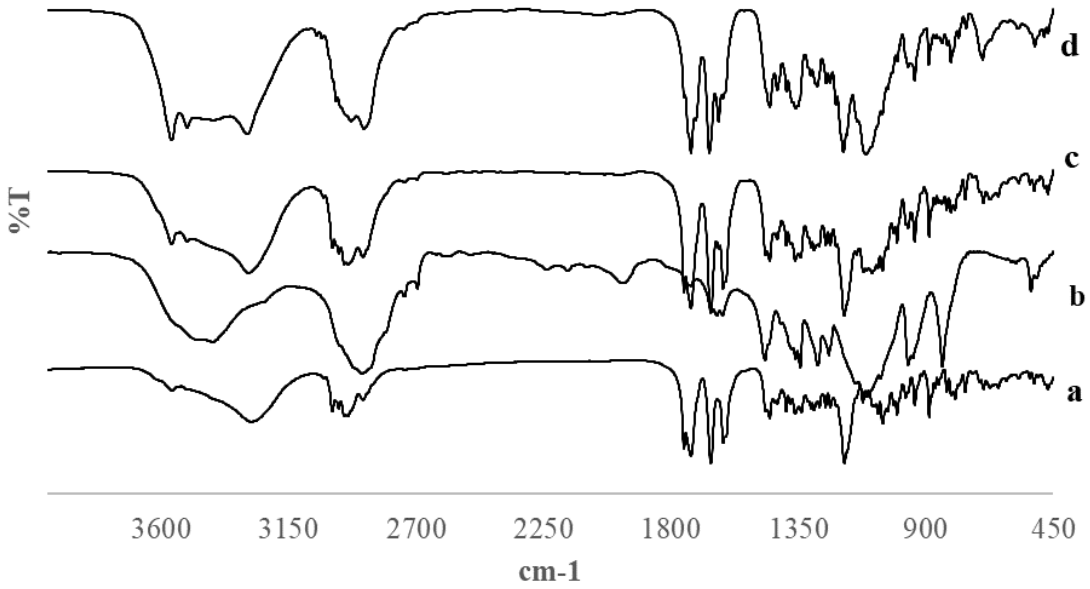

Figure 5. FT-IR analysis of BDP raw powder (a), P188 raw powder (b), physical mixture of P188 and BDP (c) and freeze-dried BDP nanocrystals (d).

The infrared spectrum (Figure 5) of commercial BDP shows the broad O-H stretching at 3562 cm^{-1}, the sharp peak of ester carbonyl group at 1754 cm^{-1}, at 1729 and 1659 cm^{-1} the bands of the conjugated and non-conjugated carbonyl groups, respectively, at 1615 cm^{-1} the carbon double bond stretching, and at 1187 cm^{-1} the C-O peak. The physical mixture spectrum contains the superimposed spectra of each component, in fact in addition to BDP bands, some typical P188 signals due to CH_2 bending (1466 cm^{-1}), in plane O-H bending (1343 cm^{-1}) and C-O stretchings (1112-1108 cm^{-1}) are recognizable. These results suggest that there are no interactions between them. However, the nanosuspension infrared spectrum evidenced the hydration of BDP. In fact, according with literature data for BDP solvates [132], NS spectrum exhibited a large decrease in intensity of BDP C=O (ester) band at 1753 cm^{-1}, the shift of the carbonyl bands at 1665 and 1631 cm^{-1}, and the appearance of a peak at 1712 cm^{-1} due to hydrogen bonding between the hydroxyl hydrogen of water and the carbonyl groups of the BDP moiety. Furthermore, peaks attributable to water hydroxyl groups appeared at 3562 and 3508 cm^{-1}.

The saturation solubility of the freeze-dried nanocrystals, the BDP bulk powder and the Poloxamer 188/BDP physical mixture was measured at 25°C in the home-made e-liquid

(water:glycerol:propylene glycol). The physical mixture was prepared maintaining the same surfactant:drug ratio (1:2, w:w).

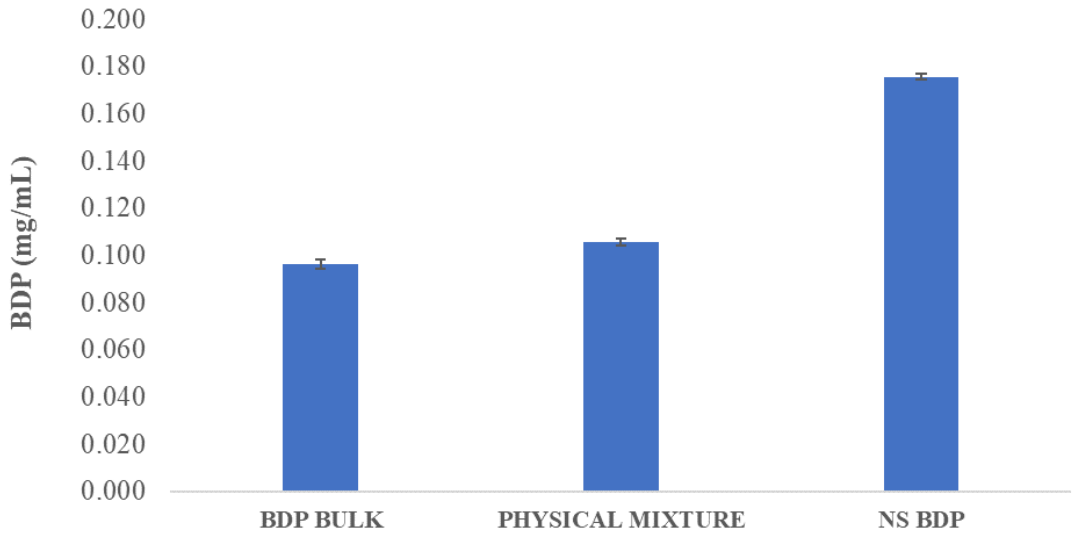

Figure 6. Saturation solubility (mg/mL) of the BDP bulk powder (BDP BULK), physical mixture of P188 and BDP (PHYSICAL MIXTURE) and freeze-dried BDP nanocrystals (NS BDP) in the e-liquid; (mean ± SD, n = 3).

As shown in the Figure 6, the solubility of BDP was found to be 96.33 ± 1.80 µg/mL for the bulk powder drug, which slightly increased to 105.73 ± 1.36 µg/mL with the addition of the surfactant P188 (physical mixture). However, the formation of nanocrystals led to an increase of approximately 80% of the bulk powder solubility, reaching a value of 175.67 ± 1.11 µg/mL. Therefore, these results are in accordance with the Freundlich-Ostwald equation and the drug solubility is enhanced not only by the action of the surfactant, but also by the nanosizing of the particles [63].

3.2 E-Cigarette vaping test

BDP nanosuspensions were frozen and then freeze-dried for 24 hours. The obtained nanocrystals were resuspended in the vehicle (water, glycerol and propylene glycol) to prepare the *nanosuspensions-containing E-liquid*, which was analysed through DLS and TEM, in order to verify if the properties of the nanocrystals had changed.

As shown in the Table 2, the average diameter of the nanocrystals slightly increased after lyophilization and dispersion in the vehicle. This can be correlated, not only to the different

nature of the vehicle – only water in the first case, water:glycerol:propylene glycol in the second one – but also to the lyophilization process itself, that might modify the morphology of the nanocrystals and promote nanocrystal aggregation. The *nanosuspensions-containing E-liquid* was then loaded in the SMOK® QBOX (SmokTech, China) e-cigarette and the vaping act was simulated. The analysis of the condensed vapour obtained by the test with DLS revealed the presence of nanoparticles – supposedly BDP nanocrystals – with an average diameter of 210 nm, a value comparable to the mean diameter of the freeze-dried nanocrystals dispersed in the vehicle (230 nm). However, the PDI value of the nanoparticles found in the condensed vapour (0.187) was smaller than that of the freeze-dried nanocrystals in the vehicle 0.234. This behaviour could be explained by the ability of the vapour to transport preferably the smallest nanocrystals, thus decreasing the width of the dimensional population (the PDI value). Furthermore, the high temperature reached in the E-cigarette might lead to a partial fusion of the BDP nanoparticles followed by a re-crystallisation in crystals with a smaller diameter.

Table 2. Average diameter, polydispersity index (PDI) of freshly prepared BDP nanosuspension, freeze-dried BDP nanocrystals dispersed in the E-cigarette liquid and BDP nanocrystals in the condensed aerosol of the vaping test; (n=3).

	Average diameter (nm)	PDI
Freshly prepared nanosuspensions	165 ± 4	0.125 ±0.037
Freeze-dried Nanocrystals dispersed in the E-liquid	231 ± 1	0.234 ±0.019
Nanocrystals in the condensed aerosol	211 ± 4	0.187 ±0.020

The *nanosuspensions-containing E-liquid* and the condensed aerosol of the vaping test were studied through TEM analysis. As shown in the micrographs, the morphology of the nanocrystals in the E-liquid (Figure 7a-b) slightly changed if compared to the starting nanosuspensions prepared in water (Figure 3c-d). Moreover, the presence of the

nanocrystals in the condensed vapours was revealed by the TEM images, confirming the ability of the E-cigarette to transport the nanoparticles.

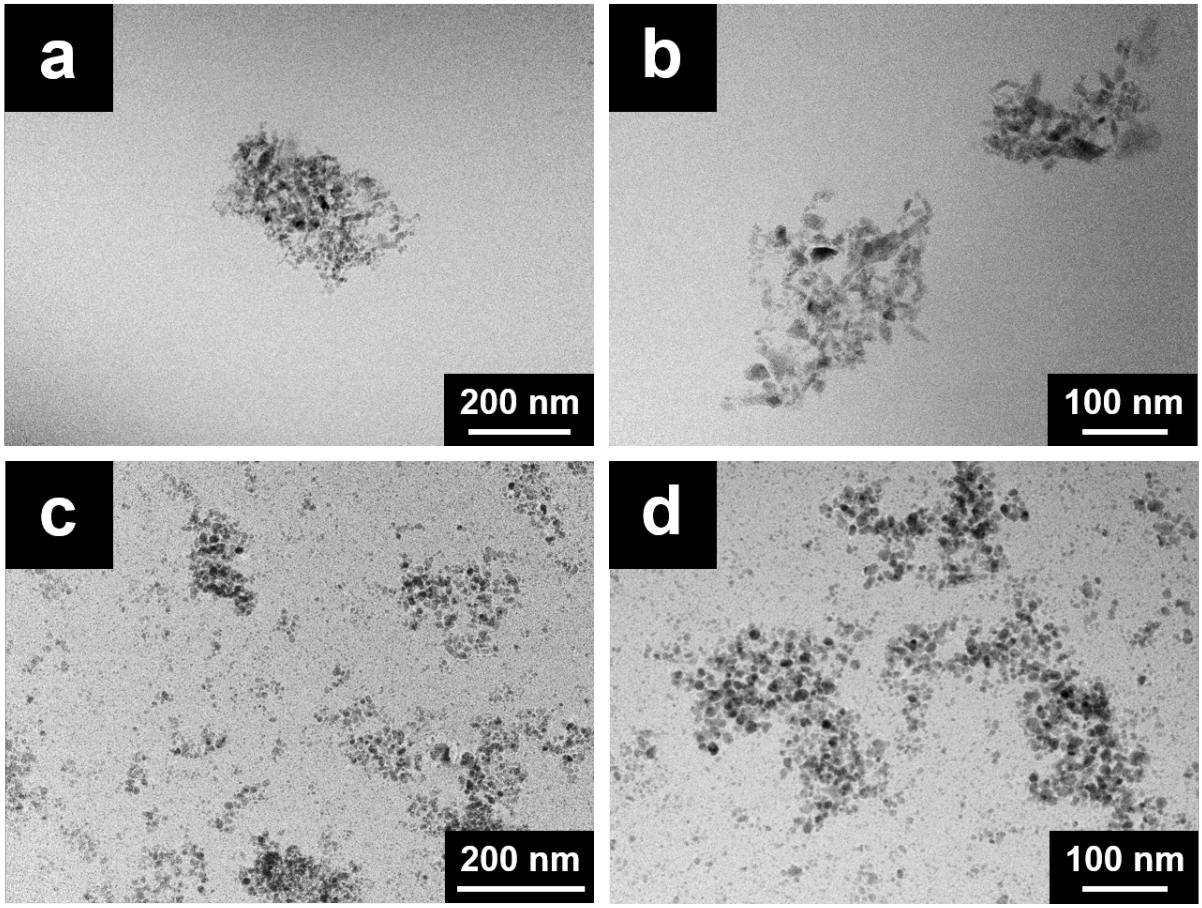

Figure 7. TEM micrographs of freeze-dried BDP nanocrystal dispersed in the e-liquid (a-b) and nanocrystals found in the condensed aerosol of the vaping test (c-d).

In order to verify the hypothesis of the BDP nature of these nanocrystals, the collected samples were diluted with methanol and the obtained solutions were analysed through HPLC. The obtained chromatogram showed the characteristic peak of the drug, eluting at 4.15 min and absorbing at 240 nm.

BDP raw powder was also dispersed in the E-cigarette vehicle and the obtained E-liquid was used for further vaping tests. The total drug amount (BDP in solution and the suspended (nano)crystals) in the condensed aerosol obtained by vaping E-liquid containing freeze-dried BDP nanosuspensions or BDP raw powder was compared to their solubility values (Figure 8).

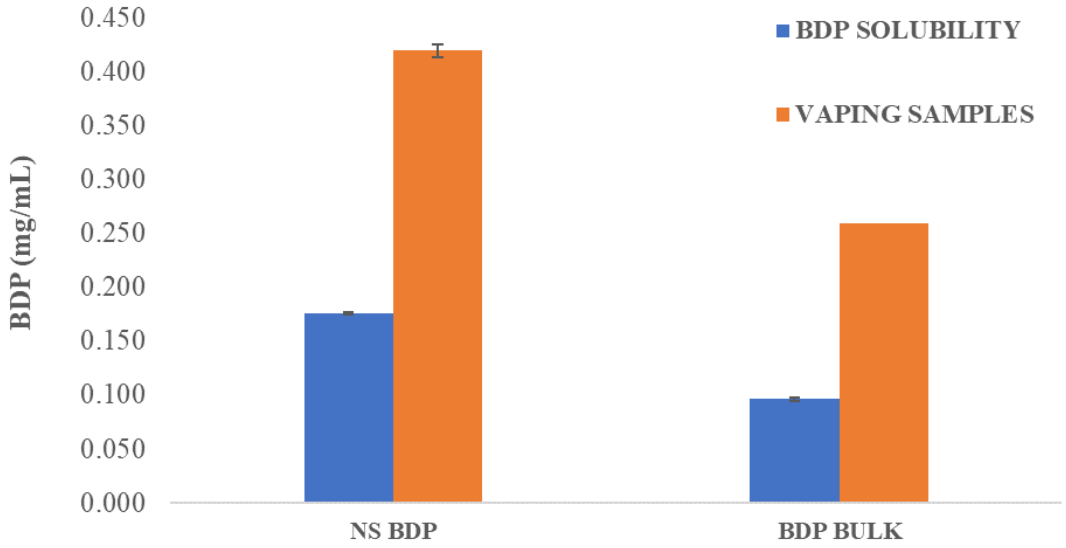

Figure 8. Comparison between BDP solubility values and total BDP amount in the condensed vapour obtained vaping E-liquid containing BDP raw powder (right) or BDP nanosuspensions (left); (n=3).

As shown in the Figure 8, for both nanocrystals and bulk BDP crystals, the total drug amount (BDP in solution and suspended nanocrystals or bulk crystal) in the condensed aerosol is more than two-fold higher than its solubility value at 25°C. This might be partly explained by the high temperatures reached in the vicinity of the electrodes, which might lead to an increase of the drug solubility. Therefore, the produced vapour is capable of transporting more drug, and thus explaining the higher total drug amount in the condensed vapour, compared to the expected values according to its solubility at 25 °C.

On the other hand, as can be seen by the comparison in the Figure 8, the amount of drug transported by the vapours is higher when the nanosuspension-loaded E-liquid is used instead of the raw powder loaded E-liquid, demonstrating the advantage of using nanocrystals. This data not only confirms that ENDS aerosol is able to transport BDP molecules dissolved in the e-vehicle but demonstrates that also suspended BDP (nano)crystals are delivered.

In fact, the analysis of the condensed samples through TEM micrographs prove the presence of drug nanocrystals, as can be seen in the Figure 7c-d, whose morphology and diameter resemble those of the nanocrystals dispersed in the e-liquid (Figure 7a-b).

4 Conclusion

In this study, a BDP nanosuspension was successfully prepared and characterized. The resulting nanocrystals were small in size and homogeneously dispersed, showing an increased solubility compared to the bulk drug. Overall results obtained by the vaping test demonstrated the presence of drug nanocrystals in the produced aerosol. Although we cannot exclude that new particles are formed in the heating chamber, the structural similarity assessed by DLS and TEM suggests that the original BDP nanocrystals were transported by the aerosol. Thus, the ability of ENDS to deliver nanocrystals was confirmed, drawing attention to its possible alternative use as a medical device for poorly soluble drugs. ENDS have nowadays become common all around the world, due to the proven benefits and less toxicity compared to traditional cigarette smoking [133], [134]. The largest number of adults declare to use ENDS to help them stop smoking [135], and a significant part claimed to have satisfactorily stopped [136]. Therefore, using e-cigarettes with bronchodilators or corticosteroids nanosuspensions – such as BDP – might be advantageous in the treatment of COPD in those patients that are chronic smokers in pursuit of a stop-smoking aid [137]. The use of e-cigarette rather than another inhaler device for therapy administration might not only play a key role on the smoking habit cessation, but also ensure better compliance therapy. In fact, patients with chronic respiratory conditions have frequently shown to achieve negative treatment outcomes, linked to inadequate adherence and poor compliance to prescribed therapy [138]. It is well documented that an effective inhaler technique, which is required to assess an adequate adherence to inhaled medications, is often lacking in many patients, due to scarcity of training or necessary abilities [139], [140]. Hence, owing to the easy operations needed for the activation and the handheld and portable structure, ENDS might represent an inexpensive and simple medical device for the inhalation therapy. All things considered, the eventual regulation of electronic cigarettes as medical device would require an evaluation in terms of quality, safety and efficacy [141]. Consequently, further studies will be needed to assure the drug delivery potential of the device and the appropriate drug dosing.

Chapter 2: Curcumin and Beclomethasone Dipropionate Multicomponent Nanosuspension for the Treatment of Bronchial Asthma

The majority of this chapter has been directly copied or modified from *Pharmaceutics* ***2021****, 1300; https://doi.org/10.3390/pharmaceutics13081300* "Pulmonary Delivery of Curcumin and Beclomethasone Dipropionate in a Multicomponent Nanosuspension for the Treatment of Bronchial Asthma" by **Casula, L.**, Lai, F., Pini, E., Valenti, D., Sinico, C., Cardia, M.C., Marceddu, S., Ailuno, G., Fadda, A.M.

1 Introduction

Bronchial asthma is a chronic inflammatory disease, characterized by a complex interplay of airway inflammation and hyper-responsiveness, reversible airway obstruction, mucus hypersecretion and pulmonary edema. The main common symptoms include cough, chest tightness, dyspnea and wheezing [142], [143]. The well-known 'umbrella' asthma diagnosis helps to describe the heterogeneity of the disease and to identify the involved endotypes and phenotypes [144]. In particular, the prevalent phenotypes can be classified as: early-onset allergic, late-onset eosinophilic, exercise-induced, obesity-related and neutrophilic [145]. As regards the pathogenesis of asthma, the disease development is associated with the expression of several transcription factors and in particular the Nuclear Factor- κB (NF-κB), [8]. Medications for the long-term treatment of asthma can be classified into: (i) controller medications, to control the symptoms and reduce exacerbations, (ii) reliever/rescue medications, to provide an immediate relief of breakthrough symptoms, and (iii) add-on therapies for patients with severe asthma. Treatment includes inhaled corticosteroids (CS), long-acting beta2-agonist (LABA), leukotriene receptor antagonist (LTRA), oral corticosteroids (OCS) and short-acting beta2-agonist (SABA) [146]. In the recent years, an increasing interest in complementary and alternative treatments in asthma patients has been shown. Natural extracts, also known as herbal medicinal products, are the most used complementary products or health-promoting agents, due to their health benefits and reduced side effects [147]. Among others, curcumin, a polyphenol extracted

from the rhizome of Curcuma longa, has shown a potential therapeutic value and promising pharmacological activities in a variety of chronic diseases, including bronchial asthma [148]. Its antioxidant and anti-inflammatory activities act synergically to stop the inflammatory process. In particular, curcumin ability to attenuate airway inflammation seems to be due to the inhibition of NF-kB in the asthmatic lung tissue, which is highly involved in the pathogenesis of the disease [149], [150]. Moreover, levels of pro-inflammatory and pro-fibrotic cytokines, chemokines and heat shock proteins were found to be reduced by the polyphenol action, whereas aquaporin expression increased, leading to reduction of pulmonary oedema [151]. However, the low aqueous solubility is limiting for its potential therapeutic applications. A possible strategy to improve the pulmonary delivery of curcumin might be its administration as nanocrystals [152]. Nanocrystals suspensions are nanoparticles of pure drug without any matrix material, suspended in an outer liquid phase, usually composed of water and/or water-miscible solvents, and stabilized using an ionic or non-ionic surfactant or polymers [50]. The drug nanocrystals average diameter is below 1 μm (typically in the range of 200-500 nm). Due to the increased particle surface area and the decreased diffusion layer thickness (compared to coarse and micronized drugs), the dissolution rate is sped up, as described by the Prandtl equation [62]. The Freundlich–Ostwald equation shows that nanocrystals are also characterized by an enhanced saturation solubility [63]. Furthermore, poorly soluble drugs for lung delivery have shown to have superior pharmacokinetics properties when formulated as nanocrystals, compared to solutions or coarse suspensions of the same drug [114]–[119]. Therefore, the aim of our work was to formulate a multi-component nanocrystal suspension for the inhalation therapy, composed of beclomethasone dipropionate – corticosteroid agent, well-known for its activity to reduce the symptoms [120], [146] – and curcumin as natural complementary agent. At first, curcumin nanosuspension (CUR-NS) was prepared by a top down - media milling method [153]. The multi component nanosuspension (CUR+BDP-NS) was then prepared using a beclomethasone dipropionate nanosuspension (BDP-NS) studied in our previous work [154]. Characterization of the nanosuspensions was carried out via different techniques: dynamic light scattering (DLS), scanning electron microscopy (SEM), differential scanning calorimetry (DSC), X-ray powder diffractometry (XRPD) and Attenuated Total Reflectance-Fourier Transform Infrared (ATR-FTIR) spectroscopy. Finally, nebulization tests

with Next Generation Impactor (NGI, Apparatus E Ph. Eu) were carried out to study the aerodynamic properties of the obtained formulations.

2 Materials and Methods

2.1 Materials

Beclomethasone dipropionate, curcumin, Kolliphor P188 (Poloxamer 188, P188) were obtained from Sigma Aldrich (Italy). All the other products were of analytical grade.

2.2 Preparation of nanosuspension

The nanosuspensions were prepared through a wet ball media milling technique, using a 2:1 (w/w) drug:stabilizer ratio. The drug was dispersed in a (0.5 and 1%, w/w) Poloxamer 188 (P188) water solution using an Ultra Turrax T25 basic (IKA, Werke) for 6 min at 8000 rpm. This coarse suspension was divided in 1.5 ml conical microtubes containing about 0.4 g of 0.1-0.2 mm yttrium-stabilized zirconia-silica beads (Silibeads® Typ ZY Sigmund Lindner, Germany). For the CUR-NS, the microtubes were oscillated at 3000 rpm for 70 minutes using a beads-milling cell disruptor equipment (Disruptor Genie®, Scientific Industries, USA). The obtained nanosuspensions of each microtube were gathered and then separated from the milling beads by sieving. As concerns the BDP-NS, the formulation was prepared as previously reported [154]. The procedure was the same as for the CUR-NS, and the oscillation time of the microtubes at 3000 rpm was 150 minutes. The formulations had a final concentration of 1% (w/w) active compound (CUR or BDP) and 0.5% (w/w) P188.

2.3 Particle size analysis

Average diameter and polydispersity index (PDI, as a measure of the size distribution width) of the samples were determined by Dynamic Light Scattering (DLS) using a Zetasizer nano (Malvern Instrument, Worcestershire, United Kingdom). Samples were backscattered by a helium–neon laser (633 nm) at an angle of 173° and a constant temperature of 25°C. Zeta potential was estimated using the Zetasizer nano by means of the M3-PALS (Phase Analysis Light Scattering) technique. Just before the analysis, nanosuspensions were diluted with distilled water. Furthermore, a medium-term stability study of the CUR nanosuspension stored at room temperature was performed by monitoring average size, polydispersity index, and zeta potential for 90 days. All the measurements were made in triplicate.

2.4 Scanning electron microscopy

In order to investigate the (nano)crystals morphology, CUR raw powder and CUR-NS were analysed through a Zeiss ESEM EVO LS 10 (Germany) environmental scanning electron microscope (SEM), operating at 20 KV in high vacuum modality with secondary electron detector (SEI). For the CUR raw powder, the sample was mounted on an aluminium stub with carbon adhesive discs and coated with gold in an Agar Automatic Sputter Coater B7341. As regards the CUR-NS, a drop of the sample was firstly placed on a glass slide and air dried, and then mounted on the stub following the procedure stated above.

2.5 Solubility studies

CUR apparent solubility in water was measured for the CUR bulk powder, CUR-NS and the CUR/P188 physical mixture with the same drug:surfactant ratio. The formulations (n = 3) were kept under constant stirring for 72 h at 37°C. Samples were withdrawn and centrifuged at 21,380 G for 60 min; the supernatant was centrifuged again at 21,380 G for 60 min. Then, a known amount of the clear supernatant was withdrawn and diluted with methanol for the HPLC analysis.

2.6 Solid state characterization

CUR, BDP, P188, physical mixtures of CUR:P188 and BDP:P188 in amounts equivalent to the ratios present in the formulations, and the two single-component formulations (CUR-NS and BDP-NS) were investigated by using different technologies such as DSC, XRPD, and ATR-FTIR spectroscopy.

In order to obtain the powder samples, CUR-NS and BDP-NS were frozen at -80 °C and then freeze dried for 24 h at -86 °C and 0 mTorr, using an FDU-8606 Freeze Dryer (Operon Co, Korea).

DSC analysis (Perkin Elmer DSC 6 Waltham, MA, USA) was used to characterize the thermal behaviour of the different components used for the formulations. Samples were hermetically sealed in an aluminium pan and heated at a speed of 10 °C/min in the range between 30 and 220°C. Inert atmosphere was maintained by purging nitrogen at a flow rate of 10 mL/min. A control empty pan subjected to the same heating conditions was used as a reference.

ATR-FT-IR spectra were acquired with a Perkin Elmer Spectrum One FT-IR (Perkin Elmer, Waltham, MA, USA), equipped with a Perkin Elmer Universal ATR sampling accessory consisting of a diamond crystal. Analyses were performed in a spectral region between 4000 and 650 cm^{-1} and analysed by transmittance technique with 32 scansions and 4 cm^{-1} resolution.

XRPD patterns were collected with a Rigaku MiniFlex diffractometer, operating at 30 kV and at 15 mA, with Cu Kα radiation (1.54056 Å) in the range from 3 to 60 2θ, in steps of 0.02, using a scan step time of 2.00 seconds. The results were then obtained as peak height (intensity) versus 2θ.

2.7 Preparation of nanosuspension

CUR-NS and BDP-NS were prepared as described above (2.2). The multicomponent nanosuspension (CUR+BDP-NS) was prepared right before the nebulization test by mixing equal parts of CUR-NS and BDP-NS. The formulation was adequately vortexed and then visually inspected to check the absence of large precipitated aggregates or phase separation. Finally, particle size analysis was carried out by DLS.

2.8 Nebulization and aerodynamic behaviour of nanosuspensions

CUR-NS, BDP-NS and CUR+BDP-NS were nebulized using a Pari SX® air jet nebulizer attached to a Pari TurboBoy® compressor (Pari GmnH, Starnberg, Germany) and connected to the Next Generation Impactor (NGI, Apparatus E, Eur. Ph 10^{th} ed., Copley Scientific Ltd., Nottingham, United Kingdom). All the parts of the NGI were washed in methanol and allowed to dry. The collection plates were not sprayed with silicone fluid in accordance with the European Pharmaceutical Aerosol Group (EPAG) recommendations [155]. Pre-separator, which is mostly indicated for dry powder inhalers to separate very large particles and avoid blockage of NGI stages, was not used during this study.

The formulation (2 ml) was placed in the nebulizer and aerosolized to dryness directly into the throat of the NGI, using a flow rate of 15 L/min [156]. At the end of the experiment, the drug amount deposited in each stage of the impactor and the residual (undelivered) was collected, using methanol, in a glass vial, properly diluted and analysed by HPLC. The following nebulization parameters were evaluated: (1) the Emitted Dose (ED%), calculated

as the percentage of drug recovered in the NGI versus the amount of drug placed in the nebulizer; (2) the Fine Particle Dose (FPD), which represents the amount of drug contained in droplets of size less than 5 µm; and (3) the Fine Particle Fraction (FPF%), calculated as percentage of FPD versus the amount of drug recovered in the NGI.

The cumulative amount of drug-containing droplets with a diameter lower than the stated size of each stage was plotted as a percentage of the recovered drug versus the cut-off diameter, not including the mass deposited in the induction port due to the unavailability of a precise upper size limit for particles deposited in this section [157]. Finally, the Mass median aerodynamic diameter (MMAD) of the particles was extrapolated from the graph according to the Eur. Ph. 10^{th} ed., and the geometric standard deviation (GSD) value was calculated.

2.9 HPLC analysis

Quantitative determination of BDP and CUR was performed by HPLC using a liquid chromatograph Alliance 2690 (Waters Corp, Milford, MA) equipped with a photodiode array detector and a computer integrating apparatus (Empower 3). Analyses were performed with a Sunfire C18 column (3.5 µm, 4.6 mm × 150 mm, Waters). The mobile phase was a mixture of acetonitrile, water and acetic acid (95:4.84:0.16 v/v), delivered at a flow rate of 0.5 mL/min. Samples (10µL) were injected using an auto sampler. CUR was revealed at 421 nm, whereas BDP at 240 nm. The stock standard solutions of CUR and BDP were prepared by dissolving the drug in methanol and stored at 4 °C. A standard calibration curve (peak area of CUR/BDP vs. known drug concentration) was built up by using standard solutions prepared by dilution of the stock standard solution with the mobile phase. Calibration graphs were plotted according to the linear regression analysis, which gave a correlation coefficient value (R2) of 0.999. The described HPLC method was also used to quantify the drug in the obtained nanosuspensions and to evaluate the presence of any degradation products. The limit of quantification was 1 ng/µL for CUR and 0.5 ng/µL for BDP, while the limit of detection was 0.2 ng/µL for both compounds. Sample preparation and analyses were performed at room temperature.

2.10 Statistical analysis of data

Results are expressed as the mean ± SD. Multiple comparisons of means (one-way ANOVA) were used to substantiate statistical differences between groups, while Student's t-test was used to compare two samples. Data analysis was carried out with the software package XLStatistic for Microsoft Excel. Significance was tested at 0.05 level of probability (p).

3 Results and Discussion

3.1 Preparation and characterization of nanosuspension

A preliminary study was carried out to optimize the protocol for the CUR-NS preparation through the wet ball media milling technique. Two parameters were investigated, namely the stabilizer concentration and the milling time. CUR concentration was fixed at 1% (w/w), whereas two concentrations of the stabiliser P188 were studied: 0.5 and 1 % (w/w). The two formulations were milled for 60, 70, 80, and 90 minutes. Average diameter, PDI and zeta potential as a function of the milling time are shown in Figure 1.

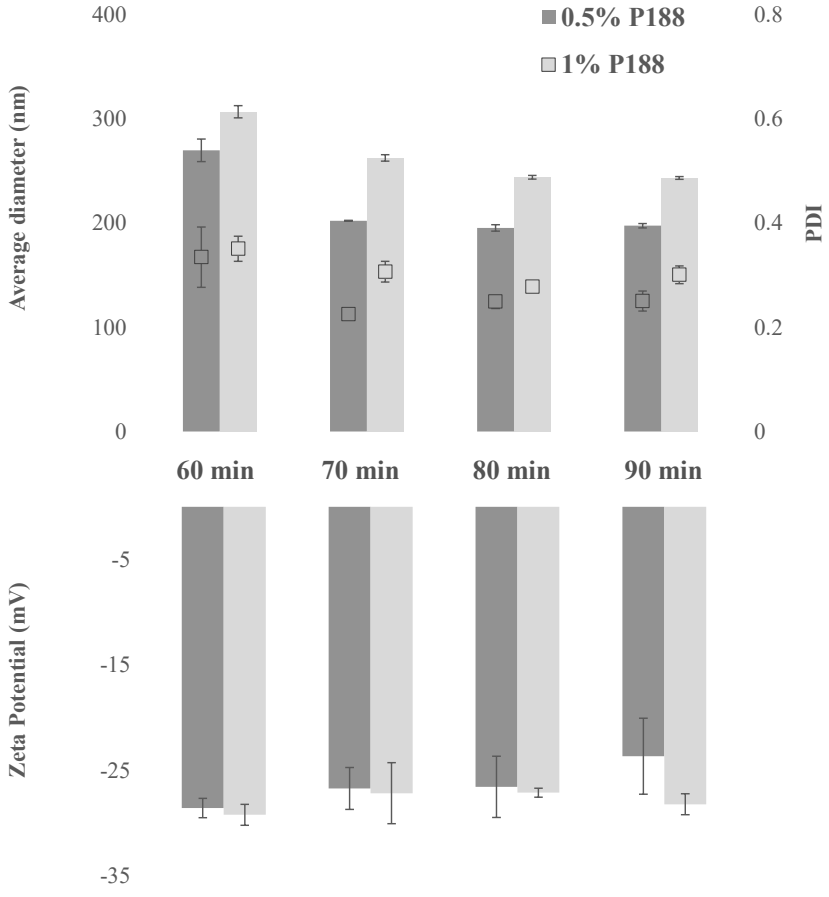

Figure 1. Average diameter (nm), PDI and Zeta Potential (mV) as a function of milling time (minutes) for the formulation with 1% (w/w) CUR and 0.5% (w/w) P188, and with 1% (w/w) CUR and 1% (w/w) P188. (n=3; mean ± SD).

Both formulations showed a significant decrease in the nanocrystal average diameter by increasing the milling time from 60 to 70 minutes. As highlighted in Figure 1, also the PDI

value improved for formulation with 0.5% P188, decreasing from 0.34 to 0.23. On the other hand, by increasing the milling time from 70 to 90 minutes, the variation of the nanocrystal dimensional properties was less pronounced. It is worth to notice that after all the milling protocols, the zeta potential values were maintained at approximately -30 mV, representative of promising formulation stability. However, as can be seen in the Figure 1, when the 1:1 drug:surfactant ratio (w/w) was used, the PDI never decreased to values less than approximately 0.30, even after 90 minutes of milling. Therefore, the formulation containing 1% CUR and 0.5% P188 obtained after 70 minutes of milling (CUR-NS) was selected for further studies.

CUR solubility studies were performed in water at 37 °C to evaluate the properties of nanocrystal CUR-NS in comparison with CUR raw powder and the physical mixture. The raw drug powder showed an apparent solubility of 0.97 ± 0.1 µg/mL, which increased 38-fold in the physical mixture with the P188 (38.10± 1.2 µg/mL). After the nanosizing process, the CUR nanocrystal apparent solubility increased further (53.08 ± 1.7 µg/mL). Consequently, preparation of nanocrystals stabilised by P188, allowed us to improve CUR apparent solubility by approximately 54-fold in comparison with the raw material, in accordance with the Freundlich-Ostwald equation [63].

These results suggest that drug formulated as nanocrystals would improve therapeutic efficacy. However, it is worth to highlight that, depending on the drug characteristic, increased biological medium concentration can also lead to more toxic effects. As widely reported in literature, very challenging safety issues need to be addressed [158], [159]. Indeed, many factors influence nanosuspension safety in drug delivery, such as particle surface area, formulation, external environment, and temperature. Moreover, most nanosuspension drug delivery studies were carried out in animal models instead of in humans, therefore full knowledge of them is still limited [160].

The evaluation of the morphological changes of CUR crystals after the milling process was carried out by ESEM (Figure 2).

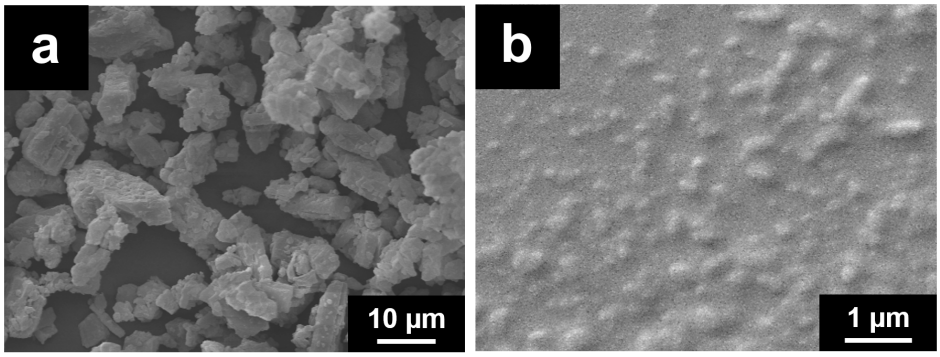

Figure 2. ESEM micrographs of CUR raw powder (a) and CUR-NS (b).

As it can be seen in the ESEM micrographs, the milling process modified both shape and size of the CUR crystals. The considerable amount of energy required to reduce the nanocrystal size below one micron is provided during the milling process by the collision of the drug crystals and the milling beads – and of the drug crystals themselves – that generate high shear forces. Before the milling, Figure 2a, the raw drug material appears to have large crystals with irregular elongated shape while, after the milling with the stabilizer, as shown in Figure 2b, CUR nanocrystals show a regular and rounded shape, with a homogenous particle size distribution, in accordance with DLS analysis.

The stability of the obtained CUR-NS was evaluated by monitoring size distribution and zeta-potential over a period of 90 days at room temperature (Figure 3).

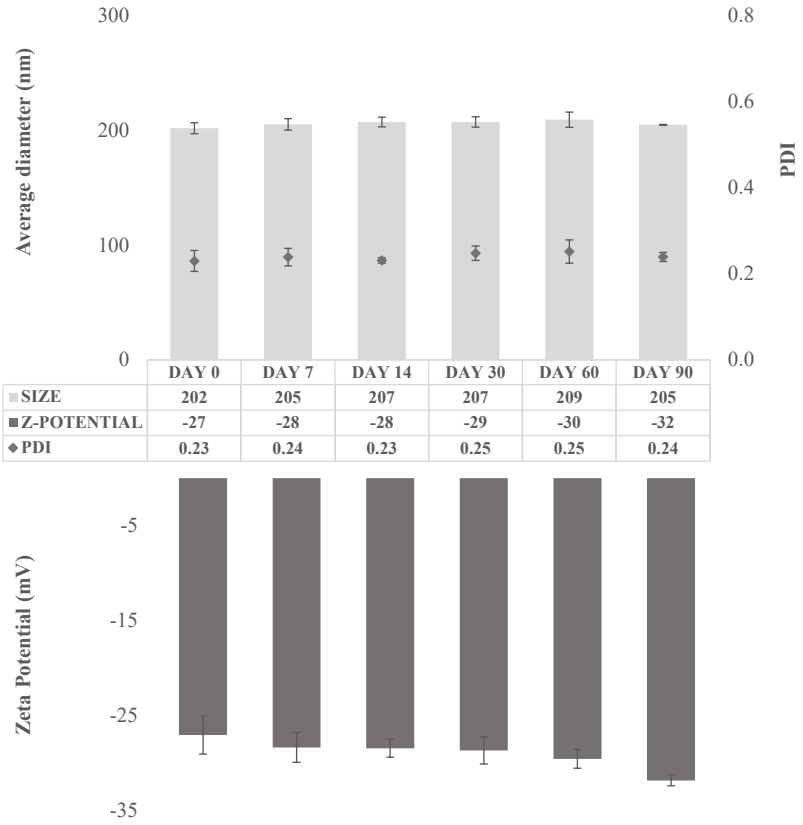

Figure 3. Average diameter (nm), polydispersity index (PDI) and Zeta Potential (mV) of CUR-NS over 90 days of storage at room temperature. (n=5; mean ± SD).

Size distribution study revealed a long-term stability of the CUR-NS. Indeed, the mean diameter did not vary appreciably during the 90 days on storage showing an average diameter of 202 nm in the day 1 and of 205 nm in day 90. Furthermore, the PDI was almost constant and below 0.25, confirming the stability of the formulation since the retention of the homogeneous size distribution on storage [124]. Moreover, the zeta potential value was almost constant during the stability test (approximately -30 mV). Finally, HPLC analysis revealed no decomposition and the absence of degradation products in the obtained chromatograms.

The final multicomponent nanosuspension (CUR+BDP-NS) was obtained by mixing CUR-NS with BDP-NS, which was prepared according to the previously reported procedure [21] with a 1% (w/w) BDP concentration and 0.5% (w/w) P188. BDP nanocrystals exhibited a mean

diameter of approximately 240 nm, with a low PDI (0.24) indicating a well-dispersed colloidal dispersion.

Solid state characterization of CUR-NS, BDP-NS and their components as raw material and physical mixture was carried out by DSC, ATR-FTIR and XRPD.

3.2 DSC analysis

To evaluate the possible interactions between the active ingredients and the stabilizer in the preparation, thermal analysis was performed; results are expressed as onset temperature. CUR thermogram revealed the presence of an endothermic peak at 165.05 °C, while P188 at 53.71°C, which implies that both are in the crystalline state. In the physical mixture, both the sharp endothermic peak of the stabilizer and the broad CUR peak, showed less intensity and a shift towards lower temperatures, (47.96 °C and 147.35 °C, respectively) compared to the component melting points, suggesting a molecular dispersion of CUR in P188. This trend became even more evident in the optimized formulation, thus, suggesting that the CUR existed in a less crystalline state.

As it concerns BDP-NS and its components, the BDP thermal behaviour revealed an endothermic peak at 212.09 °C followed by an exothermic event, thus, indicating that the recrystallized BDP undergoes a melting process followed by chemical degradation. Furthermore, in BDP-NS thermogram an endothermic event between 60 and 90 °C is visible, suggesting the formation of hydrate BDP, as reported in literature [161], [162].

The melting peak of P188 was at an onset temperature of 53.71 °C. Physical mixture and nanosuspension thermograms showed some similarities, in fact, the melting peaks were all present but drifted, and with a sharp decrease in the BDP peak intensity, implying that no amorphous forms were produced during the preparation process.

3.3 ATR-FTIR analysis

ATR spectroscopy was carried out to further elucidate the interactions between the active compounds and P188 in the solid state. These interactions are detected by any changes in the position or disappearance of a characteristic vibration or stretching region of the compounds.

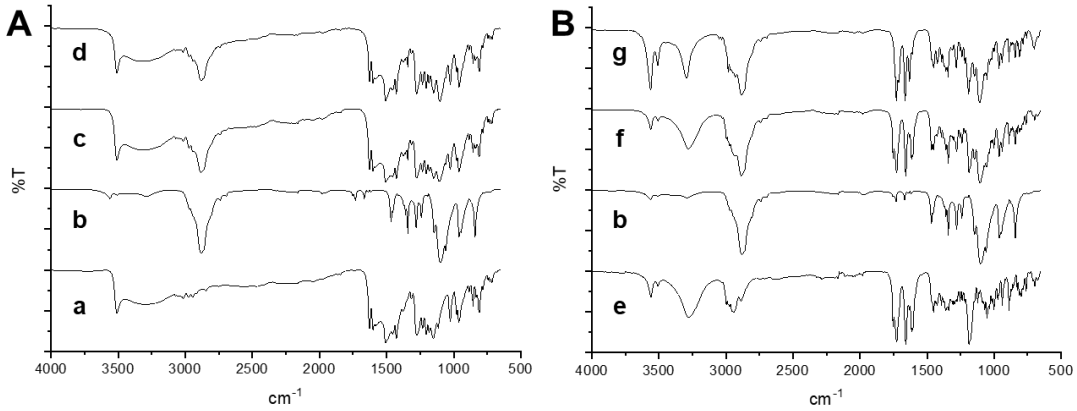

Figure 4. ATR-FTIR analysis of (A) CUR formulation and its components: raw powder (a), P188 (b). physical mixture of CUR+P188 (c), CUR-NS (d); and (B) BDP formulation and its components: raw powder (e), physical mixture of BDP+P188 (f) and BDP-NS (g).

The ATR spectrum of CUR (Figure 4A) exhibited a sharp peak at 3509 and a broad one at 3326 cm^{-1} attributed to phenolic OH stretching. Furthermore, it can be observed a peak at 1626 cm^{-1} owing to the carbonyl in CUR, consistent with the formation of a keto-enol tautomer, at 1602 and 1510 cm^{-1} the bands of the strong vibrations of C==C and C=O stretching, while at 1274 cm^{-1} the C- O peak of enol. At 1027 cm^{-1} the C -O- C peak was visible, while at 962 cm^{-1} and 810 cm^{-1} the trans-C-H vibration of the unsaturated chain and the C-H vibration of aromatic ring, respectively, were clearly shown. Finally, the characteristic absorption peaks of P188 around 3600, 2881, and 1099 cm−1 were attributed to O-H, C–H, and C–O–C stretching vibrations. The spectrum of the physical mixture was the combination of CUR and P188. These results clearly demonstrated that no interactions occurred between the physically mixed CUR and P188. The spectra of CUR-NS exhibited the same peak position of raw CUR demonstrating that the addition of the stabilizer and physical process would not affect its molecular structure.

The ATR spectrum of BDP (Figure 4B) showed the O-H free and associated vibrations at 3559 and 3280 cm^{-1}, the ester carbonyl stretching at 1753, the conjugated and non-conjugated C=O stretching bands at 1727 and 1658 cm^{-1}, respectively. The C=C stretching was at 1615 and 1608 cm^{-1}, and the C-O bands at 1186 cm^{-1}. The characteristic absorption peaks of P188 at 3500, 2881, and 1099 cm−1 were attributed to O-H, C–H, and C–O–C stretching vibrations, respectively. In the physical mixture spectrum, bands of both raw materials were visible, no absence of any functional peaks or addition of new peaks, thus, revealing that there is no significant chemical interaction between the drug and P188. In the

nanosuspension spectrum, as reported in our previous article [21], the COO peak, the C=O and C=C stretchings at 1711, 1663 and 1631 respectively disappeared while a peak at 1712 cm^{-1} appeared, suggesting that the BDP carbonyl group is involved in a hydrogen bond with water. The presence of water was also confirmed by the increase of peak intensities at 3562 and 3508 cm^{-1}, confirming the presence of BDP as monohydrate.

3.4 XRPD analysis

The crystalline state of the active ingredients in nanosuspensions was estimated by a XRPD study.

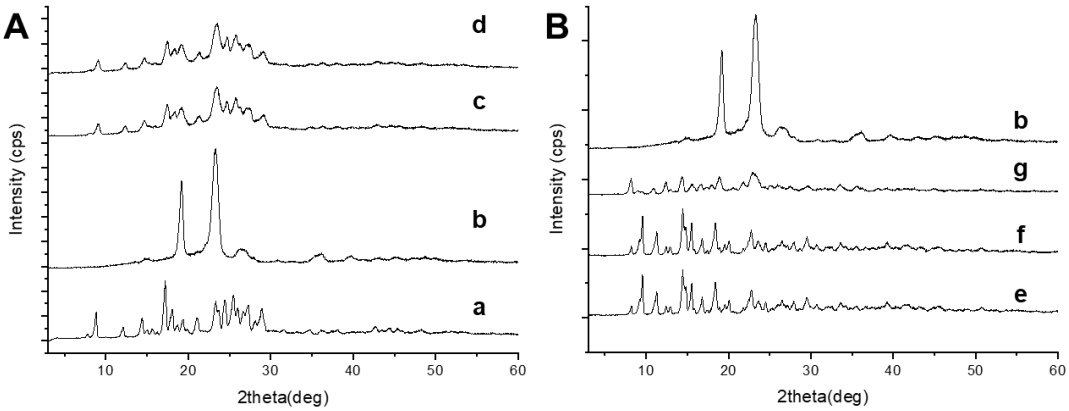

Figure 5. XRPD analysis of (A) CUR formulation and its components: raw powder (a), P188 (b). physical mixture of CUR+P188 (c), CUR-NS (d); and (B) BDP formulation and its components: raw powder (e), physical mixture of BDP+P188 (f) and BDP-NS (g).

The diffraction patterns of CUR (Figure 5A) showed intense sharp peaks at 8.8, 12.1, 14.4, 17.2, 18.08, 19.36, 21.08, 21.66, 23.32, 24.46, 25.48, 27.28 and 28.10 2θ (deg), while P188 at 19.32 and 23.48 2θ (deg) implying the crystalline structure of the both raw materials. The physical mixture and the nanosuspension profiles were very similar; reflection peaks of the raw materials were still present indicating that CUR partially retained its crystallinity in the formulation.

To confirm the crystalline nature of BDP nanosuspension, X-ray diffraction analysis was performed (Figure 5B). BDP and P188 have crystalline profiles. The XRPD analysis of BDP showed a pattern with sharp and intense peaks at 9.54, 11.28, 14.44 and 20.06 2θ (deg) values, P188 at 19.32 and 23.48 2θ (deg). The physical mixture pattern indicated that the crystalline structure remained unchanged; the characteristic peaks of the drug were still

present, even if their intensities were attenuated due to the lower drug content. The optimized NS retained the crystalline profile, but the increased intensity of the peaks at 8.5° and 12 2θ (deg) suggested the presence of BDP monohydrate, thus supporting ATR and DSC results.

3.5 Preparation of the multicomponent nanosuspension

After the optimization and characterization of the two single-component nanosuspensions, CUR+BDP-NS was prepared by mixing equal amounts of CUR-NS and BDP-NS right before the nebulization test. The composition of the obtained formulation is indicated in the Table 1. A preliminary visual inspection revealed the absence of macroscopic precipitated aggregates or phase separation. This information was also confirmed by DLS analysis. Indeed, the nanocrystals average diameter of the CUR+BDP-NS (221nm) did not differ appreciably from CUR-NS (202 nm) and BDP-NS (241 nm.) Furthermore, the PDI maintained a value of approximately 0.25.

Table 1. Composition of the two single-component (CUR-NS, BDP-NS) and the multicomponent formulation (CUR+BDP-NS) and their dimensional properties expressed as average diameter (nm) and polydispersity index (PDI). (n=3; mean ± SD).

	Composition			Dimensional Analysis	
	Curcumin (% w/w)	Beclomethasone dipropionate (% w/w)	P188 (% w/w)	Average diameter (nm)	PDI
CUR-NS	1	-	0.5	202 ± 5	0.23 ± 0.02
BDP-NS	-	1	0.5	241 ± 2	0.24 ± 0.01
CUR+BDP-NS	0.5	0.5	0.5	221 ± 7	0.25 ± 0.02

3.6 Nebulization test

To evaluate the drug deposition and determine the aerodynamic parameters, samples (CUR-NS, BDP-NS, CUR+BDP-NS) were nebulized using the PariSX® air jet nebulizer connected to the NGI. It is well known that nebulizers might generate aerosol particles with different aerodynamic diameters. In particular, only those characterized by a MMAD value in the range 5 – 0.5 µm are believed to deposit on the lungs [163]. Operating with a flow rate of 15 L/min, the overall range of the impactor is 0.98–14.1 µm. Notably, four stages have cut sizes in the range of 0.5–5.0 µm aerodynamic diameter, and a fifth stage only slightly larger than the upper limit [156]. Nebulization time to dryness, which is the time required to complete cessation of aerosol formation, was shown to be 10 minutes.

The percentage of drug deposited in each stage of the impactor was very similar for all the formulations, as shown in the Figure 6.

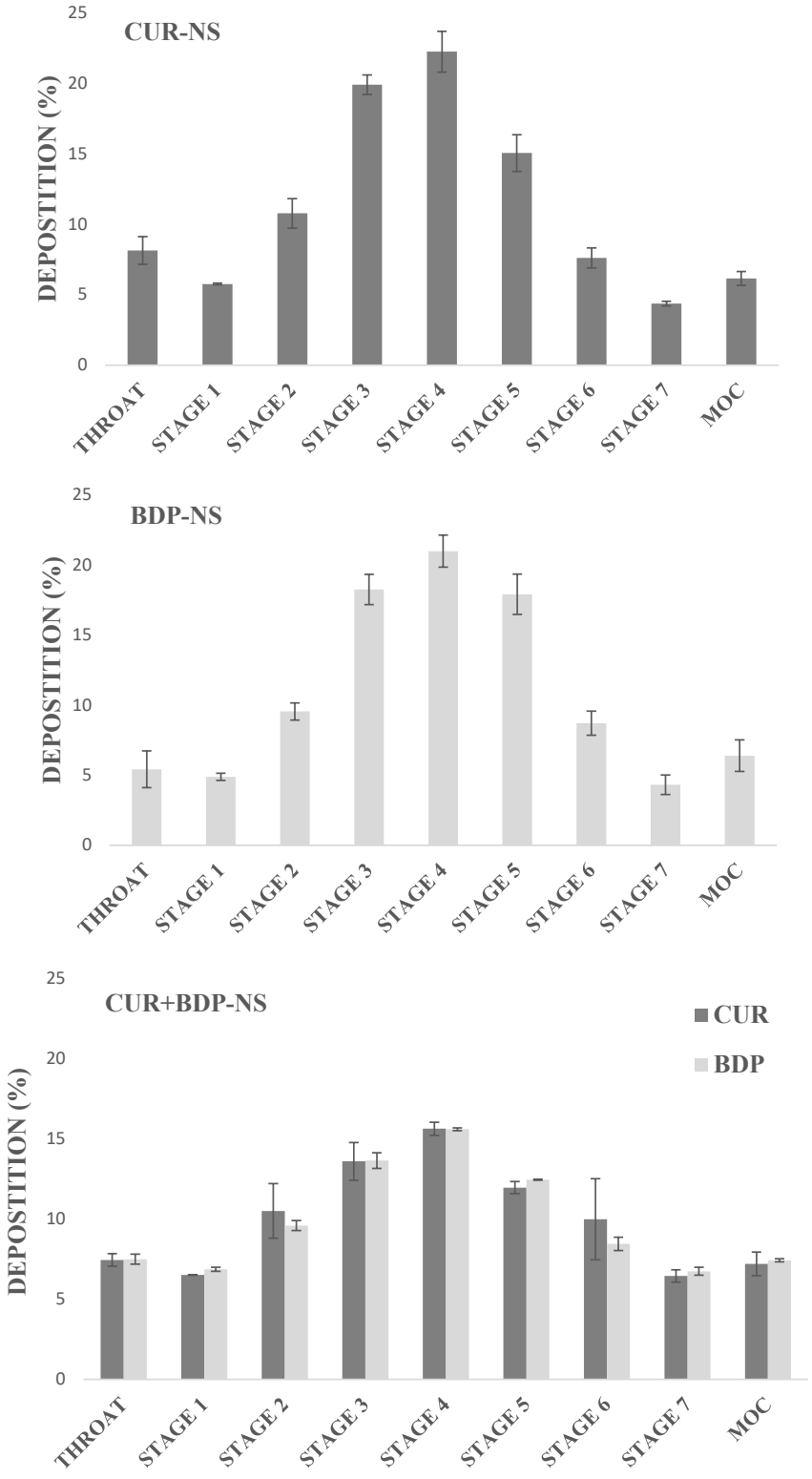

Figure 6. Deposition of CUR and BDP in the different stages of the NGI after nebulization with a flow rate of 15 L/min, for the single-component formulations (CUR-NS and BDP-NS), and the multicomponent formulation (CUR+BDP-NS). (n=3; mean ± SD).

Approximately 5 – 7% of the generated aerosol particles tend to deposit on the induction port (throat), thus showing their inability to reach the deeper stages. However, the majority of the drug was found to be in the intermediate/middle stages (3 – 5). Interestingly, approximately 6-7% of the droplets is able to reach the MOC stage, showing an aerodynamic diameter < 0.98 µm, and thus the ability to hypothetically deposit on the alveolar region of the lungs. To better evaluate the nanosuspension behaviour during the nebulization process, the aerodynamic parameters were analysed for each formulation (Table 2). In the case of CUR+BDP-NS, values were calculated separately for each active ingredient.

Table 2. Aerodynamic parameters of the three tested formulations: Emitted dose (ED), Fine Particle Dose (FPD), Fine Particle Fraction (FPF), Mass Median Aerodinamic Diameter (MMAD) and Geometric Standard Deviation (GSD). (n=3; mean ± SD).[§] Data are not statistically different (p>0.05).

		CUR+BDP-NS		
	CUR-NS	CUR	BDP	BDP-NS
ED%	57.0 ± 0.9	81.9 ± 1.1	83.4 ± 3.7	65.5 ± 4.9
FPD (mg)	7.8 ± 0.3	6.8 ± 0.8	6.1 ± 0.1	7.6 ± 0.2
FPF (%)	60.3 ± 1.9 [§]	64.7 ± 4.0 [§]	62.7 ± 0.5 [§]	68.1 ± 7.2 [§]
MMAD (µm)	4.1 ± 0.1	3.4 ± 0.6	3.8 ± 0.1	3.7 ± 0.2
GSD	2.6 ± 0.1	3.1 ± 0.4	2.9 ± 0.1	2.6 ± 0.1

As can be seen, the Emitted Dose (ED) for CUR-NS and BDP-NS reached a value of 57% and 65.5%., respectively. It is interesting to highlight that this value increases more than 80% in the case of the multicomponent formulation, thus, demonstrating that more than 80% of the formulation loaded in the nebulizer may be properly delivered to the patient. Results showed that the mean FPF% value for the CUR in the multicomponent nanosuspension was higher than that in the CUR-NS while the opposite was for the BDP. However, statistical analysis revealed that these differences are not significant (p>0.05).

Finally, all the nebulized formulations showed a MMAD <5 µm, a mandatory condition for the droplets to be able to reach the deeper parts of the respiratory system, and therefore to carry out their therapeutic action at the site of inflammation.

4 Conclusion

In this study, a CUR nanosuspension was optimized and characterized. The resulting nanocrystals were small in size and homogeneously dispersed, showing an increased solubility compared to the bulk drug. Furthermore, the BDP-NS was successfully prepared as reported previously [154], and used for the preparation of the multicomponent nanosuspension, containing CUR and BDP nanocrystals. The obtained formulation showed a narrow distribution and the absence of aggregation phenomena. In vitro nebulization tests were carried out and highlighted that all prepared formulations, especially CUR+BDP-NS, had high values of ED% and MMAD < 5 µm.

In conclusion, the obtained multicomponent nanosuspension has shown optimal dimensional properties and aerodynamic parameters, suggesting a correct and efficient delivery of the formulation in the deeper lung regions.

Owing to the improved solubility of the active ingredients formulated as nanocrystals, our formulation represents a promising lung delivery system which can improve the course of the asthmatic inflammation.

Part 2: Development of electrospun nanofibers with simvastatin loaded liposomes for wound healing

The work described in this chapter was carried out at the Department of Pharmaceutical Technology, Faculty of Pharmacy, University of Ljubljana under the supervision of Professor Julijana Kristl and Assistant Professor Špela Zupančič, and the home mentorship of Professor Anna Maria Fadda. The results presented in this chapter will be the content of common publication.

1 Introduction

The wound can be described as a discontinuity of the normal anatomic structure of the tissue due to an exogenous laceration on the skin, which might be caused by a thermal, physical, mechanical or electrical trauma. In general, wounds can be classified according to the depth of the damage as: superficial, involving only the epidermis and the papillary dermis, partial thickness or deep dermal, and full thickness wounds. Wound healing is an incredibly complex process, which depends on an elaborated interaction of highly controlled mechanisms and chemical mediators to re-establish the tissue structure and functionality [164], [165]. There are four wound healing stages: haemostasis, inflammation, proliferation and remodelling. Several inflammatory cells are involved in this process and, among the others, macrophages and fibroblasts are the most important ones for their phagocytose action, stimulation of granulation tissue formation, cell proliferation and structural elements restoration. The last phase, the remodelling process, might take weeks to years and, the mature scar strength might be about 80% of the normal skin [166]. Although the skin exhibits rapid self-regenerative capacity with no to minimal scarring in case of acute wounds, the chronic wounds healing takes months to show progress and it shows thus susceptible to external attack such as bacterial infections. Therefore, an appropriate wound care and dressing is often needed to provide a physical barrier, to avoid infections or contaminations, and to form a controlled environment that aids and accelerates wound healing [164], [167].

Several nanomaterial-based systems have been introduced into the area of wound healing and skin regeneration. As a result of innovative and outstanding development of nanotechnology, they offer unique properties with respect to conventional wound care products. These systems have shown to be non-toxic, biocompatible and to create a favourable moist environment to facilitate the wound healing process. Furthermore, they can incorporate bioactive molecules, protecting drugs from degradation and providing a sustained drug release when desired [168], [169].

Among them, electrospun polymeric nanofibers have been recognized as efficient systems to promote skin regeneration [170]–[172]. Nanofibers can be described as solid fibers with various outstanding nanoscale features, such as a high surface-to-volume ratio, a porous structure, and a theoretically unlimited length. Owing to their morphological similarity with the extracellular matrix, combined with their mechanical performance and flexibility, they provide structural support to the damaged tissues and improve cell growth and proliferation [91]. The interconnected fibrous structure ensures gas exchange, nutrient supply, and control of fluid loss, maintaining a moist environment that avoids dehydration of the wound and augment angiogenesis and collagen synthesis. Moreover, systems composed of a wide range of synthetic and nature-derived polymers can reduce scar formation, since biodegradation of fibers offer a desirable roadmap for tissue reconstruction [173], [174]. Preparation of nanofibrous scaffolds can be adapted for a specific area of the body, and several active ingredients can be incorporated to facilitate the healing process and improve the patients compliance [173], such as anti-inflammatory agents, anaesthetics, antimicrobial agents or growth factors [58], [175]–[177].

In the midst of the numerous active pharmaceutical ingredients used for wound treatment, recent studies have shown the remarkable effects of simvastatin (SIM) as anti-inflammatory and immunomodulatory agents [178]–[181]. SIM is part of the lipid-lowering statin drugs, which are well known as 3-hydroxy-3-methyl-gutaryl coenzyme A (HMG-CoA) reductase inhibitors. As concerns the anti-inflammatory activity, statins have exhibited (i) a reduction in the endothelial adhesion by decreasing the levels of nitric oxide and intercellular adhesion molecules, (ii) an interference with the recruitment of mononuclear cells by reducing the expression or the activation of various chemoattractant cytokines (MCP-1, IL-8), nuclear factor-kB (NF-kB), proinflammatory enzymes (COX-2), tissue factors (TF) and plasminogen

activator inhibitor-1 (PAI-1) and (iii) a reduction in inflammatory serum markers such as high-sensivity C-reactive proteins (hs-CRP), E-selectin, matrix metalloproteinases (MMPs), tumor necrosis factor- α (TNF-α), IL-1β. Regarding the immunomodulatory activity, they have shown a suppression of proliferation of natural killer cell activity, an inhibition of the expression of major histocompatibility class II (MHC II) antigens by macrophages and endothelial cells (required for the antigen presentation and T-cell activation (Th1 and Th2)), which results in a reduction of the activation of several anti-inflammatory cytokines [182]–[185]. Moreover, SIM demonstrated a surprising antimicrobial activity and remarkable therapeutic effects on the healing of infected skin wounds [186]–[188].

The aim of this work was to produce a SIM-loaded biocompatible nanofibrous scaffold for wound healing purpose. Due to the low aqueous solubility of SIM [189], the drug was in first step incorporated in liposomes with different concentrations of butylated hydroxyanisole (BHA), which can as an antioxidant prevent SIM degradation as shown in previous study [190]. In the next step, the nanofibrous scaffolds were obtained through the green electrospinning technique from the liposomal dispersions where alginate and poly(ethylene) oxide (PEO) were dissolved in mass ratio 80:20. Alginate was chosen as biopolymer due to its appropriate properties, such as biocompatibility and non-toxicity. The nanofibrous were characterised in terms of morphology investigation, drug content and entrapment efficiency, release studies and chemical stability. Finally, *in vitro* cell tests were carried out to evaluate the cytotoxicity and the immunomodulatory activity of the formulations. The combination of two nanocarrier technologies – liposomes and nanofibers – used in this work to produce liposome-scaffold composite systems represent a promising approach for more suitable clinical applications, merging the excellent biocompatibility, controlled release and mechanical properties.

2 Materials and Methods

2.1 Materials

SIM and butylated hydroxyanisole (BHA) were of pharmaceutical grade and a supplied by Krka d.d.. Phosphatidylcholine (Phospolipon 90G) was a gift from Phospholipid GmbH (Germany). Sodium alginate (Mw, 1.38 × 105 g/mol [138 kDa]; Protanal LF 10/60) was from FMC BioPolymer (Haugesund, Norway), and was defined by the manufacturer as 65%–75% α-l-guluronate and 25%–35% β-d-mannuronate. PEO (MW = 2 MDa) was purchased from Sigma-Aldrich, (Steinheim, Germany). Water was purified with a Milli-Q system with a 0.22 µm Millipak 40 filter (Millipore, Ireland). All the chemicals were used as received, without any further purification or change.

2.2 Liposome preparation and characterization

The different components of the formulations were weighed in a glass vial and hydrated with 5 mL of water to obtain liposomes. The dispersions were immediately sonicated (5 sec on, 2 sec off, 2.20 min 3 cycles, 40% amplitude) with a high intensity ultrasonic processor (Cole-Parmer, USA). The composition of the samples is reported in Table 1 and the nomenclature was made by taking into consideration BHA concentration (mg/mL). Additional samples were prepared and used only as control for the *in vitro* tests (section 2.11) with the same concentration of P90G without SIM (EMPTY-LIPO) and without SIM and with 1.2 mg/mL of BHA (1.2-BHA LIPO).

Table 1. Composition of the vesicular formulation.

SAMPLE	COMPOSITION			
	P90G (mg)	SIM (mg)	BHA (mg)	H_2O (mL)
0-BHA SIM LIPO	500	100	0	5
0.3-BHA SIM LIPO	500	100	1.5	5
0.6-BHA SIM LIPO	500	100	3	5
0.9-BHA SIM LIPO	500	100	4.5	5
1.2-BHA SIM LIPO	500	100	6	5

The average diameter and polydispersity index (P.I., a measure of the width of size distribution) of the vesicles were determined by Dynamic Light scattering (DLS) using a Zetasizer Ultra (Malvern Instrument, UK). Samples were backscattered by a helium-neon laser (633 nm) at 174.7° and a constant temperature of 25 °C. Zeta potential was estimated using the Zetasizer Ultra by means of the M3-PALS (Mixed Mode Measurement-Phase Analysis Light Scattering) technique, which measures the particle electrophoretic mobility.

To evaluate the effective drug concentration and the encapsulation efficiency of the liposomal formulations, the samples were filtered with 0.45 µm filters to remove undissolved drug particles. The filtered samples were then ultracentifuged for 2 h at 100,000 g (Ultracentrifuge Sorvall WX100, Thermo Scientific, USA) to separate the liposomes from the free drug. All the obtained samples (non-filtrated, filtrated and centrifuged samples) were diluted and analized with UPLC. The encapsulation efficiency (EE) was calculated as follows:

$$EE(\%) = \frac{SIM\ (filtrated\ sample) - SIM\ (surnatant)}{SIM\ (initial\ sample)}$$

2.3 UPLC analysis

All the samples were analyzed using an UPLC method described by Pohlen et al. [191]. SIM was determined by the chromatographic system Acquity UPLC (Waters Corp., USA). A UV–VIS photodiode array (PDA) module equipped with a high sensitivity flow cell was used for detection. The column used was a reverse phase column Acquity UPLC BEH C18 1.7 µm; 2.1 × 100 mm (Waters Corp., USA). A gradient elution was used containing mobile phase A (water, containing 0.1% formic acid and 10% acetonitrile) and mobile phase B (98% acetonitrile, 2% water). The gradient method was the following: start at 50:50 (A:B); 0 – 6 min, 50:50 – 40:60; 6 – 7 min, 40:60; 7 – 8 min, 40:60 – 50:50; 8 – 10 min, 50:50. The flow rate was set at 0.3 mL/min and the column temperature was kept at 45 °C. The auto-sampler temperature was set at 10 °C. The injection volume was 5 µL and the run time was 10 min. SIM was detected at the wavelength of 238 nm.

2.4 Electrospinning of nanofibers mats

The polymeric solutions were prepared at a total polymer concentration of 3.75% (w/w) by dissolving sodium alginate and PEO (weight ratio 80:20) in water – in case of the empty nanofibers (EMPTY-NF) – or using three chosen liposomal dispersions (0, 0.6 and 1.2 -BHA SIM LIPO) to obtain liposomes-loaded nanofibers, respectively: 0-BHA SIM LIPO-NF, 0.6-BHA SIM LIPO-NF and 1.2-BHA SIM LIPO-NF). The solutions were left stirring overnight at room temperature and then placed in a plastic syringe, fixed into the electrospinning machine (Fluidnatek LE100; BioInicia SL, Valencia, Spain). The flow rate of the electrospinning solution was 600 ± 200 µL and the applied voltage was 22 ± 2 kV. In case of the solutions with BHA, an additional negative voltage of -5 ± 2 kV was applied on the collector. The distance between the needle and the grounded flat collector was 15 cm, and a cycling option in the y axis (100-200 mm, speed 8 mm/s) was used to obtain a homogeneous nanofiber mat. The whole process was carried out in a climatic chamber with a controlled environment of 37 ± 0.5 °C and 15% ± 2% relative humidity.

2.5 Electron microscopy analysis

The morphology of the electrospun products was evaluated using scanning electron microscopy (SEM). Samples were fixed with double sided adhesive and conductive tape onto metallic stubs. The morphology of the samples was observed using high resolution SEM (235 Supra 35VP-24-13; Carl Zeiss, Jena, Germany) operated at the increasing voltage of 1 kV at different magnifications. The average diameter (d) and its standard deviation (SD) were determined measuring at least 50 nanofibers randomly selected using the Image J 1.53e software (NHI, USA).

2.6 Determination of the drug content in the nanofibers

A known amount of sample (about 5 mg) was put in 5 mL of water and then put in an ultrasonic bath to allow the complete dissolution of the nanofiber mat. The obtained solution was diluted with methanol and then analyzed with UPLC. The drug loading (DL) in the nanofibers was determined according to the following equation:

$$DL\ (\%) = \frac{mass\ of\ measured\ SIM}{mass\ of\ added\ lipids\ and\ polymers + mass\ of\ measured\ SIM}\ x\ 100\%$$

The drug entrapment efficiency (DEE) was calculated according to the ratio of the experimental to the theoretical drug content in the nanofibers:

$$DEE\ (\%) = \frac{experimental\ DL}{theoretical\ DL}\ x\ 100\%$$

2.7 Solubility studies

Prior drug release studies, SIM solubility in the buffer solutions was investigated. The phosphate buffer solution was prepared by dissolving 3.39 g of $NaH_2PO_4 \bullet H_2O$ and 10.70 g of anhydrous Na_2HPO_4 in water. The pH was then adjusted to 7.4 and the solution was made up to 1 L with water. To perform the sink conditions experiments, 0.2% (w/v) sodium dodecyl sulphate (SDS) was added to the phosphate buffer. For the solubility study, an excess amount of drug powder was added to both buffers. The vials were shaken at 150 rpm at 37 °C, and after 48 h, 2 mL were taken, immediately filtered through a 0.22 µm syringe filter, diluted and analyzed using UPLC.

2.8 Release studies

SIM release studies were performed under sink and non-sink conditions using phosphate buffer with SDS and phosphate buffer, respectively, as release medium described in the section 2.6. Nanofibers mats of approximately 10 mg were immersed in 15 mL of release medium. The glass vials were shaken at 150 rpm at 37 °C throughout the test. At predetermined time points, 0.5 mL medium was withdrawn and replenished with fresh medium for the sink conditions test, whereas 2 mL of medium were withdrawn without replenishment for the non-sink conditions test. The samples were immediately filtered, diluted and analyzed using UPLC. The release was calculated as follows:

$$Drug\ release\ (\%) = \frac{drug\ released\ (\mu g)}{drug\ loading\ (\%) \times NF\ mass\ (mg) \times 1000} \times 100\ \%$$

2.9 Investigation of the liposome formation after nanofibers dissolution

Zetasizer Ultra (Malvern Instrument, UK) was used to investigate the formation of liposomes after dissolution of the nanofibrous samples through the Multi Angle Dynamic Light Scattering (MADLS®) and the Particle Concentration technique following the manufacturer's instructions [192], [193]. To this purpose, EMPTY-NF of approximately 1.22 mg (which correspond to the same mass of polymers in 5 mg of LIPO-NF) were dissolved in 5 mL of water and analysed using a backscatter analysis, in order to evaluate the dispersant scattering count rate. The three LIPO-NF samples were then dissolved in water and analysed through the coupled MADLS®-Particle Concentration technique, setting the obtained dispersant scattering count rate as background scattering. The instrument automatically removes the dispersant-background scattering contribution and measures the particle size distribution using MADLS® with the detection angles of 12.8, 90.0, 174.7°.

2.10 Stability study

The prepared nanofibrous scaffolds (with and without BHA) were stored for one month at room conditions (25 °C, 30% RH) and for 20 days in a humidity chamber (40 °C, 75% RH) to simulate accelerated conditions [190]. After this period, the samples were then analyzed as described in the section 2.6 to evaluate the drug chemical stability. The degradation rate in the samples was calculated as the relative content of SIM as described:

$$Drug\ content\ (\%) = \frac{drug\ content\ (t = n)}{drug\ content\ (t = 0)} \times 100\ \%$$

2.11 *In vitro* cell tests

Different formulations with SIM and without it were tested on cells to determine the effect of each component and formulations, which were: SIM, BHA, physical mixture of the ingredients (SIM-BHA mix), EMPTY-LIPO, 0-BHA SIM LIPO, 1.2-BHA LIPO, 1.2-BHA SIM LIPO, EMPTY-NF, 0-BHA SIM LIPO-NF, 1.2-BHA SIM LIPO-NF. Due to insolubility of SIM 0.2 % of DMSO was added to solubilize the highest concentrations of simvastatin. The nanofiber

samples were weighed and then dissolved in vials filled with 50 % FBS serum in DMEM and after disintegration the liquid was sampled and diluted to be added to the test wells.

Cytotoxicity study

Human keratinocyte (HaCat) cells were seeded at a density of 5,000 cells per well in a 96-well tissue culture plate (TPP, CH) in DMEM media and incubated overnight at 37 °C to facilitate adherence. Then cells were treated with SIM formulations at different concentrations 0, 0.4, 4, 40 and 400 µg/ml (the amount of empty formulations were the same as in formulations with SIM) 72 h and 0,2 % of DMSO was added. After incubation MTS assay reagent, 3-(4,5-dimethylthiazol-2-yl)-5-(3carboxymethoxyphenyl)-2-(4-sulfophenyl)-2H-tetrazolium) (Promega, Madison, WI, USA) was added. After 4 h of incubation at 37 °C, absorbance was measured using microplate reader (Agilent BioTek Synergy H4, CA, USA). Viability of treated cells was calculated relative to the untreated cells.

Keratinocyte proliferation assay

The proliferation of keratinocytes was measured the same as cytotoxicity study but multiple timepoints were introduced. The proliferation was measured at 40 µg/ml in final solution at 24 h, 48 h and 72 h using the same protocol as above.

Lymphocyte proliferation inhibition assay

Lymphocytes in 96-well plates were treated with different formulations in two parallels with phytohemagglutinin (PHA) a polyclonal lymphocyte activator and without PHA and then cultured for 72 h at 37 °C in a 5% CO_2 incubator. Ten microliters of the MTS solution were added to each well, and the plates were incubated for another 4 h. The absorbance at 490 nm was measured using a microplate reader (Agilent BioTek Synergy H4, CA, USA). The proliferation inhibition was calculated with the equation:

$$\%\ \text{Proliferation Inhibition} = \frac{\text{Mean OD}_{\text{Positive Control}} - \text{Mean OD}_{\text{Positive Control + Formulation}}}{\text{Mean OD}_{\text{Positive Control}} - \text{Mean OD}_{\text{Untreated Cells}}} \times 100\%$$

2.12 Statistical analysis

All of the experiments were performed at least in triplicate and data are presented as means ± SD. Multiple comparisons of means (one-way ANOVA, post-hoc Tukey HSD) were used to substantiate statistical differences between groups, while Student's t-test was used

to compare two samples. Data analysis was carried out with the software package XLStatistic for Microsoft Excel. Significance was tested at 0.05 level of probability (p).

Release profiles from the nanofiber mats were compared using the statistically derived mathematical parameter known as the similarity factor (f_2):

$$f_2 = 50 \times \log \left\{ \left[1 + \frac{1}{n} \sum_{t=1}^{n} (S_{1t} - S_{2t})^2 \right]^{-0.5} \times 100) \right\}$$

where n is the number of time points, S_{1t} is the released percentage of drug in sample 1, and S_{2t} is the released percentage of drug in sample 2, at time t. Evaluation of the release profiles was performed using the exacted same time points and was concluded at the first sampling time where the drug release was ≥ 85%. As highlighted by the US Food and Drug Administration and the European Medicines Agency, when the f_2 value is between 50 and 100 the sameness or equivalence of the two curves is confirmed [194], [195].

3 Results and discussion

3.1 Optimization of the liposomal formulations

To develop the optimal liposomal formulation with high SIM loading and content and small size of liposomes, different formulations with increasing concentrations of SIM and soy phosphatidylcholine were prepared in a preliminary study (data not shown). Liposomes with concentration of 100 mg/mL P90G and 20 mg/mL SIM resulted to be the most promising formulation with average diameter of 65.1 ± 0.8 nm, zeta potential of -14 ± 3 mV and very high encapsulation efficiency of 96 ± 5 % (Table 2). Since SIM concentration in dispersion was near the theoretical one (20 mg/mL), none or minimal drug degradation occurred during the sonication process.

To prevent oxidative degradation of SIM, formulations with fixed concentration of phospholipid and SIM, and increasing concentration of BHA were prepared. BHA is a synthetic antioxidant commonly added to food, cosmetics, and other products to prevent oxidative degradation [190], [196]. Increasing the antioxidant concentration leads to a slight increase of the average diameter of the obtained vesicles, ranging from 65.09 nm (0 mg/mL BHA) to 105.87 nm (1.2 mg/mL BHA). Nevertheless, even the formulation with the higher amount of BHA was characterized by a narrow size distribution. All the formulations showed negative zeta potential and high values of encapsulation efficiency, which became lower as the concentration of the antioxidant was augmented.

Table 2. Characterization of the different liposomal formulations.

sample	Average diameter (nm)	PDI	ZP (mV)	EE (%)
0-BHA SIM LIPO	65.1 ± 0.8	0.19 ± 0.01	-14 ± 3	96 ± 5
0.3-BHA SIM LIPO	73.6 ± 4.0	0.16 ± 0.01	-16 ± 1	88 ± 3
0.6-BHA SIM LIPO	77.9 ± 1.2	0.16 ± 0.01	-18 ± 1	88 ± 5
0.9-BHA SIM LIPO	86.4 ± 4.6	0.18 ± 0.01	-21 ± 2	82 ± 5
1.2-BHA SIM LIPO	105.9 ± 4.4	0.17 ± 0.01	-18 ± 3	80 ± 4

3.2 Optimization of the nanofibrous scaffolds

Alginate was chosen as biopolymer due to its appropriate properties, such as biocompatibility and non-toxicity. Moreover, dry alginate dressings are able to absorb wound fluids and form a gel-like system that can maintain a physiologically moist environment, reduce bacterial contaminations and facilitate the granulation tissue formation and a rapid re-epithelialization [174], [197]. Since its electrospinning is challenging, due to its polyelectrolyte nature and chain conformation characteristics [198], [199], a blend polymer solution of alginate and PEO was used.

A preliminary study was carried out to investigate the optimal solution parameters for the production of EMPTY-NF. Different polymer concentrations were prepared, namely 3, 3.25, 3.5, 3.75, 4 % (w/w), whereas the alginate/ PEO ratio was kept constant at 80:20 [200]. The electrospinning solutions with a total polymer concentration of 3 and 4% (w/w) were respectively not enough viscous, and too viscous to be electrospun. In the first case, the polymer solution was constantly dripping on the collector, with high jet instability that led to unsolidified polymer aggregates on the collector. In the second case, solidification of the polymer at the end of the nozzle occurred, preventing the Taylor cone formation and the consequent nanofibers production. SEM images (data not shown) revealed lower defects

and higher homogeneity of the sample obtained with the 3.75% (w/w) dispersion, which was then chosen to prepare the drug loaded nanofibers.

Since all the liposomal formulations exhibited promising characteristics, three of them were selected for the preparation of the polymeric solutions for electrospinning, namely 0, 0.6 and 1.2 -BHA SIM LIPO. The electrospinning of LIPO-NF resulted to be more challenging than the EMPTY-NF, and in case of the samples with the antioxidant (0.6-BHA SIM LIPO-NF and 1.2-BHA SIM LIPO-NF) an additional negative voltage on the collector was required to obtain an optimal Taylor cone and to maintain a stable process.

3.3 Characterisation of the nanofibrous scaffolds

Importantly, nanofibers were prepared by green electrospinning, which is a technique employed for the fabrication of biomaterials for tissue engineering and regenerative medicine, to reduce the drawbacks of organic solvents use, such as environmental safety and human toxicity issues due to residual solvents impurities [201], [202].

SEM micrographs of EMPTY-NF (**Figure 1**a) showed smooth and beadless nanofibers with a homogeneous morphology and an average diameter of 159.8 ± 25.2 nm. In contrast, when the liposomal dispersions were used (instead of water) as vehicle for the polymeric solutions preparation, the LIPO-NF (**Figure 1**b-d) appeared with a widen and irregular shape, with some areas of fusion between the single fibers. This might be due to the presence of the phospholipid itself and of liposomes incorporated in the fibers structure, as highlighted with white arrows in the Figure 1d, which also affected the nanofibers diameter distribution. Likewise, this particular structure was observed by Mickova et al., where liposomes were incorporated in core-shell nanofibers of PCL/PVA [203]. The average nanofiber diameter of 0-BHA SIM LIPO-NF was found to be 273.3 ± 64.6. However, the addition of BHA further increased the nanofiber diameter to 315.4 ±79.0 nm for the 0.6-BHA SIM LIPO-NF, and 311.6 ±88.5 nm for the 1.2-BHA SIM LIPO-NF (Table 3).

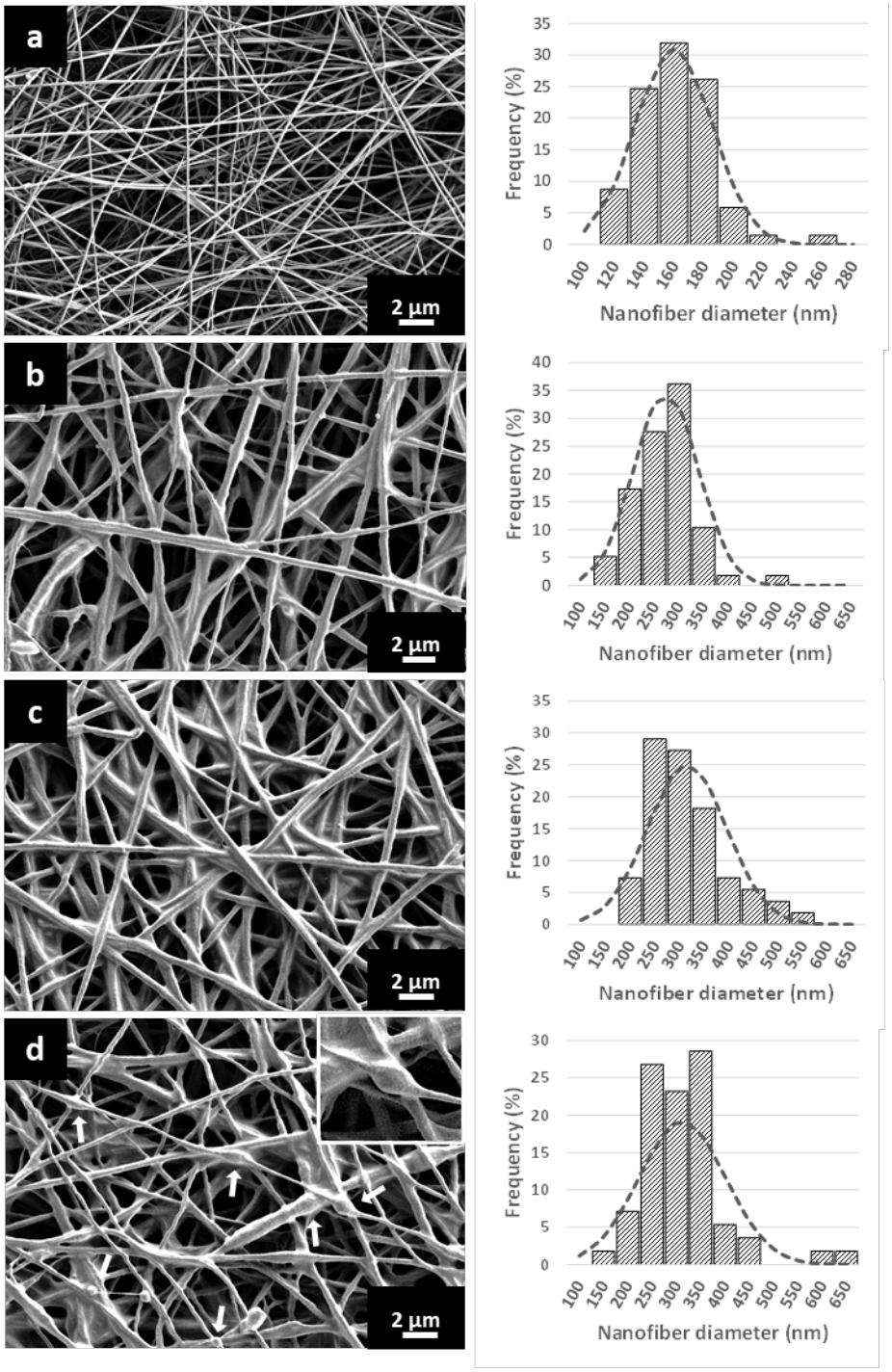

Figure 1. SEM images (LEFT) and diameter distribution (RIGHT) of 3.75% (w/w) alginate/PEO nanofibers as: a) EMPTY-NF, b) 0-BHA SIM LIPO-NF, c) 0.6-BHA SIM LIPO-NF, d) 1.2-BHA SIM LIPO-NF. White arrows represent the liposomes incorporated in the nanofibers.

The nanofibers were composed of theoretically 62.9 % of P90G, 24.5 % of polymers and 12.6% of SIM, presenting a very high content of both, phospholipids and drug. The experimental DL was slightly lower than the theoretical one and all the three formulations reached a drug entrapment efficiency of approximately 80% (Table 3). In particular, the BHA-

loaded samples showed average values slightly lower than the 0-BHA SIM LIPO-NF. However, statistical analysis revealed no significance difference among the results obtained with the three samples.

Table 3. Characterization of the nanofibrous samples in terms of nanofiber diameter (nm), drug loading (% w/w), and entrapment efficiency (%). Each symbol (*, §) indicates couple of values statistically different.

	nanofiber diameter (nm)	DL (% (w/w))	DEE (%)
EMPTY-NF	159.8 ± 25.2	-	-
0-BHA SIM LIPO-NF	273.3 ± 64.6 * §	10.61 ± 0.28	83.6 ± 2.4
0.6-BHA SIM LIPO-NF	315.4 ±79.0 *	10.38 ± 0.45	80.9 ± 3.5
1.2-BHA SIM LIPO-NF	311.6 ±88.5 §	10.41 ± 0.27	81.3 ± 2.0

3.4 Release tests

SIM release from the nanofibrous scaffolds was evaluated under sink and non-sink conditions. The European Pharmacopoeia defines the sink conditions as a volume of release medium that is at least 3-10 times greater than the saturation volume [204]. SIM solubility in phosphate buffer 7.4 (non-sink release medium) was found to be 22.56 ± 1.72 µg/mL, whereas in phosphate buffer 7.4 + 0.2 % (w/v) (sink release medium), it was 717.69 ± 11.54 µg/mL. The highest theoretical SIM concentration achievable in release medium was 70 µg/mL in both cases, therefore, both release conditions were achieved. The release profiles of the three formulations are shown in the Figure 2.

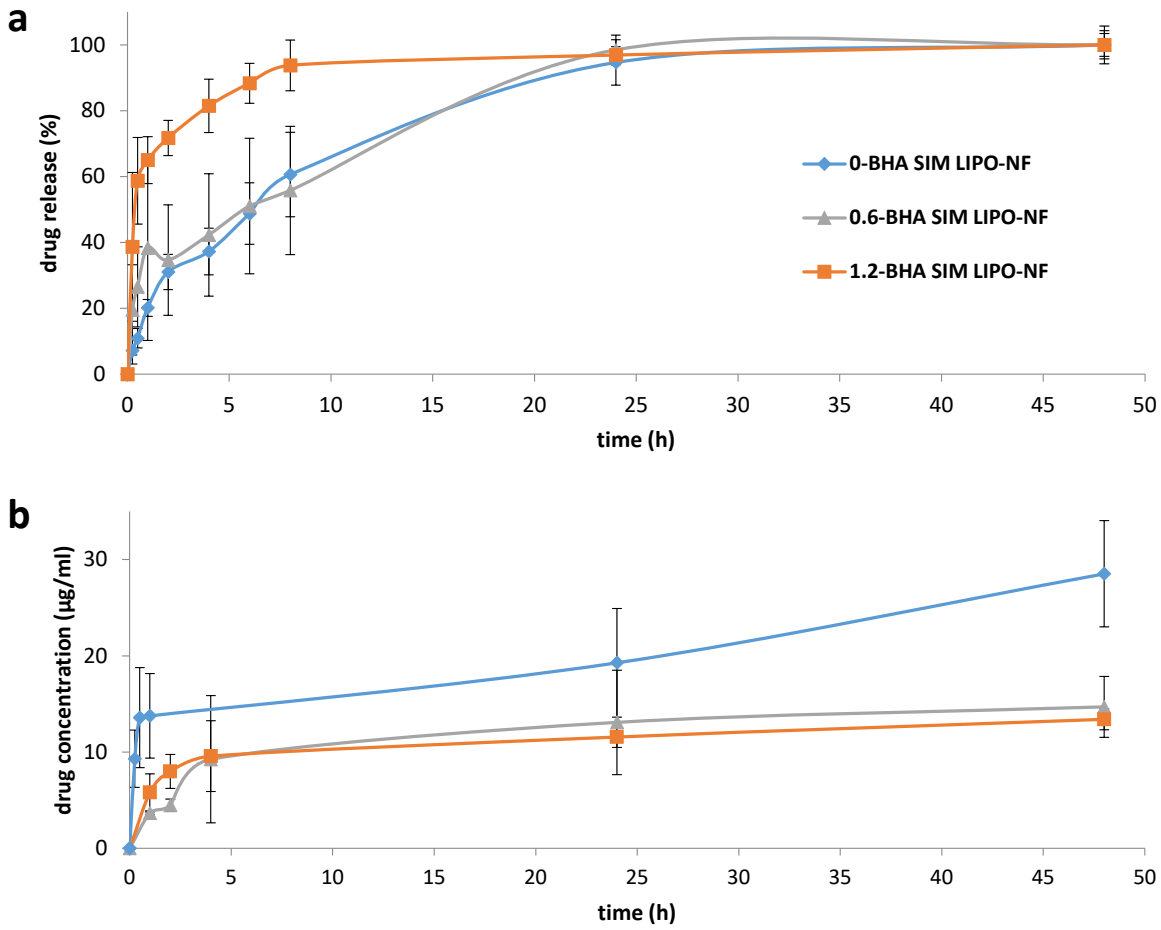

Figure 2. Release profiles of the three drug-loaded liposomes nanofibers under a) sink conditions expressed as % of SIM released over time, and b) non-sink conditions expressed as SIM concentration.

0-BHA SIM LIPO-NF and 0.6-BHA SIM LIPO-NF showed a similar release profile under sink conditions, releasing approximately 50% SIM between 5 and 6 h, and reaching 100% of released drug after 24 h. On the other hand, 1.2-BHA SIM LIPO-NF exhibited a faster release with almost 70% SIM released after 1 h. As concerns the non-sink conditions, 0-BHA SIM LIPO-NF displayed a higher SIM release than the other two samples, reaching an average concentration of 28.5 ± 5.5 (µg/ml) after 48 h, which was not statistically different from the saturation solubility value. On the other hand, BHA seems to decrease SIM solubility in the BHA-loaded samples, where after 48 h the concentration was 14.7 ± 3.2 and 13.4 ± 1.1 µg/ml, for 0.6-BHA SIM LIPO-NF and 1.2-BHA SIM LIPO-NF respectively. A similar result was highlighted by Zorec et al., where BHA decreased SIM solubility in PVP nanoparticles [190]. To better understand the release profiles and to compare the different samples, the similarity factor (f_2) was calculated (**Table 4**). The similarity factor is described as a

logarithmic reciprocal square root transformation of one plus the mean squared (the average sum of squares) differences of drug percent dissolved between the test and the reference products, or two test products. It can vary between 0 and 100 and values higher than 50 reveal similarity of the release profiles. The analysis confirmed the similarity of SIM release in sink conditions from 0-BHA SIM LIPO-NF and 0.6-BHA SIM LIPO-NF, showing a f_2 value of 50. Moreover, a similar profile was also highlighted between 0.6-BHA SIM LIPO-NF and 1.2-BHA SIM LIPO-NF under non-sink conditions, with a f_2 value of 77.

Table 4. Similarity factor (f_2) of the release profiles of the three formulations under sink and non-sink conditions.

f_2	**0-BHA SIM LIPO-NF** ***vs*** **0.6-BHA SIM LIPO-NF**	**0-BHA SIM LIPO-NF** ***vs*** **1.2-BHA SIM LIPO-NF**	**0.6-BHA SIM LIPO-NF** ***vs*** **1.2-BHA SIM LIPO-NF**
sink conditions	50	19	24
non-sink conditions	45	45	77

3.5 Investigation of the liposome formation after nanofibers dissolution

As highlighted by the SEM micrographs, some spheres-like systems were observed in the nanofibers structures, allegedly SIM liposomes. To confirm our hypothesis, the innovative Particle Concentration technique coupled with MADLS® was used. MADLS® is a high-resolution technique that works by combining scattering information from multiple angles (backscatter, side scatter and forward scatter), providing a better insight in the particle size distribution of the sample. Particle concentration can be considered as an extension of MADLS® to give the total particle concentration and the particle concentration of each size population [192], [205] and thus, it has gained remarkable importance in the characterization of micro and nano-sized systems [206]–[213]. Prior to the experiments, EMPTY-NF were dissolved in water to obtain the background dispersant scattering value. The LIPO-NF samples were then dissolved and analysed. The results are shown in the Table 5.

Table 5. MADLS and particle concentration results of the dissolved LIPO-NF samples.

	MADLS		particle concentration (particle/mL)	
	Peak 1 (nm)/ % intensity	**Peak 2 (nm)/ % intensity**	**Peak 1**	**Peak 2**
0-BHA SIM LIPO-NF	135.6/44.5 ± 7.2	432.2/39.0 ± 11.8	1.24E+12	2.46E+10
0.6-BHA SIM LIPO-NF	154.2/44.6 ± 12.0	438.0/45.7 ± 5.2	3.17E+10	1.31E+11
1.2-BHA SIM LIPO-NF	141.2/33.2 ± 6.6	436.3/48.8 ± 6.4	1.11E+09	2.12E+12

As it can be seen by the analysis, two main size populations were formed highlighted. One is characterized by an average diameter of approximately 430 nm, whereas the other varies between 135 and 154 nm. The % intensity of the two peaks slightly varies, showing none or low predominance of one population over the other one. From these results, it can be hypothesised the formation of two populations of liposomes after nanofibers dissolution.

3.6 Chemical stability of SIM in the nanofibrous scaffolds

SIM is well known as unstable molecule for its oxidative degradation, hence antioxidants ingredients have often been used in different formulations to prevent or reduce this process [190], [196], [214]. To this purpose, the chemical stability of SIM in the different nanofibrous formulations with increasing concentration of BHA was evaluated (Figure 3).

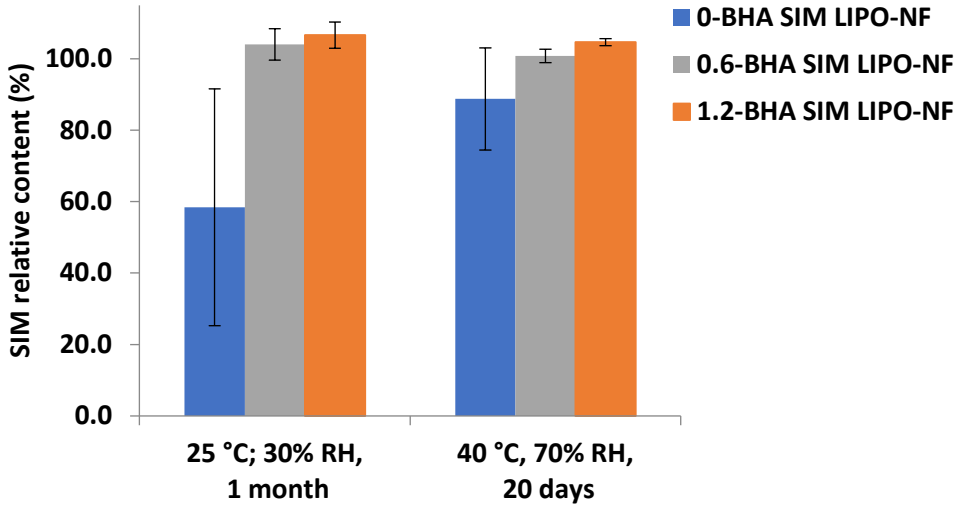

Figure 3. SIM relative content for the three nanofibrous formulations expressed as relative drug content of after production and after one month at room conditions, or 20 days at accelerated conditions.

The three formulations were exposed to room temperature with low humidity on one hand, and to accelerated stability conditions on the other. SIM degradation was observed in the 0-BHA SIM LIPO-NF in both room and accelerated conditions, and the relative drug content was respectively 58.4% and 88.8%. However, as shown by the standard deviation, there was a high variability among replicates. On the other hand, BHA acts by protecting the active ingredient from degradation in both samples – 0.6-BHA SIM LIPO-NF and 1.2-BHA SIM LIPO-NF – where the average relative drug content is maintained at values of approximately 100% for all the replicates (low standard deviation).

3.7 *In Vitro* tests

Safety of the formulations in mammalian cells was evaluated against human keratinocyte cells (HaCat) by MTS assay. The formulations did not show any toxicity up to 40 µg/ml of simvastatin. The results on **Figure 4**a demonstrate that half maximal inhibitory concentrations (IC50) are: EMPTY-LIPO ~ 1998 µg/ml; 0-BHA SIM LIPO ~ 47.16 µg/ml; 1.2-BHA SIM LIPO ~ 9.48 µg/ml; 0-BHA SIM LIPO-NF ~ 322,7 µg/ml and 1.2-BHA SIM LIPO-NF ~ 392,1 µg/ml required to inhibit 50% of HaCat cells.

Proliferation induction of keratinocytes by final formulations (40 µg/ml of SIM in formulations 0-BHA SIM LIPO-NF and 1.2-BHA SIM LIPO-NF) was subtle and not consistent through different time points shown on **Figure 4**b. A statistically significant increase in

proliferation can be seen at 24 h in formulation 1.2-BHA SIM LIPO-NF, but the trend does not continue in the next timepoints. The same is true for formulation 0-BHA SIM LIPO-NF only the value is increased at 72 h but not before.

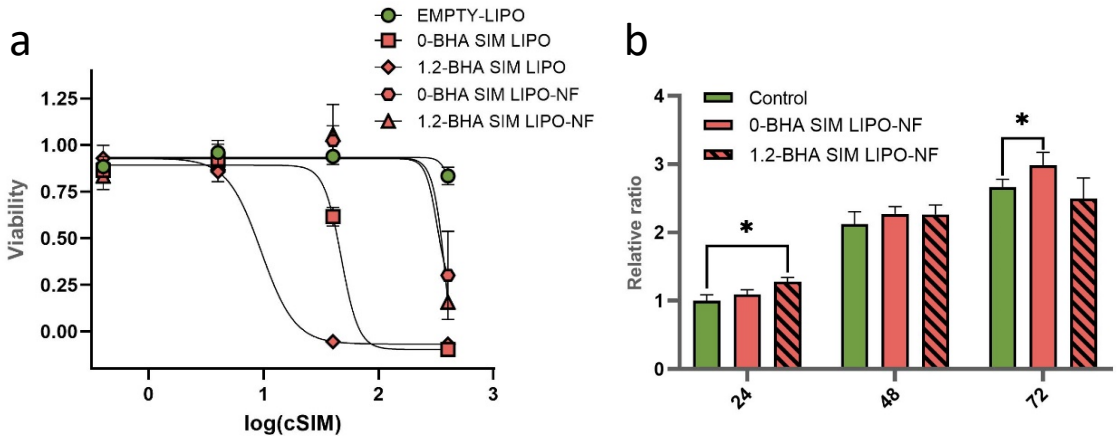

Figure 4. Keratinocyte a) LC50 curves and b) proliferation with different formulations.

SIM alone and incorporated in different formulations has proven to inhibit lymphocyte proliferation in a PHA stimulated environment Figure 5. The largest inhibition effect can be seen in the liposomal formulation 1.2-BHA SIM LIPO: 445.12 % compared to the control sample. Some inhibition can be observed in EMPTY-LIPO and 1.2-BHA LIPO, but it is significantly lower than the SIM-loaded liposomal formulations. As concerns the nanofibrous formulations, it is clear that EMPTY-NF does not significantly decrease lymphocyte proliferation, whereas the inhibition provided by 0-BHA SIM LIPO-NF and 1.2-BHA LIPO-NF is 356.50 % and 315.85 % respectively.

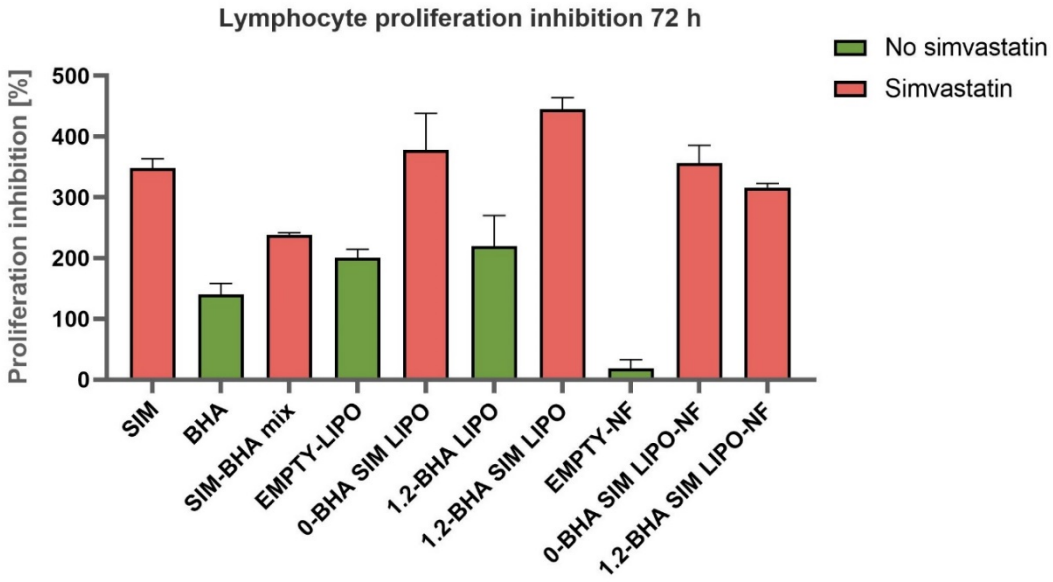

Figure 5. Lymphocyte proliferation inhibition after 72h with different formulations.

4 Conclusion

In this study, different SIM-loaded liposomal formulations with increasing concentrations of the antioxidant compound BHA were successfully prepared and characterized. The resulting phospholipid vesicles were small in size and homogeneously dispersed, showing high values of EE%. Using three selected SIM-loaded liposomal formulations, with 0, 0.6 and 1.2 mg/mL BHA respectively, liposome-scaffold composite systems were efficiently produced using a green electrospinning technique. The obtained nanofibrous samples, made of alginate/PEO, showed an average diameter ranging from 273 to 311 nm, in the different samples. Release studies in sink conditions showed a faster release rate for the formulation with the higher concentration of antioxidant, and a slower and similar release for the two other formulations. SEM images showed embedded liposomes in the nanofibers structure and their release after nanofibers dissolution was confirmed through MADLS® analysis, showing two main size population of approximately 144 ± 10 and 436 ± 2 nm. *In vitro* tests revealed that the formulations were not cytotoxic on human keratinocyte cells and were able to inhibit lymphocyte proliferation in a PHA stimulated environment. The overall results showed that the combination of the two nanotechnological approaches led to the production of biocompatible and more functional scaffolds, optimal as dressing systems for chronic wound healing. In fact, drug incorporation in liposomes allows a high content of SIM in the nanofibrous system, avoiding the use of organic solvents, and the morphology of nanofibers themselves provides the desired mechanical support. Moreover, it is reasonable to believe that the liposomes-embedded nanofibrous scaffolds helps drug retain a certain concentration in situ for a longer period than with liposomes local application alone.

General conclusions

Anti-inflammatory drugs are widely used for pain management and inflammation resolution. However, a large number of these drugs are characterized by poor water solubility which can lead to low bioavailability and suboptimal drug delivery. Therefore, in this thesis different nanotechnological approaches were investigated to overcome the drug delivery limits of conventional formulations.

Part 1 target was the production of nanosuspension for inhalation drug delivery for the treatment of pulmonary inflammatory conditions. In the two chapters of this part, nanocrystals suspensions were efficiently prepared with a wet media milling technique and the resulting nanocrystals were small in size and homogeneously dispersed, showing an increased solubility compared to the bulk drug. In Chapter 1, the ability an electronic cigarette to deliver drug nanocrystals with the produced aerosol of was confirmed through TEM, DLS and HPLC results, highlighting the opportunity of using it as an alternative medical device for poorly soluble drugs. This section presents the first report (to the best of our knowledge) of a combined use of a commercial ENDS with a nanosuspension formulation. In Chapter 2, a multicomponent nanosuspension of a conventional glucocorticoid drug and a natural active compound as adjuvant showed optimal aerodynamic parameters, proving to be a promising formulation for an efficient delivery in the deeper lung regions.

In Part 2 of the thesis, a liposomes-nanofibrous composite scaffold was developed by combining two different technological approaches, namely liposomes and nanofibers. Liposomes with high values of encapsulation efficiency, prepared using a direct sonication method, allowed the production of more functional scaffolds through a green electrospinning technique. The obtained composite samples revealed optimal release profiles, *in vitro* biocompatibility and immunomodulatory activity.

The different approaches investigated in the two parts of this thesis highlight the great versatility of the nano-based drug delivery systems, which can be efficiently used to improve drug bioavailability, safety and patient compliance, guaranteeing excellent therapeutic performances.

References

[1] S. Krishnamoorthy and K. V. Honn, “Inflammation and disease progression,” *Cancer Metastasis Rev.*, vol. 25, no. 3, pp. 481–491, Nov. 2006, doi: 10.1007/s10555-006-9016-0.

[2] P. Libby, “Inflammatory Mechanisms: The Molecular Basis of Inflammation and Disease,” *Nutr. Rev.*, vol. 65, no. 12, pp. 140–146, Dec. 2007, doi: 10.1301/nr.2007.dec.s140-s146.

[3] P. M. Henson, “Dampening Inflammation,” *Nat. Immunol.*, vol. 6, no. 12, pp. 1179–1181, 2005.

[4] C. N. Serhan, N. Chiang, and T. E. Van Dyke, “Resolving inflammation: Dual anti-inflammatory and pro-resolution lipid mediators,” *Nat. Rev. Immunol.*, vol. 8, no. 5, pp. 349–361, 2008, doi: 10.1038/nri2294.

[5] A. U. Ahmed, “An overview of inflammation: Mechanism and consequences,” *Front. Biol. China*, vol. 6, no. 4, pp. 274–281, 2011, doi: 10.1007/s11515-011-1123-9.

[6] S. Akira, S. Uematsu, and O. Takeuchi, “Pathogen recognition and innate immunity,” *Cell*, vol. 124, no. 4, pp. 783–801, Feb. 2006, doi: 10.1016/J.CELL.2006.02.015.

[7] R. Medzhitov, “Recognition of microorganisms and activation of the immune response,” *Nature*, vol. 449, no. 7164, pp. 819–826, Oct. 2007, doi: 10.1038/NATURE06246.

[8] J. W. Christman, R. T. Sadikot, and T. S. Blackwell, “The role of nuclear factor-κ B in pulmonary diseases,” *Chest*, vol. 117, no. 5, pp. 1482–1487, 2000, doi: 10.1378/chest.117.5.1482.

[9] A. D. Luster, R. Alon, and U. H. Von Andrian, “Immune cell migration in inflammation : present and future therapeutic targets,” vol. 6, no. 12, pp. 1182–1190, 2005, doi: 10.1038/ni1275.

[10] C. Nathan, “Points of control in inflammation,” *Nature*, vol. 420, no. 6917, pp. 846–852, 2002, doi: 10.1038/nature01320.

[11] T. L. Moore and T. D. Weiss, “Mediators of inflammation,” *Semin. Arthritis Rheum.*, vol. 14, no. 4, pp. 247–262, 1985, doi: 10.1016/0049-0172(85)90044-7.

[12] M. White, “Mediators of inflammation and the inflammatory process,” *J. Allergy Clin. Immunol.*, vol. 103, no. 3 SUPPL., pp. 378–381, 1999, doi: 10.1016/S0091-

6749(99)70215-0.

[13] L. A. Abdulkhaleq, M. A. Assi, R. Abdullah, M. Zamri-Saad, Y. H. Taufiq-Yap, and M. N. M. Hezmee, “The crucial roles of inflammatory mediators in inflammation: A review,” *Vet. World*, vol. 11, no. 5, pp. 627–635, 2018, doi: 10.14202/vetworld.2018.627-635.

[14] H. Z. Movat, “The role of histamine and other mediators in microvascular changes in acute inflammation,” *Can. J. Physiol. Pharmacol.*, vol. 65, no. 3, pp. 451–457, 1987, doi: 10.1139/y87-077.

[15] G. MAJNO and G. E. PALADE, “Studies on inflammation. 1. The effect of histamine and serotonin on vascular permeability: an electron microscopic study.,” *J. Biophys. Biochem. Cytol.*, vol. 11, no. 3, pp. 571–605, Dec. 1961, doi: 10.1083/jcb.11.3.571.

[16] J. N. Sharma and S. S. J. Mohsin, “The role of chemical mediators in the pathogenesis of inflammation with emphasis on the kinin system,” *Exp. Pathol.*, vol. 38, no. 2, pp. 73–96, Jan. 1990, doi: 10.1016/S0232-1513(11)80241-0.

[17] J. M. Zhang and J. An, “Cytokines, Inflammation and Pain,” *Int. Anesthesiol. Clin.*, vol. 45, no. 2, p. 27, Mar. 2007, doi: 10.1097/AIA.0B013E318034194E.

[18] A. Cerami, “Inflammatory cytokines,” *Clin. Immunol. Immunopathol.*, vol. 62, no. 1 PART 1, pp. S3–S10, Jan. 1992, doi: 10.1016/0090-1229(92)90035-M.

[19] C. A. Dinarello, “Proinflammatory cytokines,” *Chest*, vol. 118, no. 2, pp. 503–508, Aug. 2000, doi: 10.1378/chest.118.2.503.

[20] S. M. Opal and V. A. DePalo, “Anti-Inflammatory Cytokines,” *Chest*, vol. 117, no. 4, pp. 1162–1172, Apr. 2000, doi: 10.1378/CHEST.117.4.1162.

[21] D. Rossi and A. Zlotnik, “The biology of chemokines and their receptors,” *Annual Review of Immunology*, vol. 18. Annual Reviews 4139 El Camino Way, P.O. Box 10139, Palo Alto, CA 94303-0139, USA, pp. 217–243, Nov. 28, 2000, doi: 10.1146/annurev.immunol.18.1.217.

[22] A. Viola and A. D. Luster, “Chemokines and their receptors: Drug targets in immunity and inflammation,” *Annual Review of Pharmacology and Toxicology*, vol. 48. Annual Reviews, pp. 171–197, Jan. 09, 2008, doi: 10.1146/annurev.pharmtox.48.121806.154841.

[23] W. R. Henderson, “Lipid-derived and other chemical mediators of inflammation in the lung,” *J. Allergy Clin. Immunol.*, vol. 79, no. 4, pp. 543–553, Apr. 1987, doi:

10.1016/S0091-6749(87)80146-X.

[24] S. Palumbo, “Pathogenesis and Progression of Multiple Sclerosis: the Role of Arachidonic Acid-mediated Neuroinflammation,” *Exon Publ.*, pp. 111–123, Nov. 2017, doi: 10.15586/CODON.MULTIPLESCLEROSIS.2017.CH7.

[25] C. D. Funk, “Prostaglandins and leukotrienes: Advances in eicosanoid biology,” *Science (80-.).*, vol. 294, no. 5548, pp. 1871–1875, 2001, doi: 10.1126/science.294.5548.1871.

[26] B. Kis, J. A. Snipes, S. A. Simandle, and D. W. Busija, “Acetaminophen-sensitive prostaglandin production in rat cerebral endothelial cells,” *Am. J. Physiol. - Regul. Integr. Comp. Physiol.*, vol. 288, no. 4 57-4, pp. 897–902, Apr. 2005, doi: 10.1152/AJPREGU.00613.2004/ASSET/IMAGES/LARGE/ZH60050526790004.JPEG.

[27] N. V. Chandrasekharan *et al.*, “COX-3, a cyclooxygenase-1 variant inhibited by acetaminophen and other analgesic/antipyretic drugs: Cloning, structure, and expression,” *Proc. Natl. Acad. Sci. U. S. A.*, vol. 99, no. 21, pp. 13926–13931, Oct. 2002, doi: 10.1073/pnas.162468699.

[28] J. J. Int *et al.*, “Prostaglandins as Potentiators of Increased Vascular Permeability in Inflammation,” *Nat. 1973 2465430*, vol. 246, no. 5430, pp. 215–217, 1973, doi: 10.1038/246215a0.

[29] B. Wang *et al.*, “Metabolism pathways of arachidonic acids: mechanisms and potential therapeutic targets,” *Signal Transduct. Target. Ther.*, vol. 6, no. 1, 2021, doi: 10.1038/s41392-020-00443-w.

[30] B. D. Levy, C. B. Clish, B. Schmidt, K. Gronert, and C. N. Serhan, “Lipid mediator class switching during acute inflammation: Signals in resolution,” *Nat. Immunol.*, vol. 2, no. 7, pp. 612–619, 2001, doi: 10.1038/89759.

[31] K. D. Rainsford, *Aspirin and related drugs*. 2004.

[32] K. D. Rainsford, “Anti-inflammatory drugs in the 21st century,” *Subcell. Biochem.*, vol. 42, pp. 3–27, 2007, doi: 10.1007/1-4020-5688-5_1.

[33] C. M. Wilcox, B. Cryer, and G. Triadafilopoulos, “Patterns of use and public perception of over-the-counter pain relievers: focus on nonsteroidal antiinflammatory drugs.,” *J. Rheumatol.*, vol. 32, no. 11, 2005.

[34] K. Brune and P. Patrignani, “New insights into the use of currently available non-steroidal anti-inflammatory drugs,” *Journal of Pain Research*, vol. 8. Dove Press, pp.

105–118, Feb. 20, 2015, doi: 10.2147/JPR.S75160.

[35] S. Bacchi, P. Palumbo, A. Sponta, and M. F. Coppolino, “Clinical pharmacology of non-steroidal anti-inflammatory drugs: a review,” *Antiinflamm. Antiallergy. Agents Med. Chem.*, vol. 11, no. 1, pp. 52–64, Oct. 2012, doi: 10.2174/187152312803476255.

[36] M. L. Capone, S. Tacconelli, L. Garcia Rodriguez, and P. Patrignani, “NSAIDs and cardiovascular disease: transducing human pharmacology results into clinical read-outs in the general population,” 2010.

[37] W. Ericson-Neilsen and A. D. Kaye, “Steroids: Pharmacology, Complications, and Practice Delivery Issues,” *Ochsner J.*, vol. 14, no. 2, p. 203, 2014, Accessed: Nov. 28, 2021. [Online]. Available: /pmc/articles/PMC4052587/.

[38] T. Rhen and J. A. Cidlowski, “Antiinflammatory Action of Glucocorticoids — New Mechanisms for Old Drugs,” *N. Engl. J. Med.*, vol. 353, no. 16, pp. 1711–1723, 2005, doi: 10.1056/nejmra050541.

[39] R. Y. Reins, S. D. Hanlon, S. Magadi, and A. M. McDermott, “Effects of topically applied Vitamin D during corneal wound healing,” *PLoS One*, vol. 11, no. 4, pp. 1–19, 2016, doi: 10.1371/journal.pone.0152889.

[40] P. J. Barnes and S. Pedersen, “Efficacy and safety of inhaled corticosteroids in asthma,” *Am. Rev. Respir. Dis.*, vol. 148, no. 4 SUPPL., 1993, doi: 10.1164/ajrccm/148.4_pt_2.s1.

[41] D. H. P. Streeten, “Corticosteroid Therapy: II. Complications and Therapeutic Indications,” *JAMA J. Am. Med. Assoc.*, vol. 232, no. 10, pp. 1046–1049, Jun. 1975, doi: 10.1001/jama.1975.03250100042028.

[42] S. Siebert, A. Tsoukas, J. Robertson, and I. McInnes, “Cytokines as therapeutic targets in rheumatoid arthritis and other inflammatory diseases,” *Pharmacol. Rev.*, vol. 67, no. 2, pp. 280–309, 2015, doi: 10.1124/pr.114.009639.

[43] T. O. B. Y. L. Awrence, D. E. W. G. Ilroy, P. A. U. L. R. C. O. Ash, and D. E. A. W. Illoughby, “Possible new role for NF-κB in the resolution of inflammation,” vol. 2, pp. 1291–1297, 2001.

[44] J. F. Schindler, J. B. Monahan, and W. G. Smith, “P38 pathway kinases as anti-inflammatory drug targets,” *J. Dent. Res.*, vol. 86, no. 9, pp. 800–811, Sep. 2007, doi: 10.1177/154405910708600902.

[45] A. de Prati *et al.*, "STAT1 as a New Molecular Target of Anti-Inflammatory Treatment," *Curr. Med. Chem.*, vol. 12, no. 16, pp. 1819–1828, Jul. 2005, doi: 10.2174/0929867054546645.

[46] C. A. Lipinski, "Drug-like properties and the causes of poor solubility and poor permeability," *J. Pharmacol. Toxicol. Methods*, vol. 44, no. 1, pp. 235–249, Jul. 2000, doi: 10.1016/S1056-8719(00)00107-6.

[47] M. Rodriguez-Aller, D. Guillarme, J. L. Veuthey, and R. Gurny, "Strategies for formulating and delivering poorly water-soluble drugs," *J. Drug Deliv. Sci. Technol.*, vol. 30, pp. 342–351, Dec. 2015, doi: 10.1016/J.JDDST.2015.05.009.

[48] S. Kalepu and V. Nekkanti, "Insoluble drug delivery strategies: review of recent advances and business prospects," *Acta Pharm. Sin. B*, vol. 5, no. 5, pp. 442–453, Sep. 2015, doi: 10.1016/J.APSB.2015.07.003.

[49] W. Badri, K. Miladi, Q. A. Nazari, H. Greige-Gerges, H. Fessi, and A. Elaissari, "Encapsulation of NSAIDs for inflammation management: Overview, progress, challenges and prospects," *Int. J. Pharm.*, vol. 515, no. 1–2, pp. 757–773, 2016, doi: 10.1016/j.ijpharm.2016.11.002.

[50] F. Lai, M. Schlich, R. Pireddu, F. Corrias, A. Fadda, and C. Sinico, "Production of nanosuspensions as a tool to improve drug bioavailability: focus on topical delivery," *Curr. Pharm. Des.*, vol. 21, no. 42, pp. 6089–6103, 2015, doi: 10.2174/1381612821666151027152350.

[51] R. Pireddu *et al.*, "Novel nanosized formulations of two diclofenac acid polymorphs to improve topical bioavailability," *Eur. J. Pharm. Sci.*, vol. 77, pp. 208–215, Sep. 2015, doi: 10.1016/J.EJPS.2015.06.006.

[52] C. Sinico and A. M. Fadda, "Vesicular carriers for dermal drug delivery," *Expert Opinion on Drug Delivery*, vol. 6, no. 8. pp. 813–825, Aug. 02, 2009, doi: 10.1517/17425240903071029.

[53] M. A. Iqbal, S. Md, J. K. Sahni, S. Baboota, S. Dang, and J. Ali, "Nanostructured lipid carriers system: Recent advances in drug delivery," *J. Drug Target.*, vol. 20, no. 10, pp. 813–830, 2012, doi: 10.3109/1061186X.2012.716845.

[54] F. Lai, C. Sinico, D. Valenti, M. L. Manca, and A. M. Fadda, "Nanoemulsions as Vehicle for Topical 8-Methoxypsoralen Delivery," *J. Biomed. Nanotechnol.*, vol. 4, no. 3, pp. 1–5, 2008, doi: 10.1166/jbn.2008.042.

[55] A. Amri *et al.*, “Resveratrol self-emulsifying system increases the uptake by endothelial cells and improves protection against oxidative stress-mediated death,” *Eur. J. Pharm. Biopharm.*, vol. 86, no. 3, pp. 418–426, 2014, doi: 10.1016/j.ejpb.2013.10.015.

[56] F. Lai *et al.*, “Trimethyl chitosan hydrogel nanoparticles for progesteronedelivery inneurodegenerativedisorders,” *Pharmaceutics*, vol. 11, no. 12, Dec. 2019, doi: 10.3390/pharmaceutics11120657.

[57] E. Larrañeta, M. T. C. McCrudden, A. J. Courtenay, and R. F. Donnelly, “Microneedles: A New Frontier in Nanomedicine Delivery,” *Pharm. Res.*, vol. 33, no. 5, pp. 1055–1073, 2016, doi: 10.1007/s11095-016-1885-5.

[58] Š. Zupančič *et al.*, “Sustained release of antimicrobials from double-layer nanofiber mats for local treatment of periodontal disease, evaluated using a new micro flow-through apparatus,” *J. Control. Release*, vol. 316, pp. 223–235, Dec. 2019, doi: 10.1016/j.jconrel.2019.10.008.

[59] L. Gao, D. Zhang, and M. Chen, “Drug nanocrystals for the formulation of poorly soluble drugs and its application as a potential drug delivery system,” *J. Nanoparticle Res.*, vol. 10, no. 5, pp. 845–862, May 2008, doi: 10.1007/s11051-008-9357-4.

[60] A. A. Noyes and W. R. Whitney, “The rate of solution of solid substances in their own solutions,” *J. Am. Chem. Soc.*, vol. 19, no. 12, pp. 930–934, Dec. 1897, doi: 10.1021/ja02086a003.

[61] B. E. Rabinow, “Nanosuspensions in drug delivery,” *Nat. Rev. Drug Discov.*, vol. 3, no. 9, pp. 785–796, 2004, doi: 10.1038/nrd1494.

[62] M. Mosharraf and C. Nyström, “The effect of particle size and shape on the surface specific dissolution rate of microsized practically insoluble drugs,” *Int. J. Pharm.*, vol. 122, no. 1–2, pp. 35–47, Aug. 1995, doi: 10.1016/0378-5173(95)00033-F.

[63] R. H. Müller and K. Peters, “Nanosuspensions for the formulation of poorly soluble drugs. I. Preparation by a size-reduction technique,” *Int. J. Pharm.*, vol. 160, no. 2, pp. 229–237, Jan. 1998, doi: 10.1016/S0378-5173(97)00311-6.

[64] V. K. Pawar, Y. Singh, J. G. Meher, S. Gupta, and M. K. Chourasia, “Engineered nanocrystal technology : In-vivo fate , targeting and applications in drug delivery,” *J. Control. Release*, vol. 183, pp. 51–66, 2014, doi: 10.1016/j.jconrel.2014.03.030.

[65] B. Sinha, R. H. Müller, and J. P. Möschwitzer, “Bottom-up approaches for preparing

drug nanocrystals: Formulations and factors affecting particle size," *International Journal of Pharmaceutics*, vol. 453, no. 1. Elsevier, pp. 126–141, Aug. 30, 2013, doi: 10.1016/j.ijpharm.2013.01.019.

[66] S. L. A. Hennart, P. van Hee, V. Drouet, M. C. Domingues, W. J. Wildeboer, and G. M. H. Meesters, "Characterization and modeling of a sub-micron milling process limited by agglomeration phenomena," *Chem. Eng. Sci.*, vol. 71, pp. 484–495, Mar. 2012, doi: 10.1016/J.CES.2011.11.010.

[67] M. Juhnke, J. Berghausen, and C. Timpe, "Accelerated Formulation Development for Nanomilled Active Pharmaceutical Ingredients Using a Screening Approach," *Chem. Eng. Technol.*, vol. 33, no. 9, pp. 1412–1418, Sep. 2010, doi: 10.1002/CEAT.201000062.

[68] D. D. Lasic and D. Papahadjopoulos, "Liposomes revisited," *Science (80-.).*, vol. 267, no. 5202, pp. 1275–1276, Mar. 1995, doi: 10.1126/SCIENCE.7871422/ASSET/3A787D91-0017-4135-B7B9-9A352DC7BA93/ASSETS/SCIENCE.7871422.FP.PNG.

[69] M. Sala, R. Diab, A. Elaissari, and H. Fessi, "Lipid nanocarriers as skin drug delivery systems: Properties, mechanisms of skin interactions and medical applications," *Int. J. Pharm.*, vol. 535, no. 1–2, pp. 1–17, 2018, doi: 10.1016/j.ijpharm.2017.10.046.

[70] B. Mukherjee *et al.*, "Recent Trends for Nanomedicine Safety," *Nano Med. Nano Saf.*, pp. 469–509, 2020, doi: 10.1007/978-981-15-6255-6_18.

[71] M. K. Lee, "Liposomes for enhanced bioavailability of water-insoluble drugs: In vivo evidence and recent approaches," *Pharmaceutics*, vol. 12, no. 3, 2020, doi: 10.3390/pharmaceutics12030264.

[72] F. Lai, C. Caddeo, M. L. Manca, M. Manconi, C. Sinico, and A. M. Fadda, "What's new in the field of phospholipid vesicular nanocarriers for skin drug delivery," *Int. J. Pharm.*, vol. 583, no. March, p. 119398, 2020, doi: 10.1016/j.ijpharm.2020.119398.

[73] B. Iqbal, J. Ali, and S. Baboota, "Recent advances and development in epidermal and dermal drug deposition enhancement technology," *Int. J. Dermatol.*, vol. 57, no. 6, pp. 646–660, 2018, doi: 10.1111/ijd.13902.

[74] M. J. Valle and A. Navarro, "Liposomes Prepared in Absence of Organic Solvents: Sonication Versus Lipid Film Hydration Method," *Curr. Pharm. Anal.*, vol. 11, no. 2, pp. 86–91, 2015, doi: 10.2174/1573412910666141114221935.

[75] D. Van Swaay and A. Demello, “Microfluidic methods for forming liposomes,” *Lab on a Chip*, vol. 13, no. 5. The Royal Society of Chemistry, pp. 752–767, Feb. 05, 2013, doi: 10.1039/c2lc41121k.

[76] A. R. Bilia, M. C. Bergonzi, C. Guccione, M. Manconi, A. M. Fadda, and C. Sinico, “Vesicles and micelles: Two versatile vectors for the delivery of natural products,” *J. Drug Deliv. Sci. Technol.*, vol. 32, pp. 241–255, Apr. 2016, doi: 10.1016/j.jddst.2015.09.007.

[77] E. Touitou, N. Dayan, L. Bergelson, B. Godin, and M. Eliaz, “Ethosomes - novel vesicular carriers for enhanced delivery: characterization and skin penetration properties.,” *J. Control. Release*, vol. 65, no. 3, pp. 403–18, Apr. 2000, Accessed: Jul. 04, 2017. [Online]. Available: http://www.ncbi.nlm.nih.gov/pubmed/10699298.

[78] N. I. Payne, P. Timmins, C. V. Ambrose, M. D. Ward, and F. Ridgway, “Proliposomes: A novel solution to an old problem,” *J. Pharm. Sci.*, vol. 75, no. 4, pp. 325–329, 1986, doi: 10.1002/jps.2600750402.

[79] V. Nekkanti, N. Venkatesan, and G. Betageri, “Proliposomes for Oral Delivery: Progress and Challenges,” *Curr. Pharm. Biotechnol.*, vol. 16, no. 4, pp. 303–312, 2015, doi: 10.2174/1389201016666150118134256.

[80] Š. Zupančič, P. Kocbek, and J. Kristl, “Contribution of Nanotechnology to Improved Treatment of Periodontal Disease,” *Curr. Pharm. Des.*, vol. 21, no. 33, pp. 3257–3271, 2015.

[81] V. Beachley and X. Wen, “Polymer nanofibrous structures: Fabrication, biofunctionalization, and cell interactions,” *Prog. Polym. Sci.*, vol. 35, no. 7, pp. 868–892, Jul. 2010, doi: 10.1016/j.progpolymsci.2010.03.003.

[82] J. Gunn and M. Zhang, “Polyblend nanofibers for biomedical applications: perspectives and challenges,” *Trends Biotechnol.*, vol. 28, no. 4, pp. 189–197, Apr. 2010, doi: 10.1016/j.tibtech.2009.12.006.

[83] J. Pelipenko, P. Kocbek, and J. Kristl, “Critical attributes of nanofibers: Preparation, drug loading, and tissue regeneration,” *Int. J. Pharm.*, vol. 484, no. 1–2, pp. 57–74, 2015, doi: 10.1016/j.ijpharm.2015.02.043.

[84] I. Sebe, P. Szabó, B. Kállai-Szabó, and R. Zelkó, “Incorporating small molecules or biologics into nanofibers for optimized drug release: A review,” *Int. J. Pharm.*, vol. 494, no. 1, pp. 516–530, 2015, doi: 10.1016/j.ijpharm.2015.08.054.

[85] N. Bhardwaj and S. C. Kundu, “Electrospinning: A fascinating fiber fabrication technique,” *Biotechnol. Adv.*, vol. 28, no. 3, pp. 325–347, May 2010, doi: 10.1016/j.biotechadv.2010.01.004.

[86] A. Szentivanyi, T. Chakradeo, H. Zernetsch, and B. Glasmacher, “Electrospun cellular microenvironments: Understanding controlled release and scaffold structure,” *Adv. Drug Deliv. Rev.*, vol. 63, no. 4–5, pp. 209–220, Apr. 2011, doi: 10.1016/j.addr.2010.12.002.

[87] M. Gandhi, R. Srikar, A. L. Yarin, C. M. Megaridis, and R. A. Gemeinhart, “Mechanistic examination of protein release from polymer nanofibers.,” *Mol. Pharm.*, vol. 6, no. 2, pp. 641–7, 2009, doi: 10.1021/mp800160p.

[88] C. N. Manning *et al.*, “Controlled delivery of mesenchymal stem cells and growth factors using a nanofiber scaffold for tendon repair,” *Acta Biomater.*, vol. 9, no. 6, pp. 6905–6914, Jun. 2013, doi: 10.1016/j.actbio.2013.02.008.

[89] R. Zelkó, D. A. Lamprou, and I. Sebe, “Recent Development of Electrospinning for Drug Delivery,” *Pharm. 2020, Vol. 12, Page 5*, vol. 12, no. 1, p. 5, Dec. 2019, doi: 10.3390/PHARMACEUTICS12010005.

[90] T. Subbiah, G. S. Bhat, R. W. Tock, S. Parameswaran, and S. S. Ramkumar, “Electrospinning of nanofibers,” *J. Appl. Polym. Sci.*, vol. 96, no. 2, pp. 557–569, 2005, doi: 10.1002/app.21481.

[91] R. Rosic, J. Pelipenko, J. Kristl, P. Kocbeck, and S. Baumgartner, “Properties, Engineering and Applications of PolymericNanofibers: Current Research and Future Advances,” *Chem. Biochem. Eng. Q.*, vol. 26, no. 4, pp. 417–425, 2012.

[92] J. Pelipenko, J. Kristl, B. Jankovi, and P. Kocbek, “The impact of relative humidity during electrospinning on the morphology and mechanical properties of nanofibers,” *Int. J. Pharm.*, vol. 456, pp. 125–134, 2013.

[93] R. Rošic, J. Pelipenko, P. Kocbek, S. Baumgartner, M. Bešter-Rogač, and J. Kristl, “The role of rheology of polymer solutions in predicting nanofiber formation by electrospinning,” *Eur. Polym. J.*, vol. 48, no. 8, pp. 1374–1384, 2012, doi: 10.1016/j.eurpolymj.2012.05.001.

[94] B. Cramariuc, R. Cramariuc, R. Scarlet, L. R. Manea, I. G. Lupu, and O. Cramariuc, “Fiber diameter in electrospinning process,” *J. Electrostat.*, vol. 71, no. 3, pp. 189–198, Jun. 2013, doi: 10.1016/j.elstat.2012.12.018.

[95] Q. P. Pham, U. Sharma, and A. G. Mikos, “Electrospinning of Polymeric Nanofibers for Tissue Engineering Applications: A Review,” *Tissue Eng.*, vol. 12, no. 5, pp. 1197–1211, May 2006, doi: 10.1089/ten.2006.12.1197.

[96] S. Megelski, J. S. Stephens, D. Bruce Chase, and J. F. Rabolt, “Micro- and nanostructured surface morphology on electrospun polymer fibers,” *Macromolecules*, vol. 35, no. 22, pp. 8456–8466, 2002, doi: 10.1021/ma020444a.

[97] A. Trtchounian, M. Williams, and P. Talbot, “Conventional and electronic cigarettes (e-cigarettes) have different smoking characteristics.,” *Nicotine Tob. Res.*, vol. 12, no. 9, pp. 905–912, 2010, doi: 10.1093/ntr/ntq114.

[98] C. J. Brown and J. M. Cheng, “Electronic cigarettes: Product characterization and design considerations,” *Tob. Control*, vol. 23, no. SUPPL. 2, pp. ii4–ii10, 2014, doi: 10.1136/tobaccocontrol-2013-051476.

[99] T. Cheng, “Chemical evaluation of electronic cigarettes,” *Tob. Control*, vol. 23, no. SUPPL. 2, pp. ii11–ii17, 2014, doi: 10.1136/tobaccocontrol-2013-051482.

[100] M. Williams, A. Villarreal, K. Bozhilov, S. Lin, and P. Talbot, “Metal and Silicate Particles Including Nanoparticles Are Present in Electronic Cigarette Cartomizer Fluid and Aerosol,” *PLoS One*, vol. 8, no. 3, pp. 1–11, 2013, doi: 10.1371/journal.pone.0057987.

[101] M. L. Goniewicz, M. Gawron, D. M. Smith, M. Peng, P. Jacob, and N. L. Benowitz, “Exposure to nicotine and selected toxicants in cigarette smokers who switched to electronic cigarettes: A longitudinal within-subjects observational study,” *Nicotine Tob. Res.*, vol. 19, no. 2, pp. 160–167, 2017, doi: 10.1093/ntr/ntw160.

[102] M. L. Goniewicz *et al.*, “Comparison of Nicotine and Toxicant Exposure in Users of Electronic Cigarettes and Combustible Cigarettes,” *JAMA Netw. open*, vol. 1, no. 8, p. e185937, 2018, doi: 10.1001/jamanetworkopen.2018.5937.

[103] E. K. Round, P. Chen, A. K. Taylor, and E. Schmidt, “Biomarkers of Tobacco Exposure Decrease After Smokers Switch to an E-Cigarette or Nicotine Gum,” *Nicotine Tob. Res.*, vol. 21, no. 9, pp. 1239–1247, 2019, doi: 10.1093/ntr/nty140.

[104] European Parliament and the Council of the European Union, “Directive 2014/40/EU,” *Off. J. Eur. Union*, vol. 127, pp. 1–38, 2014.

[105] V. Varlet, “Drug Vaping: From the Dangers of Misuse to New Therapeutic Devices,” *Toxics*, vol. 4, no. 4, p. 29, 2016, doi: 10.3390/toxics4040029.

[106] A. K. Breitbarth, J. Morgan, and A. L. Jones, “E-cigarettes - An unintended illicit drug delivery system,” *Drug Alcohol Depend.*, vol. 192, no. 0, pp. 98–111, 2018, doi: 10.1016/j.drugalcdep.2018.07.031.

[107] V. Varlet *et al.*, “Drug vaping applied to cannabis: Is ‘cannavaping’ a therapeutic alternative to marijuana,” *Sci. Rep.*, vol. 6, no. May, pp. 1–13, 2016, doi: 10.1038/srep25599.

[108] C. Giroud, M. de Cesare, A. Berthet, V. Varlet, N. Concha-Lozano, and B. Favrat, “E-cigarettes: A review of new trends in cannabis use,” *Int. J. Environ. Res. Public Health*, vol. 12, no. 8, pp. 9988–10008, 2015, doi: 10.3390/ijerph120809988.

[109] J. D. Nguyen *et al.*, “Inhaled delivery of Δ9-tetrahydrocannabinol (THC) to rats by e-cigarette vapor technology,” *Neuropharmacology*, vol. 109, pp. 112–120, Oct. 2016, doi: 10.1016/j.neuropharm.2016.05.021.

[110] C. Miliano *et al.*, “Modeling drug exposure in rodents using e-cigarettes and other electronic nicotine delivery systems,” *Journal of Neuroscience Methods*, vol. 330. Elsevier B.V., p. 108458, Jan. 15, 2020, doi: 10.1016/j.jneumeth.2019.108458.

[111] J. Pourchez, F. de Oliveira, S. Perinel-Ragey, T. Basset, J. M. Vergnon, and N. Prévôt, “Assessment of new-generation high-power electronic nicotine delivery system as thermal aerosol generation device for inhaled bronchodilators,” *Int. J. Pharm.*, vol. 518, no. 1–2, pp. 264–269, 2017, doi: 10.1016/j.ijpharm.2017.01.009.

[112] H. J. Cho, P. Balakrishnan, H. Lin, M. K. Choi, and D. D. Kim, “Application of biopharmaceutics classification system (BCS) in drug transport studies across human respiratory epithelial cell monolayers,” *J. Pharm. Investig.*, vol. 42, no. 3, pp. 147–153, Jun. 2012, doi: 10.1007/s40005-012-0020-9.

[113] N. Wauthoz and K. Amighi, “Formulation Strategies for Pulmonary Delivery of Poorly Soluble Drugs,” in *Pulmonary Drug Delivery*, John Wiley & Sons, Ltd, 2015, pp. 87–122.

[114] C. Jacobs and R. H. Müller, “Production and characterization of a budesonide nanosuspension for pulmonary administration,” *Pharm. Res.*, vol. 19, no. 2, pp. 189–194, 2002, doi: 10.1023/A:1014276917363.

[115] P. C. Chiang, J. W. Alsup, Y. Lai, Y. Hu, B. R. Heyde, and D. Tung, “Evaluation of aerosol delivery of nanosuspension for pre-clinical pulmonary drug delivery,” *Nanoscale Res. Lett.*, vol. 4, no. 3, pp. 254–261, Mar. 2009, doi: 10.1007/s11671-

008-9234-1.

[116] Y. Zhang and J. Zhang, “Preparation of budesonide nanosuspensions for pulmonary delivery: Characterization, in vitro release and in vivo lung distribution studies,” *Artif. Cells, Nanomedicine Biotechnol.*, vol. 44, no. 1, pp. 285–289, Jan. 2016, doi: 10.3109/21691401.2014.944645.

[117] B. Van Eerdenbrugh, G. Van den Mooter, and P. Augustijns, “Top-down production of drug nanocrystals: Nanosuspension stabilization, miniaturization and transformation into solid products,” *International Journal of Pharmaceutics*, vol. 364, no. 1. Elsevier, pp. 64–75, Nov. 19, 2008, doi: 10.1016/j.ijpharm.2008.07.023.

[118] S. Britland, W. Finter, H. Chrystyn, D. Eagland, and M. E. Abdelrahim, “Droplet aerodynamics, cellular uptake, and efficacy of a nebulizable corticosteroid nanosuspension are superior to a micronized dosage form,” *Biotechnol. Prog.*, vol. 28, no. 5, pp. 1152–1159, 2012, doi: 10.1002/btpr.1616.

[119] J. Z. Yang, A. L. Young, P. C. Chiang, A. Thurston, and D. K. Pretzer, “Fluticasone and budesonide nanosuspensions for pulmonary delivery: Preparation, characterization, and pharmacokinetic studies,” *J. Pharm. Sci.*, vol. 97, no. 11, pp. 4869–4878, Nov. 2008, doi: 10.1002/jps.21380.

[120] E. Dompeling, C. P. van Schayck, J. Molema, H. Folgering, P. M. van Grunsven, and C. van Weel, “Inhaled beclomethasone improves the course of asthma and COPD.,” *Eur. Respir. J.*, vol. 5, no. 8, pp. 945–52, Sep. 1992, Accessed: Dec. 06, 2018. [Online]. Available: http://www.ncbi.nlm.nih.gov/pubmed/1426202.

[121] D. A. De Coster, M. Jones, and N. Thakrar, “Beclometasone for chronic obstructive pulmonary disease,” *Cochrane Database of Systematic Reviews*, vol. 2013, no. 10. John Wiley & Sons, Ltd, Oct. 09, 2013, doi: 10.1002/14651858.CD009769.pub2.

[122] A. J. j. Wood and P. J. Barnes, “Inhaled glucocorticoids for asthma,” *New England Journal of Medicine*, vol. 332, no. 13. pp. 868–875, 1995, doi: 10.1056/NEJM199503303321307.

[123] J. G. Moloughney and N. Weisleder, “Poloxamer 188 (P188) as a Membrane Resealing Reagent in Biomedical Applications,” *Recent Pat. Biotechnol.*, vol. 6, no. 3, pp. 200–211, 2013, doi: 10.2174/1872208311206030200.

[124] V. B. Patravale, A. A. Date, and R. M. Kulkarni, “Nanosuspensions: a promising drug delivery strategy,” *J. Pharm. Pharmacol.*, vol. 56, pp. 827–840, Jul. 2004, doi:

10.1211/0022357023691.

[125] S. Pabisch, B. Feichtenschlager, G. Kickelbick, and H. Peterlik, “Effect of interparticle interactions on size determination of zirconia and silica based systems - A comparison of SAXS, DLS, BET, XRD and TEM,” *Chem. Phys. Lett.*, vol. 521, pp. 91–97, Jan. 2012, doi: 10.1016/j.cplett.2011.11.049.

[126] H. Hinterwirth *et al.*, “Comparative method evaluation for size and size-distribution analysis of gold nanoparticles,” *J. Sep. Sci.*, vol. 36, no. 17, pp. 2952–2961, 2013, doi: 10.1002/jssc.201300460.

[127] G. Unsoy, S. Yalcin, R. Khodadust, G. Gunduz, and U. Gunduz, “Synthesis optimization and characterization of chitosancoated iron oxide nanoparticles produced for biomedical applications,” *J. Nanoparticle Res.*, vol. 14, no. 11, pp. 1–13, Oct. 2012, doi: 10.1007/s11051-012-0964-8.

[128] D. H. Lee, G. S. Cho, H. M. Lim, D. S. Kim, C. Kim, and S. H. Lee, “Comparisons of particle size measurement method for colloidal silica,” *J. Ceram. Process. Res.*, vol. 14, no. 2, pp. 274–278, 2013.

[129] W. Tscharnuter, “Photon Correlation Spectroscopy in Particle Sizing,” *Encycl. Anal. Chem.*, pp. 1–16, 2006, doi: 10.1002/9780470027318.a1512.

[130] E. Tomaszewska *et al.*, “Detection limits of DLS and UV-Vis spectroscopy in characterization of polydisperse nanoparticles colloids,” *J. Nanomater.*, vol. 2013, pp. 1–10, 2013, doi: 10.1155/2013/313081.

[131] Z. Wang, J. F. Chen, Y. Le, Z. G. Shen, and J. Yun, “Preparation of ultrafine beclomethasone dipropionate drug powder by antisolvent precipitation,” *Ind. Eng. Chem. Res.*, vol. 46, no. 14, pp. 4839–4845, Jul. 2007, doi: 10.1021/ie0615537.

[132] C. Weiss, P. McLoughlin, P. Manesiotis, W. Redington, and H. Cathcart, “Preparation and characterization of beclomethasone dipropionate solvates,” *Cryst. Growth Des.*, vol. 18, no. 10, pp. 5832–5844, 2018, doi: 10.1021/acs.cgd.8b00465.

[133] D. Azzopardi *et al.*, “Electronic cigarette aerosol induces significantly less cytotoxicity than Tobacco smoke,” *Toxicol. Mech. Methods*, vol. 26, no. 6, pp. 477–491, 2016, doi: 10.1080/15376516.2016.1217112.

[134] L. Czekala, L. Simms, M. Stevenson, N. Tschierske, A. G. Maione, and T. Walele, “Toxicological comparison of cigarette smoke and e-cigarette aerosol using a 3D in vitro human respiratory model,” *Regul. Toxicol. Pharmacol.*, vol. 103, pp. 314–324,

Apr. 2019, doi: 10.1016/j.yrtph.2019.01.036.

[135] D. McNeill, A., Brose, L.S., Calder, R., Bauld, L., and Robson, "Vaping in England: an evidence update including mental health and pregnancy, March 2020: a report commissioned by Public Health England.," 2020. Accessed: Apr. 14, 2020. [Online]. Available: www.facebook.com/PublicHealthEngland.

[136] M. L. Goniewicz, E. O. Lingas, and P. Hajek, "Patterns of electronic cigarette use and user beliefs about their safety and benefits: An Internet survey," *Drug Alcohol Rev.*, vol. 32, no. 2, pp. 133–140, Mar. 2013, doi: 10.1111/j.1465-3362.2012.00512.x.

[137] http://goldcopd.org, "Pocket guide to COPD diagnosis, management and prevention: a guide for health care professionals," 2018. doi: 10.2147/copd.2006.1.1.3.

[138] P. Moroni-Zentgraf, "Impact of Patient Needs on Design and Usage of an Inhalation Device in Respiratory Medicine," in *Respiratory Drug Delivery Europe 2013*, 2013, vol. 1, no. 1, pp. 141–152, doi: 10.1586/17476348.1.1.39.

[139] A. Ari and J. B. Fink, "Guidelines for aerosol devices in infants, children and adults: Which to choose, why and how to achieve effective aerosol therapy," *Expert Review of Respiratory Medicine*, vol. 5, no. 4. Taylor & Francis, pp. 561–572, Aug. 2011, doi: 10.1586/ers.11.49.

[140] K. Nikander, "Challenges and opportunities in respiratory drug delivery devices," *Expert Opinion on Drug Delivery*, vol. 7, no. 11. Taylor & Francis, pp. 1235–1238, Nov. 2010, doi: 10.1517/17425247.2010.525231.

[141] J. Boe, J. H. Dennis, and B. R. O'Driscoll, "European respiratory society guidelines on the use of nebulizers," *Eur. Respir. J.*, vol. 18, no. 1, pp. 228–242, 2001, doi: 10.1183/09031936.01.00220001.

[142] T. F. Carr and E. Bleecker, "Asthma heterogeneity and severity," *World Allergy Organization Journal*, vol. 9, no. 1. BioMed Central Ltd, p. 41, Nov. 29, 2016, doi: 10.1186/s40413-016-0131-2.

[143] K. Nakagome and M. Nagata, "Pathogenesis of airway inflammation in bronchial asthma," *Auris Nasus Larynx*, vol. 38, no. 5. Elsevier, pp. 555–563, Oct. 01, 2011, doi: 10.1016/j.anl.2011.01.011.

[144] M. E. Kuruvilla, F. E. H. Lee, and G. B. Lee, "Understanding Asthma Phenotypes, Endotypes, and Mechanisms of Disease," *Clinical Reviews in Allergy and*

Immunology, vol. 56, no. 2. Humana Press Inc., pp. 219–233, Apr. 15, 2019, doi: 10.1007/s12016-018-8712-1.

[145] S. E. Wenzel, "Asthma phenotypes: the evolution from clinical to molecular approaches," *Nat. Med.*, 2012, doi: 10.1038/nm.2678.

[146] Global Initiative for Asthma, "Global strategy for asthma management and prevention.," 2020. Accessed: Jan. 29, 2021. [Online]. Available: www.ginasthma.org.

[147] H. S. Park, S. R. Kim, J. O. Kim, and Y. C. Lee, "The roles of phytochemicals in bronchial asthma," *Molecules*, vol. 15, no. 10, pp. 6810–6834, Oct. 2010, doi: 10.3390/molecules15106810.

[148] A. Abidi, S. Gupta, M. Agarwal, H. L. Bhalla, and M. Saluja, "Evaluation of efficacy of curcumin as an add-on therapy in patients of bronchial asthma," *J. Clin. Diagnostic Res.*, vol. 8, no. 8, p. HC19, 2014, doi: 10.7860/JCDR/2014/9273.4705.

[149] S. W. Oh *et al.*, "Curcumin attenuates allergic airway inflammation and hyper-responsiveness in mice through NF-κB inhibition," *J. Ethnopharmacol.*, vol. 136, no. 3, pp. 414–421, Jul. 2011, doi: 10.1016/j.jep.2010.07.026.

[150] L. Chong *et al.*, "Protective Effect of Curcumin on Acute Airway Inflammation of Allergic Asthma in Mice Through Notch1–GATA3 Signaling Pathway," *Inflammation*, vol. 37, no. 5, pp. 1476–1485, 2014, doi: 10.1007/s10753-014-9873-6.

[151] H. Shahid, M. Shahzad, A. Shabbir, and G. Saghir, "Immunomodulatory and Anti-Inflammatory Potential of Curcumin for the Treatment of Allergic Asthma: Effects on Expression Levels of Pro-inflammatory Cytokines and Aquaporins," *Inflammation*, vol. 42, no. 6, pp. 2037–2047, Dec. 2019, doi: 10.1007/s10753-019-01066-2.

[152] F. Lai, M. Schlich, R. Pireddu, A. M. Fadda, and C. Sinico, "Nanocrystals as Effective Delivery Systems of Poorly Water-soluble Natural Molecules," *Curr. Med. Chem.*, vol. 26, no. 24, pp. 4657–4680, Dec. 2018, doi: 10.2174/0929867326666181213095809.

[153] F. Corrias *et al.*, "Nile red nanosuspensions as investigative model to study the follicular targeting of drug nanocrystals," *Int. J. Pharm.*, vol. 524, no. 1–2, pp. 1–8, 2017, doi: 10.1016/j.ijpharm.2017.03.042.

[154] L. Casula *et al.*, "Delivery of beclomethasone dipropionate nanosuspensions with an electronic cigarette," *Int. J. Pharm.*, vol. 596, no. January, pp. 1–9, 2021, doi: 10.1016/j.ijpharm.2021.120293.

[155] E. Berg, P. Lamb, A. Ali, J. Dennis, M. Tservistas, and J. Mitchell, “Assessment of the need to coat particle collection cups of the NGI to mitigate droplet bounce when evaluating nebuliser-produced droplets.,” *Pharmeur. Sci. Notes*, vol. 2008, no. 1, pp. 21–25, Feb. 2008, Accessed: Apr. 27, 2021. [Online]. Available: https://europepmc.org/article/med/18430403.

[156] V. Marple, K. Santhanakrishnan, J. P. Mitchell, D. L. Roberts, and B. L. Hudson-curtis, “Next Generation Pharmaceutical Impactor: A New Impactor for Pharmaceutical Inhaler Testing. Part III. Extension of Archival Calibration to 15 L/min,” *J. Aerosol Med.*, vol. 17, no. 4, pp. 335–343, 2004.

[157] M. L. Manca *et al.*, “Nanoincorporation of curcumin in polymer-glycerosomes and evaluation of their in vitro-in vivo suitability as pulmonary delivery systems,” *RSC Adv.*, vol. 5, no. 127, pp. 105149–105159, 2015, doi: 10.1039/c5ra24032h.

[158] X. Li *et al.*, “Preparation and in-vitro/in-vivo evaluation of curcumin nanosuspension with solubility enhancement,” *J. Pharm. Pharmacol.*, vol. 68, no. 8, pp. 980–988, Jul. 2016, doi: 10.1111/JPHP.12575.

[159] H. Fujimura, T. Komasaka, T. Tomari, Y. Kitano, and K. Takekawa, “Nanosuspension formulations of poorly water-soluble compounds for intravenous administration in exploratory toxicity studies: in vitro and in vivo evaluation,” *J. Appl. Toxicol.*, vol. 36, no. 10, pp. 1259–1267, Oct. 2016, doi: 10.1002/JAT.3280.

[160] L. Wang, J. Du, Y. Zhou, and Y. Wang, “Safety of nanosuspensions in drug delivery,” *Nanomedicine Nanotechnology, Biol. Med.*, vol. 13, no. 2, pp. 455–469, Feb. 2017, doi: 10.1016/J.NANO.2016.08.007.

[161] F. Zani, C. Veneziani, E. Bazzoni, L. Maggi, G. Caponetti, and R. Bettini, “Sterilization of corticosteroids for ocular and pulmonary delivery with supercritical carbon dioxide,” *Int. J. Pharm.*, vol. 450, no. 1–2, pp. 218–224, 2013, doi: 10.1016/j.ijpharm.2013.04.055.

[162] S. J. Franklin, U. S. Younis, and P. B. Myrdal, “Estimating the Aqueous Solubility of Pharmaceutical Hydrates,” *J. Pharm. Sci.*, vol. 105, no. 6, pp. 1914–1919, 2016, doi: 10.1016/j.xphs.2016.03.040.

[163] W. Yang, J. I. Peters, and R. O. Williams, “Inhaled nanoparticles-A current review,” *International Journal of Pharmaceutics*, vol. 356, no. 1–2. Elsevier, pp. 239–247, May 22, 2008, doi: 10.1016/j.ijpharm.2008.02.011.

[164] N. J. Percival, “Classification of Wounds and their Management,” *Surg.*, vol. 20, no. 5, pp. 114–117, May 2002, doi: 10.1383/SURG.20.5.114.14626.

[165] G. S. Lazarus *et al.*, “Definitions and guidelines for assessment of wounds and evaluation of healing,” *Wound Repair Regen.*, vol. 2, no. 3, pp. 165–170, 1994, doi: 10.1046/j.1524-475X.1994.20305.x.

[166] L. M. Morton and T. J. Phillips, “Wound healing and treating wounds Differential diagnosis and evaluation of chronic wounds,” *J. Am. Acad. Dermatol.*, vol. 74, no. 4, pp. 589–605, 2016, doi: 10.1016/j.jaad.2015.08.068.

[167] G. Han and R. Ceilley, “Chronic Wound Healing: A Review of Current Management and Treatments,” *Adv. Ther.*, vol. 34, no. 3, pp. 599–610, Mar. 2017, doi: 10.1007/s12325-017-0478-y.

[168] M. Ashtikar and M. G. Wacker, “Nanopharmaceuticals for wound healing – Lost in translation?,” *Adv. Drug Deliv. Rev.*, vol. 129, no. March, pp. 194–218, 2018, doi: 10.1016/j.addr.2018.03.005.

[169] W. Wang, K. J. Lu, C. H. Yu, Q. L. Huang, and Y. Z. Du, “Nano-drug delivery systems in wound treatment and skin regeneration,” *Journal of Nanobiotechnology*, vol. 17, no. 1. BioMed Central Ltd., Jul. 10, 2019, doi: 10.1186/s12951-019-0514-y.

[170] R. S. Ambekar and B. Kandasubramanian, “Advancements in nanofibers for wound dressing: A review,” *European Polymer Journal*, vol. 117. Elsevier Ltd, pp. 304–336, Aug. 01, 2019, doi: 10.1016/j.eurpolymj.2019.05.020.

[171] A. Memic, T. Abudula, H. S. Mohammed, K. Joshi Navare, T. Colombani, and S. A. Bencherif, “Latest Progress in Electrospun Nanofibers for Wound Healing Applications,” *ACS Applied Bio Materials*, vol. 2, no. 3. pp. 952–969, 2019, doi: 10.1021/acsabm.8b00637.

[172] M. Liu, X. P. Duan, Y. M. Li, D. P. Yang, and Y. Z. Long, “Electrospun nanofibers for wound healing,” *Materials Science and Engineering C*, vol. 76. Elsevier Ltd, pp. 1413–1423, Jul. 01, 2017, doi: 10.1016/j.msec.2017.03.034.

[173] S. P. Miguel *et al.*, “Electrospun polymeric nanofibres as wound dressings: A review,” *Colloids and Surfaces B: Biointerfaces*, vol. 169. Elsevier B.V., pp. 60–71, Sep. 01, 2018, doi: 10.1016/j.colsurfb.2018.05.011.

[174] L. Bacakova *et al.*, “Nanofibrous Scaffolds for Skin Tissue Engineering and Wound Healing Based on Nature-Derived Polymers,” in *Current and Future Aspects of*

Nanomedicine, IntechOpen, 2020.

[175] V. U. Godakanda *et al.*, "Tunable drug release from blend poly(vinyl pyrrolidone)-ethyl cellulose nanofibers," *Int. J. Pharm.*, vol. 562, pp. 172–179, May 2019, doi: 10.1016/J.IJPHARM.2019.03.035.

[176] T. Maver, M. Kurečič, D. M. Smrke, K. S. Kleinschek, and U. Maver, "Electrospun nanofibrous CMC/PEO as a part of an effective pain-relieving wound dressing," *J. Sol-Gel Sci. Technol.*, vol. 79, no. 3, pp. 475–486, Sep. 2016, doi: 10.1007/s10971-015-3888-9.

[177] G. Jin, M. P. Prabhakaran, D. Kai, and S. Ramakrishna, "Controlled release of multiple epidermal induction factors through core-shell nanofibers for skin regeneration," *Eur. J. Pharm. Biopharm.*, vol. 85, no. 3 PART A, pp. 689–698, 2013, doi: 10.1016/j.ejpb.2013.06.002.

[178] M. Khoshneviszadeh, S. Ashkani-Esfahani, M. R. Namazi, A. Noorafshan, B. Geramizadeh, and R. Miri, "Topical Simvastatin Enhances Tissue Regeneration in Full-Thickness Skin Wounds in Rat Models," *Iran. J. Pharm. Res. IJPR*, vol. 13, no. 1, p. 263, 2014, Accessed: Jan. 02, 2022. [Online]. Available: /pmc/articles/PMC3985244/.

[179] J. Asai *et al.*, "Topical Simvastatin Accelerates Wound Healing in Diabetes by Enhancing Angiogenesis and Lymphangiogenesis," *Am. J. Pathol.*, vol. 181, no. 6, pp. 2217–2224, Dec. 2012, doi: 10.1016/J.AJPATH.2012.08.023.

[180] U. F. Aly, H. A. Abou-Taleb, Ah. A. H. Abdellatif, and N. S. Tolba, "Formulation and evaluation of simvastatin polymeric nanoparticles loaded in hydrogel for optimum wound healing purpose," *Drug Des. Devel. Ther.*, vol. 13, p. 1567, 2019, doi: 10.2147/DDDT.S198413.

[181] S. Yasasvini, R. S. Anusa, B. N. VedhaHari, P. C. Prabhu, and D. RamyaDevi, "Topical hydrogel matrix loaded with Simvastatin microparticles for enhanced wound healing activity," *Mater. Sci. Eng. C*, vol. 72, pp. 160–167, Mar. 2017, doi: 10.1016/j.msec.2016.11.038.

[182] L. M. Blanco-Colio, J. Tuñón, J. L. Martín-Ventura, and J. Egido, "Anti-inflammatory and immunomodulatory effects of statins," *Kidney Int.*, vol. 63, no. 1, pp. 12–23, 2003, doi: 10.1046/j.1523-1755.2003.00744.x.

[183] T. Fehr *et al.*, "Statin-induced immunomodulatory effects on human T cells in vivo,"

Atherosclerosis, vol. 175, no. 1, pp. 83–90, Jul. 2004, doi: 10.1016/j.atherosclerosis.2004.02.016.

[184] A. Blum and R. Shamburek, "The pleiotropic effects of statins on endothelial function, vascular inflammation, immunomodulation and thrombogenesis," *Atherosclerosis*, vol. 203, no. 2. pp. 325–330, Apr. 2009, doi: 10.1016/j.atherosclerosis.2008.08.022.

[185] F. R. Danesh, R. L. Anel, L. Zeng, J. Lomasney, A. Sahai, and Y. S. Kanwar, "Immunomodulatory effects of HMG-CoA reductase inhibitors," *Arch. Immunol. Ther. Exp. (Warsz).*, vol. 51, no. 3, pp. 139–148, 2003.

[186] A. C. M. Do Rego *et al.*, "Simvastatin improves the healing of infected skin wounds of rats," *Acta Cir. Bras.*, vol. 22, no. SUPPL. 1, pp. 57–63, 2007, doi: 10.1590/s0102-86502007000700012.

[187] S. Jerwood and J. Cohen, "Unexpected antimicrobial effect of statins," *J. Antimicrob. Chemother.*, vol. 61, no. 2, pp. 362–364, 2008, doi: 10.1093/jac/dkm496.

[188] C. C. Wang, P. W. Yang, S. F. Yang, K. P. Hsieh, S. P. Tseng, and Y. C. Lin, "Topical simvastatin promotes healing of staphylococcus aureus-contaminated cutaneous wounds," *Int. Wound J.*, vol. 13, no. 6, pp. 1150–1157, Dec. 2016, doi: 10.1111/iwj.12431.

[189] D. K. Ellison, W. D. Moore, and C. R. Petts, "Simvastatin," in *Analytical Profiles of Drug Substances and Excipients*, vol. 22, 1993, pp. 359–388.

[190] B. Sterle Zorec, Š. Zupančič, Z. Lavrič, and R. Dreu, "Particle properties and drug metastable solubility of simvastatin containing PVP matrix particles prepared by electrospraying technique," *Eur. J. Pharm. Sci.*, vol. 158, p. 105649, Mar. 2021, doi: 10.1016/j.ejps.2020.105649.

[191] M. Pohlen, L. Pirker, M. Luštrik, and R. Dreu, "A redispersible dry emulsion system with simvastatin prepared via fluid bed layering as a means of dissolution enhancement of a lipophilic drug," *Int. J. Pharm.*, vol. 549, no. 1–2, pp. 325–334, Oct. 2018, doi: 10.1016/j.ijpharm.2018.07.064.

[192] Malvern Panalytical, "Technical Note: Particle Concentration Measurements on the Zetasizer Ultra – How It Works." 2019.

[193] Malvern Panalytical, "Technical Note: Best Practice for Making Particle Concentration Measurements on the Zetasizer." 2019.

[194] FDA/CDER, “Dissolution Testing of Immediate Release Solid Oral Dosage Forms,” vol. 4, no. August. Tel, pp. 15–22, 1997, Accessed: Jan. 06, 2022. [Online]. Available: http://www.fda.gov/cder/guidance.htm.

[195] EMA, “CPMP/EWP/QWP/1401/98 Rev. 1. Guideline on the investigation of bioequivalence,” vol. 1, no. January, pp. 1–27, 2010, Accessed: Jan. 06, 2022. [Online]. Available: http://www.ema.europa.eu.

[196] S. Kajdič, Š. Zupančič, R. Roškar, and P. Kocbek, “The potential of nanofibers to increase solubility and dissolution rate of the poorly soluble and chemically unstable drug lovastatin,” *Int. J. Pharm.*, vol. 573, p. 118809, Jan. 2020, doi: 10.1016/j.ijpharm.2019.118809.

[197] B. A. Aderibigbe and B. Buyana, “Alginate in wound dressings,” *Pharmaceutics*, vol. 10, no. 2. MDPI AG, p. 42, Jun. 01, 2018, doi: 10.3390/pharmaceutics10020042.

[198] S. Safi, M. Morshed, S. A. Hosseini Ravandi, and M. Ghiaci, “Study of electrospinning of sodium alginate, blended solutions of sodium alginate/poly(viny1 alcoho1) and sodium alginate/poly(ethylene oxide),” *J. Appl. Polym. Sci.*, vol. 104, no. 5, pp. 3245–3255, Jun. 2007, doi: 10.1002/app.25696.

[199] H. Nie *et al.*, “Effect of poly(ethylene oxide) with different molecular weights on the electrospinnability of sodium alginate,” *Polymer (Guildf).*, vol. 50, no. 20, pp. 4926–4934, Sep. 2009, doi: 10.1016/j.polymer.2009.07.043.

[200] J. Mirtič *et al.*, “Effect of Solution Composition Variables on Electrospun Alginate Nanofibers: Response Surface Analysis,” *Polymers (Basel).*, vol. 11, no. 4, p. 692, Apr. 2019, doi: 10.3390/polym11040692.

[201] R. Krishnan, S. Sundarrajan, and S. Ramakrishna, “Green processing of nanofibers for regenerative medicine,” *Macromol. Mater. Eng.*, vol. 298, no. 10, pp. 1034–1058, 2013, doi: 10.1002/mame.201200323.

[202] L. Liverani, L. Vester, and A. R. Boccaccini, “Biomaterials Produced via Green Electrospinning,” *Electrospun Biomater. Relat. Technol.*, pp. 149–168, 2017, doi: 10.1007/978-3-319-70049-6_5.

[203] A. Mickova *et al.*, “Core/shell nanofibers with embedded liposomes as a drug delivery system,” *Biomacromolecules*, vol. 13, no. 4, pp. 952–962, 2012, doi: 10.1021/bm2018118.

[204] Council of Europe, “5.17.1. Reccomendations on dissolution testing,” *The European*

Pharmacopoeia 8th ed, no. 1. pp. 727–729, 2013.

[205] Malvern Panalytical, "Technical Note: Multi-angle Dynamic Light Scattering (MADLS) on the Zetasizer Ultra – How it Works," 2018.

[206] J. Austin, C. Minelli, D. Hamilton, M. Wywijas, and H. J. Jones, "Nanoparticle number concentration measurements by multi-angle dynamic light scattering," *J. Nanoparticle Res.*, vol. 22, no. 5, pp. 1–15, May 2020, doi: 10.1007/s11051-020-04840-8.

[207] P. Śliwa, K. Śliwa, E. Sikora, J. Ogonowski, J. Oszmiański, and P. Nowicka, "Incorporation of bioflavonoids from Bidens tripartite into micelles of non-ionic surfactants – experimental and theoretical studies," *Colloids Surfaces B Biointerfaces*, vol. 184, p. 110553, Dec. 2019, doi: 10.1016/j.colsurfb.2019.110553.

[208] L. Cole, D. Fernandes, M. T. Hussain, M. Kaszuba, J. Stenson, and N. Markova, "Characterization of Recombinant Adeno-Associated Viruses (rAAVs) for Gene Therapy Using Orthogonal Techniques," *Pharm. 2021, Vol. 13, Page 586*, vol. 13, no. 4, p. 586, Apr. 2021, doi: 10.3390/PHARMACEUTICS13040586.

[209] J. H. Leitão *et al.*, "Biophysical Characterization of Viral and Lipid-Based Vectors for Vaccines and Therapeutics with Light Scattering and Calorimetric Techniques," *Vaccines 2022, Vol. 10, Page 49*, vol. 10, no. 1, p. 49, Dec. 2021, doi: 10.3390/VACCINES10010049.

[210] W. M. Maccuaig *et al.*, "Active Targeting Significantly Outperforms Nanoparticle Size in Facilitating Tumor-Specific Uptake in Orthotopic Pancreatic Cancer," *ACS Appl. Mater. Interfaces*, vol. 13, no. 42, pp. 49614–49630, Oct. 2021, doi: 10.1021/ACSAMI.1C09379/SUPPL_FILE/AM1C09379_SI_001.PDF.

[211] M. Soldi *et al.*, "Laboratory-Scale Lentiviral Vector Production and Purification for Enhanced Ex Vivo and In Vivo Genetic Engineering," *Mol. Ther. - Methods Clin. Dev.*, vol. 19, pp. 411–425, Dec. 2020, doi: 10.1016/J.OMTM.2020.10.009.

[212] E. Porges *et al.*, "Antibiotic-Loaded Polymersomes for Clearance of Intracellular Burkholderia thailandensis," *ACS Nano*, 2021, doi: 10.1021/ACSNANO.1C05309/SUPPL_FILE/NN1C05309_SI_001.PDF.

[213] N. J. Pandya *et al.*, "Secreted retrovirus-like GAG-domain-containing protein PEG10 is regulated by UBE3A and is involved in Angelman syndrome pathophysiology," *Cell Reports Med.*, vol. 2, no. 8, p. 100360, Aug. 2021, doi:

10.1016/J.XCRM.2021.100360.

[214] M. J. Kaufman, “Applications of Oxygen Polarography to Drug Stability Testing and Formulation Development: Solution-Phase Oxidation of Hydroxymethylglutaryl Coenzyme A (HMG-CoA) Reductase Inhibitors,” *Pharm. Res. 1990 73*, vol. 7, no. 3, pp. 289–292, 1990, doi: 10.1023/A:1015886415210.